# Detection of very long period seismic signals and acoustic gravity waves generated by large tsunamis: Application to tsunami warning

Inauguraldissertation
zur Erlangung des akademischen Doktorgrades

eingereicht am Fachbereich Geowissenschaften,
der Freien Universität Berlin

vorgelegt von

Andriamiranto Raveloson

November 7, 2011

Als Dissertation angenommen vom Fachbereich Geowissenschaften
der Freien Universität Berlin.

auf Grund der Gutachten
von Prof. Dr. Rainer Kind
und Prof. Dr. Marco Bohnhoff

Berlin, den 01. November 2011

**Statement of Authorship**

This thesis has been submitted for the degree of Doctor of natural sciences. I, Andriamiranto Raveloson, hereby declare that:

- I am the sole author of this thesis.
- I have fully acknowledged and referenced the ideas and work of others, whether published or unpublished, in my thesis.
- I have prepared my thesis specifically for the degree of natural sciences under the supervision of Prof Rainer Kind at the Freie Universität Berlin.
- My thesis does not contain work extracted from a thesis, dissertation or research paper previously presented for another degree or diploma at this or any other university.

**Eidesstattliche Erklärung**

Die These ist für den Grad eines Doktors der NaturWissenschafter vorgelegt. Ich, Andriamiranto Raveloson, erkläre hiermit, dass:

- Ich bin der alleinige Urheber dieser These.
- Ich habe voll anerkannt und verwiesen die Ideen und die Arbeit der anderen, ob veröffentlicht oder unveröffentlicht, in meiner Diplomarbeit.
- Ich habe meine Diplomarbeit speziell für den Grad eines Doktors der NaturWissenschafter, während unter den vorbereiteten Aufsicht von Prof. Rainer Kind an der Freien Universität Berlin.
- Meine These enthält keine Arbeit aus einer Diplomarbeit, Dissertation oder Forschungsarbeit gewonnen zuvor für einen anderen Abschluss oder ein Diplom in dieser oder einer anderen Hochschule vorgestellt.

Andriamiranto Raveloson

# Abstract

Tsunamis belong to natural events, which lead to the most devastating global catastrophes, although they occur rarely. Because tsunamis caused in recent times large number of casualties and heavy destruction in wide spread coastal areas, they became the focus of intensive scientific research. The basis to mitigate casualties due to tsunamis is mainly continuous monitoring of seismic activity. Since prediction of earthquakes is not possible, early tsunami warning is the primary goal of related research. So far, direct observations of tsunamis came only from tide gauges on the shore lines and deep ocean pressure sensors (Deep Ocean Assessment and Reporting of Tsunamis, DART). However, tide gauge measurements are dominantly influenced by local conditions (shape of the harbor and resonances within the harbor) and DART stations have a very poor coverage.

In this thesis, data from seismic and infrasound stations were analyzed in order to see effects of tsunamis of the great Sumatra-Andaman 2004 and Tohuku-Oki 2011 earthquakes. Data used are from seismic stations of the Global Seismic Network (GSN) around the Indian and Pacific oceans and from infrasound stations of the International Monitoring System of the Comprehensive Test Ban Treaty Organization (IMS/CTBTO). In both data sets, seismic and infrasound, tsunami signals are observed in the period range of $500 to 2000 s$. These data may add to two new very useful observables for tsunami early warning systems. A traveling tsunami wave is causing tilting of the ocean bottom and of the coast up to $150 km$ inland, which is recorded on the horizontal components of broadband seismometers. In the source region of an earthquake, the bottom of the ocean may be displaced vertically, which causes vertical displacement of the surface of the sea, and which leads to the generation of an acoustic gravity wave propagating in the atmosphere. Infrasound signals of the Sumatra-Andaman and Tohoku-Oki earthquakes have been used successfully to locate the

sources of both tsunamis. The epicenter of the Tohoku-Oki tsunami was about 100km to the south-east of the seismic epicenter, and that of the Sumatra-Andaman event was about $200km$ to the northwest of the seismic epicenter. The great advantage of this technique is that infrasound travels with a speed of about $330m/s$ and the tsunami travels significantly slower, with a speed of about $200m/s$ in the deep ocean and much slower in shallow coastal waters. This technique not only provides the fastest evidence if a tsunami was indeed generated (which may avoid false alarms), but it also gains additional warning time and provides basic information on the tsunami source needed for modeling of tsunami propagation. Implementation of these two new observables into existing tsunami early warning systems would be relatively easy, because infrasound sensors could be integrated into seismic stations. Ultra long period seismic observations of tsunamis at coastal stations would only require some software additions.

# Zusammenfassung

Tsunamis sind Naturereignisse, die zu den verheerendsten weltweiten Katastrophen gehören, obwohl sie relativ selten auftreten. Da Tsunamis in letzter Zeit zahlreiche Opfer und schwere Zerstörungen in groβen Küstenregionen verursacht haben, sind sie Ziel intensivierter Forschungen geworden. Die Grundlage zur Reduzierung von Tsunamiopfern ist ein kontinuierliches Monitoring der Seismizität. Da eine Erdbebenvorhersage nicht möglich ist, sind Tsunamifrühwarnungen das primäre Ziel der Forschungen auf diesem Gebiet. Bisher geschehen direkte Beobachtungen von Tsunamis hauptsächlich durch Messungen des Meeresspiegels an Küsten oder durch Drucksensoren in der Tiefsee mit Hilfe von Bojen (Deep Ocean Assessment and Reporting of Tsunamis, DART). Jedoch werden Küstenpegelmessungen in Häfen dominiert von lokalen Küstenstrukturen und möglichen Resonanzeffekten und es gibt nur eine relativ geringe Anzahl von DART Stationen im offenen Ozean.

In dieser Dissertation werden Beobachtungen von Tsunamis in seismischen Daten und in Infrasound Daten der groβen Erdbeben von Sumatra-Andaman 2004 und Tohoku-Oki 2011 analysiert. Die benutzten Daten stammen von den seismischen Stationen des Global Seismic Network (GSN) im Gebiet des Pazifischen und Indischen Ozeans und von den Infrasound Stationen des International Monitoring System of the Comprehensive Test Ban Treaty Organization (IMS/CTBTO). In beiden Datensätzen, den seismischen und den Infrasound Daten, wurden Signale von Tsunamis im Periodenbereich von 500 bis $2000s$ beobachtet. Diese Daten sind neue, möglicherweise sehr nützliche Beobachtungsgröβen für Tsunamiwarnsysteme. Ein sich ausbreitender Tsunami verursacht Neigungsänderungen des Meeresbodens und der Küstenregionen bis zu $150km$ landeinwärts, die auf den Horizontalkomponenten von Breitbandseismometern messbar sind. In der Herdregion von Erdbeben bewegt sich der Meeresboden möglicherweise vertikal, was zu vertikalen Bewegungen

der Meeresoberfläche führt, die wiederum akustische Gravitationswellen in der Atmosphäre erzeugen. Solche Infrasound Signale der Sumatra-Andaman und Tohoku-Oki Erdbeben wurden erfolgreich zur Lokalisierung der Herde der Tsunamis benutzt. Das Epizentrum des Tohoku-Oki Tsunamis wurde ca. $100km$ südöstlich des seismischen Epizentrums lokalisiert, und das Epizentrum des Sumatra-Andaman Tsunamis ca. $200km$ nordwestlich des seismischen Epizentrums. Der gro$\beta$e Vorteil dieser Methode ist, dass Infrasound sich mit einer Geschwindigkeit von ca. $330m/s$ ausbreitet während der Tsunami selbst sich viel langsamer ausbreitet; mit Geschwindigkeiten von ca. $200m/s$ in der Tiefsee und mit viel kleineren Geschwindigkeiten in flachen Küstengewässern. Diese Technik liefert nicht nur die schnellsten Hinweise, ob ein Tsunami tatsächlich von einem Erdbeben erzeugt wurde (was falsche Alarme reduziert), sondern es wird auch zusätzliche Warnzeit gewonnen und wichtige Informationen für die Modellierung der Tsunamiausbreitung werden erhalten. Die Einfügung dieser neuen Beobachtungsgrö$\beta$en in existierende Tsunamiwarnsysteme sollte relativ leicht möglich sein, da Infrasoundsensoren sich in existierende seismische Stationen integrieren lassen. Ultralangperiodische seismische Beobachtungen von Tsunamis an Küstenstationen würden lediglich Softwareänderungen benötigen.

# Contents

# List of Figures

# List of Tables

# Chapter 1

# INTRODUCTION

## 1.1 Historical context

Over the past centuries tsunamis have been considered as one of the most devastating natural phenomenon on the world. Different geophysical events like landslides, volcanoes, meteorites can generate tsunamis. *Van Dorn* (1968) reported that nuclear explosion in the ocean could generate serious tsunamis. However, the most common cause of tsunamis is seismic activity in the oceanic area and we should notice that not all big submarine earthquakes generate tsunamis. Despite of its rare activity compared to other natural disasters (earthquakes, hurricanes and tornadoes), tsunamis remain one of the most destructive, extreme and deadliest hazards. Therefore tsunamis become the central focus of all organizations dealing with natural hazard management. Tsunamis occur more frequently in the "Ring of Fire" around the Pacific Ocean. More than 1300 events were recorded since 1974 [*Soloviev et al.* 1986] there. Tsunamis are also observed in the Atlantic Ocean, Caribbean, Black and Caspian Seas [*Nikonov* 1997, *Dotsenko et al.* 2000, *Lander et al.* 2002] and the Mediterranean Sea is known to experience about 300 tsunamis. As in the European coasts, a catastrophic earthquake and tsunami happened in 1755 which destroyed Lisbon,

Portugal supposedly to be the largest catastrophe of this kind. Additionally, the fifth large tsunami which hit Indonesia within a period of 13 years was in Andaman-Sumatra in December $26^{th}$ 2004 which generated the largest tsunami in the Indian Ocean. These events demonstrate that many places can be vulnerable to tsunami hazard. Facing these problem, tsunami scientists have developed reliable techniques for the early warning system in order to at least reduce the horrific disaster.

## 1.2 Present research and motivation

As opposed to earthquake and atmospheric sciences, tsunami science has evolved differently due to the unavailability until recently of instrumental recordings of tsunami in the open ocean and its rare and unsystematic occurrence. The only available recordings were from tide gauges which are known to only represent arrival times and possibly the character of the first wave polarity. While the basic governing equations have been known for over 150 years, the measurement of tsunamis in open ocean was only possible in the later 1990s by the National Oceanic and Atmospheric Administration's (NOAA). The number of the instrument responded to the excitation of the tsunami has increased in the last few years. At the initial stage, some of these instruments are not designed to monitor tsunamis. This allows theorecians to get some reference from the observation of a tsunami and to validate the state-of-the-art of their model in order to provide a good estimate of the water level which is very useful for the evacuation of the population in danger. Despite of the significant progress in tsunami research, the casualty caused by the last tsunami in Japan triggered a recurring question: what further steps would have been done to improve the tsunami early warning systems. Thus, this thesis introduces a relatively new method of observing tsunamis in seismic and infrasound data which could be applied in warning systems.

Therefore, this thesis is structured as follows:
In Chapter 2 we review a general information on tsunamis. Basic knowledge on the physics of tsunamis is explained as well as the technique of tsunami measurement followed by a description of existing tsunami warning systems.

In Chapter 3 we introduce the theory of interaction between solid earth, ocean and atmosphere. Here we briefly explain the translation of energy dissipated during the earthquake accompanied with the vertical displacement of the sea bottom to the ocean and the generation of tsunamis. The tsunami, in turn, transfers energy to the atmosphere and generate acoustic gravity waves. In addition, the tilting inferred by loading of ocean gravity waves in harbors is explained.

Chapter 4 describes the observations of tsunami effect in seismic and infrasound data. These two geophysical method may be used as a tsunameters.

In Chapter 5 we discuss our results about the possibility of using these new method in tsunami warning systems and ending up with a concluding remarks in Chapter 6

# Chapter 2

# GENERAL INFORMATION ON TSUNAMIS

Different places around the world have been identified in the past centuries to be potential sources of tsunami. When it comes to tsunami hazard, it is worth referring to the historical tsunami generated by the Lisbon earthquake in 1755. This tsunami has reached countries as far away as England and even propagated across the Atlantic Ocean to the Caribbean Isles [*Degg & Doornkamp* 1994]. The Lisbon tsunami was supposed to be one of the first well known tsunami which has killed thousands of people [Pacific Disaster Center report]. The city of Lisbon was severely destroyed and most of the coastal towns and villages were damaged. The intensity of the event was accurately illustrated by several painters. Seismologists tried to reconstruct the signal and estimated the magnitude of the earthquake to be 9.0 Mw (USGS).

In the 1950s the destructive oceanic waves were still a very complicated puzzle for scientists and considered as a mysterious event by the whole population who had experienced such a phenomenon. The word "tsunami" is the pronunciation of two Japanese hieroglyphs

(Figure 2.1) translated as "wave in the harbor". Even though more than 250 of such events were recorded since 1950s, no expression for this term has found in the Grand Soviet Encyclopedia [*Boris L. & Mikhail N.* 2009].


**Figure 2.1:** Japanese hieroglyphs pronounced as 'tsu nami' translated as 'wave in the harbor'

In 1963 the term "tsunami" was adopted by an international scientific conference for the general and academic use. Although tsunamis in the coastal area are influenced by the tide level at the time of impact, the former name "tidal wave" doesn't represent the phenomenon since tides are the result of gravitational influences of the moon, sun, and other planets but tsunamis are not caused by any of those. Sometimes some mass media still use the old nomenclature like "seismic sea wave" or "sea quake" and even the antique European term "seebeben" and "maremoto", but none of them reflects the actual mechanism of the event. Depending on the scale of the area, tsunamis can be distinguished as local, regional and remote (or tele) events. A local tsunami is an event in which the destructive effect is concentrated within distance not exceeding 100 km. The event is classified as regional when the destruction effect reaches a distance up to 1000 km and farther than 1000 km is called teletsunami. The damage caused by tsunami can be dangerous in the immediate vicinity of the source as well as thousands of kilometers away from the source depending on different parameters. As opposed to common sea waves, tsunamis have particular physical properties.

## 2.1 Physical characteristics of tsunamis

Tsunamis are considered as long period gravitational waves in the ocean.While propagating, not only does the subsurface layer move but also the entire height of the water column becomes involved. In general the size of teleseismic tsunami is proportional to the magnitude of the earthquake i.e. the size of the tsunami increases with the magnitude of the earthquake. However, the magnitude of the earthquake and its location alone are not enough to predict an occurrence of a tsunami. The November 2002 earthquake in the Simeulue island with a magnitude of 7.6 Ms did not generate any significant tsunami despite its location under water and the strong ground shaking generated. Conversely, the Java earthquake in 2006 with 7.2 Ms caused a remarkable tsunami. Note that both sources are on thrusting fault system. Therefore, different parameters must be involved to study and describe tsunami effects from the generation through propagation and up to the inundation phase. These phases are described in the following paragraphs.

### 2.1.1 Properties of tsunami

Tsunamis are mainly known as a deformation of the sea surface excited by any undersea events. Due to the complexity of the actual phenomenon, some simplifications are needed in order to determine the basic features of the physical process of the wave. For the case of tsunamis generated by submarine landslide, for instance, *Tinti et al.* (2001) simplified the source by considering a small-height slide which permits them to use linear theory of the wave motion related to a shallow-water model.

As for the tsunami earthquakes, the amplitude of the tsunami and the seismic moment are generally considered to be linearly dependent [*Kanamori* 1972;*Abe* 1973]. Although the nonlinear effect is considered to be negligible, the general feature of the wave obtained from

these assumptions, for both near and far fields, provides an ample understanding of the physical characteristics of the tsunami. In its simplified form, tsunami is then considered as surface gravity waves of an incompressible flat oceanic layer with a constant thickness (depth) $h$ over the rigid half space. The phase c($\omega$) and group u($\omega$) velocity of the tsunami are governed by the following equations:

$$\begin{cases} c(\omega) = \sqrt{\frac{g\ tanh[k(\omega)h]}{k(\omega)}} \\ u(\omega) = c(\omega)\Big[\frac{1}{2} + \frac{k(\omega)h}{sinh[2k(\omega)h]}\Big] \end{cases} \tag{2.1}$$

where, **g** is the acceleration of gravity (g=9.8 m/s$^2$) and **k** is the wavenumber associated with the frequency $\omega$.

The wavenumber is linked to wavelength by:

$$\lambda(\omega) = \frac{2\pi}{k(\omega)} \tag{2.2}$$

then,

$$(1)+(2) \rightarrow \begin{cases} c(\omega) = \sqrt{\frac{g\ tanh\Big[\frac{2\pi}{\lambda(\omega)}h\Big]\lambda(\omega)}{2\pi}} \\ u(\omega) = c(\omega)\Big[\frac{1}{2} + \frac{2\pi h}{\lambda(\omega) sinh\Big[\frac{2\pi}{\lambda(\omega)}h\Big]}\Big] \end{cases} \tag{2.3}$$

Equation 2.3 illustrates that tsunamis of different wavelengths travel at different speeds. Consequently ***tsunamis*** are considered to be ***dispersive waves***. While approaching the coast tsunamis slow down, because of depth effect, and amplitudes increase. Under these conditions, tsunamis exhibit not only frequency dispersion but also amplitude dispersion.

Variations of phase and group velocities as a function of period are illustrated in Figure 2.2. In order to generate a tsunami, a submarine earthquake must move vertically a considerable area. For the case of Sumatra 2004, for instance, the fault width across E-W

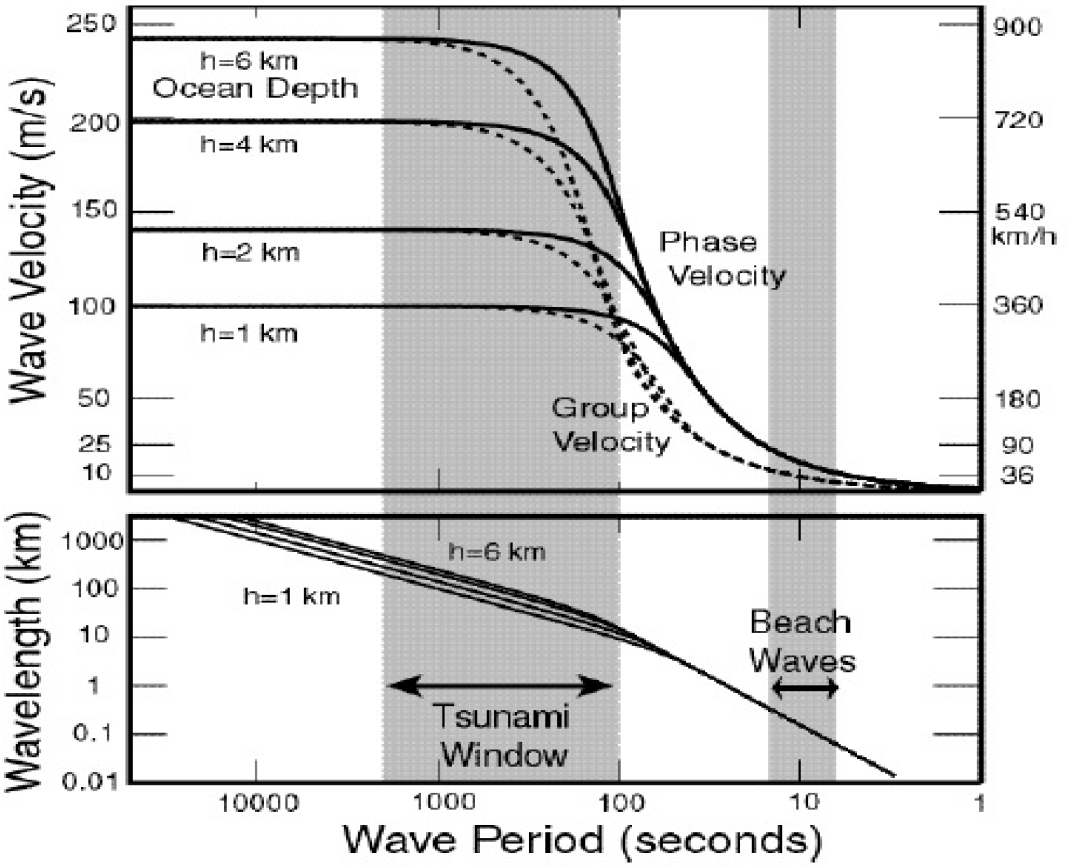


**Figure 2.2:** (top) Phase and group velocity of tsunamis on a flat earth covered by oceans. (Bottom) Wavelength as a function of wave period *(Source: Steven W., Encyclopedia of Physical Science and Technology)*

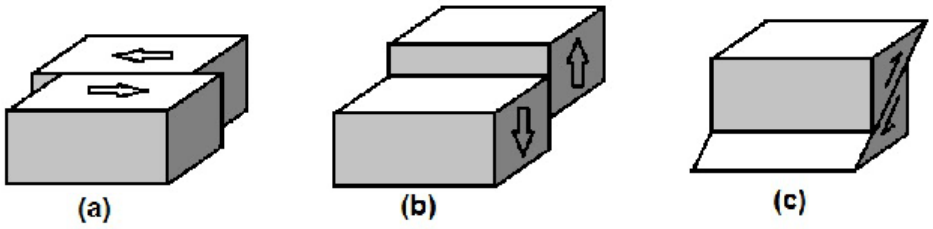


**Figure 2.3:** Faults system. (a) Strike-slip, (b) Dip-slip, (c) Thrust-dip

profile is estimated to be 120 km [*Meltzner et al.* 2006]. Assuming that the deformation at sea bottom is translated to the sea surface, we could determine the dimension of the displaced sea floor by measuring the wavelength of the observed wave at the sea surface. Figure 2.2 (bottom panel) shows that the wavelength of a tsunami can be as large as 500 km so does the size of the source area.

For a very long wavelength ($kh \rightarrow 0$) the phase velocity is c($\omega$)=u($\omega$)=$\sqrt{gh}$. This demonstrates the absence of dispersion in the very long wavelength represented by flat curve on the left hand side in Figure 2.2 (top panel). When it comes to the short wavelength ($kh \rightarrow \infty$) phase velocity becomes c($\omega$)=2u($\omega$)=$\sqrt{\frac{g\lambda(\omega)}{2\pi}}$ and waves propagate with dispersion.

### 2.1.2 Tsunami source

Tsunamis are mainly generated by three geophysical events:
Volcanic eruption can cause tsunamis. The case of the 1883 Krakatoa event is one of the relevant examples. There was a significant damage and considerable loss of lives but the mechanism which triggered the tsunamis was not very clear whether by the explosion [*Yokoyama* 1981; 1987], by caldera collapse [*Verbeek* 1885; *Francis* 1985; *Sigurdsson et al.* 1991] or by a pyroclastic flow [*Self & Rampino* 1981].

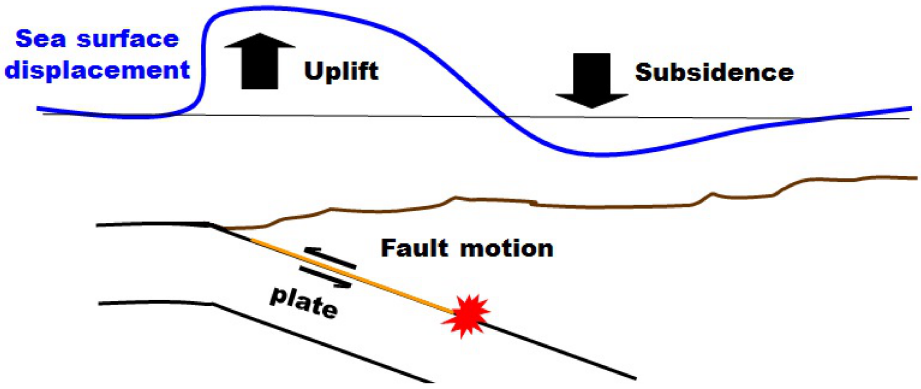


**Figure 2.4:** Tsunami nucleation by a subducting plate boundary. Rupture zone is shown by orange line while red star denotes the hypocenter.

Submarine landslides like the one in Aitape, Papua New Guinea in 1998 can a generate local tsunami which swept out 25 km along the coast with maximum water wave of 15 m above sea level [*Watts P. et al.* 2001].

But the most frequent sources of large tsunamis are submarine earthquakes with a moment magnitude stronger than 7.0 and a focal depth less than 50 km. The hypocenter is commonly on the rupture along fault lines where two plates are moving against each other. There are three main faulting systems: strike-slip system, dip-slip system and thrusting fault system (Figure 2.3).

Normally, a tsunami will be formed only if an earthquake causes vertical displacement of the sea floor and the source area is three times greater than the ocean depth at the source. As an example, the 7.9 Mw earthquake in 1906, located at 3.2 km west of San Francisco (37.75 °N, 122.55 °W) in the Pacific Ocean with a depth of only 8km [USGS], did not generate a tsunami because the motion on the fault was strike-slip (Figure 2.3a) motion with no vertical displacement. Tsunamis only occur if the earthquake source is dip-slip or thrust

type(Figure 2.3b, c). Because of this, most tsunamis are generated by earthquakes that occur near subduction boundaries of plates, usually along oceanic trenches.

Due to a driving force of plate tectonics, two plates converge and one slides beneath the other in a subduction zone. The average speed of this displacement is in the order of centimeters per year. The main thrust fault is locked during the interseismic time period (Figure 2.4). The accumulation of stress on the inter-plate contact in a subducting lithosphere is associated with crustal deformation usually pronounced by the bending of the slab.

A none strike-slip earthquake results in a sudden vertical displacement of the ocean bottom [*Bilham et al.* 2005, *Ji* 2005, *Fine et al.* 2005, *Song et al.* 2005 and *Heki et al.* 2006]. Because the ocean is an incompressible and non viscous fluid, the upward movement of the sea floor causes a vertical deformation of the sea surface. The higher the vertical displacement, the bigger the tsunami amplitude at source becomes . After the generation of the tsunami, the gravity force tends to restore equilibrium causing propagation of the waves known as "tsunami" which can travel thousands of kilometers.

### 2.1.3 Tsunami propagation

Tsunamis can propagate over a very long distance with a speed greater than typical ocean waves generated by wind. The energy which generates ocean wind waves decreases considerably with depth (Figure 2.5). This is the reason why wind waves diminish easily because there is not enough energy to push the entire body of the water. However, tsunami is caused by the up-lifting of the ocean floor and the energy released during this deformation pushes the entire water column from the ocean floor. Thus, a tsunami travels as a big wall

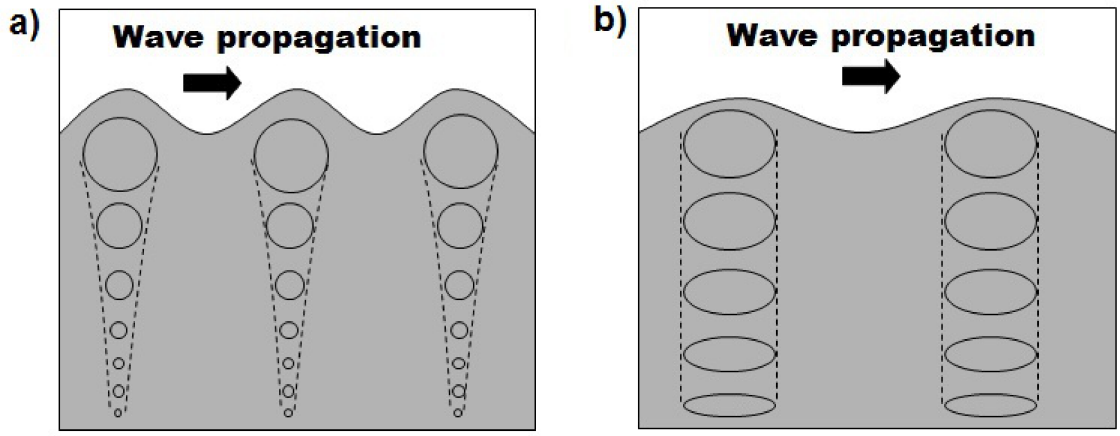


**Figure 2.5:** Anatomy of the wave: (a) Wind waves with a circular particle motion. (b) Tsunamis with elliptic particle motion

of water towards the shore at relatively constant speeds from sea bottom to surface and particles move in an elliptical trajectory.

### 2.1.4 Tsunami inundation

After traveling through the ocean, tsunamis move from deep to shallow water. In general, ocean waves break far offshore but this condition varies with the type of the wave. Typical wind waves break near the shore. Waves generated by large explosions or small asteroids in the ocean break at the continental shelf. However, typical waves from undersea earthquake don't break. This is known as "Van Dorn Effect".

Towards the shore, water depth decreases and tsunamis slow down. Coming from the deep ocean with a speed of a jet airplane ($\approx 800 km/h$), the tsunami moves a large amount of water which will pile up on the continental shelf. Thus, while moving toward the shore the wave amplitude grows up to a large swell because the shelf is small compared to the distance between crests. This amplification of the wave is given by the shoaling factor, S,

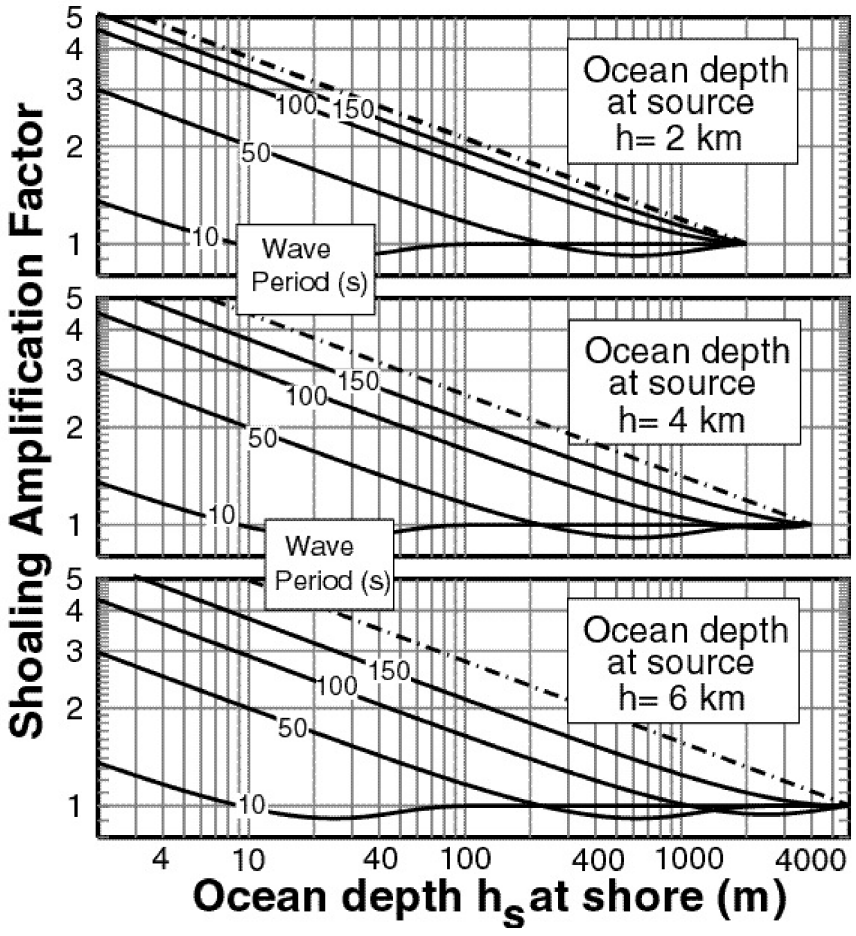


**Figure 2.6:** Shoaling amplification factor for ocean waves of various frequencies and source depth *(Source: Encyclopedia of Physical Science and Technology)*

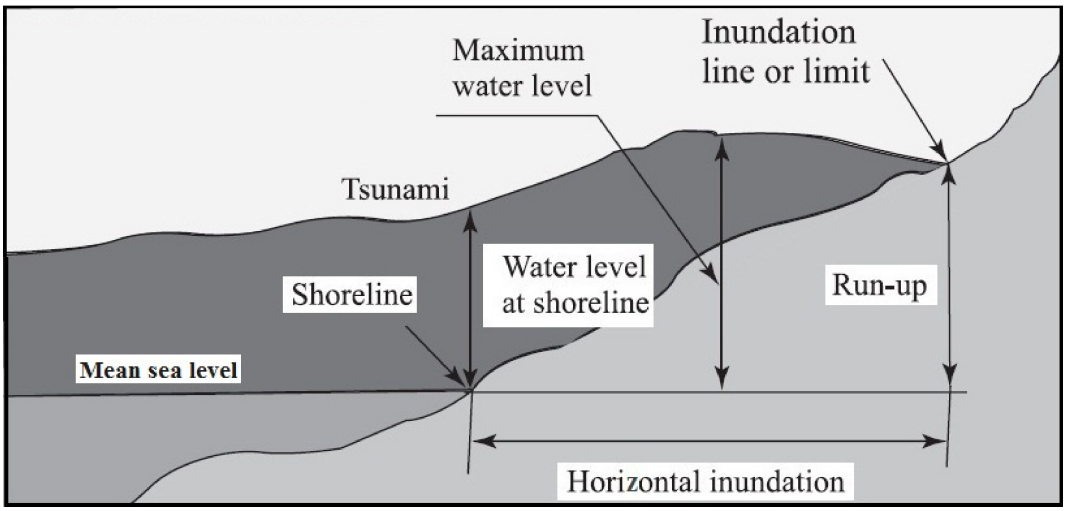


**Figure 2.7:** Tsunami cross section view. Adapted from UNESCO-IOC (Tsunami glossary)

which is a ratio between the amplitude of the wave at shore and the amplitude at source. Figure 2.6 shows the amplification on the wave height as function of depth.

$$S = \frac{a_{final}}{a_{initial}} = \sqrt{\frac{u_{initial}}{u_{final}}} \text{ (where a is the amplitude,u the group velocity)} \tag{2.4}$$

The amplification of the typical wind waves (period 10 s) is smaller than the very long period tsunami (period $>$ 100 s).

In reality, the wave height increases until it becomes instable. Then, tsunami will slosh up the beach and inundate over low-lying areas. The vertical elevation above the mean sea level reached by a tsunami in coastal areas is called ”run-up” (Figure 2.7). The geomorphology of the beach plays an important role on the seriousness of the damage caused the flooding. When tsunami propagates into a narrowing embayment,it will be funneled into one direction and the direct wave force becomes more severe. Alternatively, a considerable energy of the tsunami is reflected back due to a presence of continental margins and large part of the tsunami impact is attenuated.

## 2.2 Tsunami warning system

### 2.2.1 Tsunami registration

In general, tsunamis are supposedly generated by submarine earthquakes. With the help of the global or with local seismographic networks, seismologists are able to locate the earthquake and determine its magnitude. Knowing the origin time of the earthquake, one can estimate the probable arrival time of tsunami at shore. Besides, tide gauge has been used to register the sea level anomalies in the coastal area since in the 1900s and can be used to measure the passage of tsunami at shore. However, neither earthquake parameters nor coastal tide gauges provide data that allow accurate prediction of tsunami at different places. Firstly because strong submarine earthquake is not logically accompanied by a large tsunami and sometimes moderate earthquake can generate destructive waves to the coast. Secondly tide gauge provides the direct height of the sea at a particular coastal location but the tsunami is significantly altered by local bathymetry and harbor shapes. This might limit the use of these two techniques for tsunami warning system.

### 2.2.2 Size of a tsunamis

Even before the existence of instrumental record for tsunamis several attempts were made to quantify tsunamis. The first tsunami magnitude scale was known as "Imamura-Ida scale" $m$ which is the log base 2 of the maximum run-up height in meters [*Ida et al.*, 1967]. This scale was extended by *Hatori, (1979)* by including far-field tsunami data and the effect of distance. He constructed a diagram in log-log scale. This diagram shows a decay $R^{-1/2}$ of tsunami height with distance which is theoretically predicted for non-dispersive waves traveling a long distance [*Comer 1980*] .*Soloviev (1970)*, changed the Imamura-Iida scale and came up with a new intensity scale. In his formula, he used the mean tsunami

height and added a factor $\sqrt{2}$ in the logarithm. For the tsunami magnitude $M_t$, *Abe (1988)* defined a quantity similar to that used since the 1960s in seismology for the measurement of the surface wave earthquake magnitude (see equation 2.5):

$$M_t = a \log H + b \log \Delta + D \tag{2.5}$$

where H (m) is the maximum single (crest or trough) amplitude of tsunami; $\Delta$ (Km) is the distance epicenter-tide gauge; $a$, $b$ and $D$ are constants.

### 2.2.3 Tsunami warning system

Until recently all ideas of monitoring the evolution of waves in open ocean like tsunamis were based exclusively on coastal measurement. This idea was criticized by *Jacques and Soloviev* (1971) as they introduced a technique of measuring waves in the deep ocean to avoid any influence of the coast. However, the first prototype of such an instrument came only out 24 years later.

It is composed of a very sensitive pressure gauge placed on the ocean floor to detect the pressure changes when a tsunami passed over the instrument. Because of its functionality the system has given the name **"tsunameter"** and the first-generation of tsunameters were named DART (Deep-ocean Assessment and Reporting of Tsunamis Figure 2.8). The DART is used at NOAA/PMEL, USA and JAMSTEC, Japan for early warning system. Figure 2.9 shows the different location of DARTs deployed by several countries. Note that the data of these stations are available in real time on the internet and open for public.

Compared to coastal measurements, this system brings important advantage because they are free from the nonlinear process of shoaling and run-up at continental and island shores

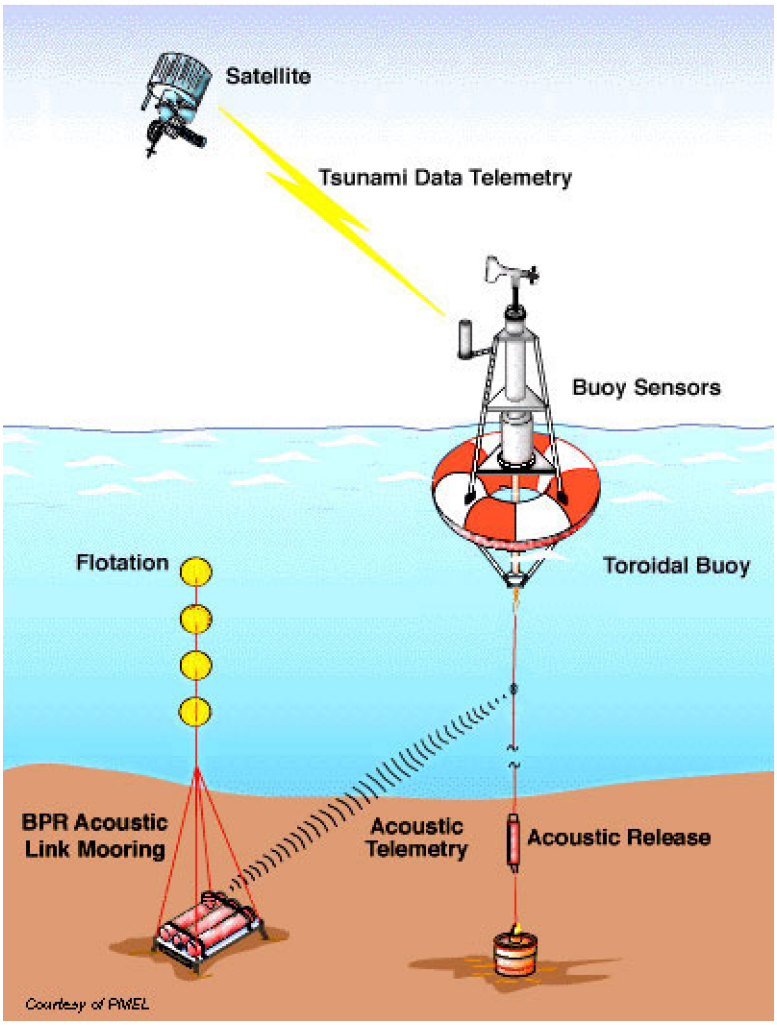


**Figure 2.8:** Prototype of Deep-ocean Assessment and Reporting of Tsunamis (DART) *(Source: http://www.ndbc.noaa.gov/)*

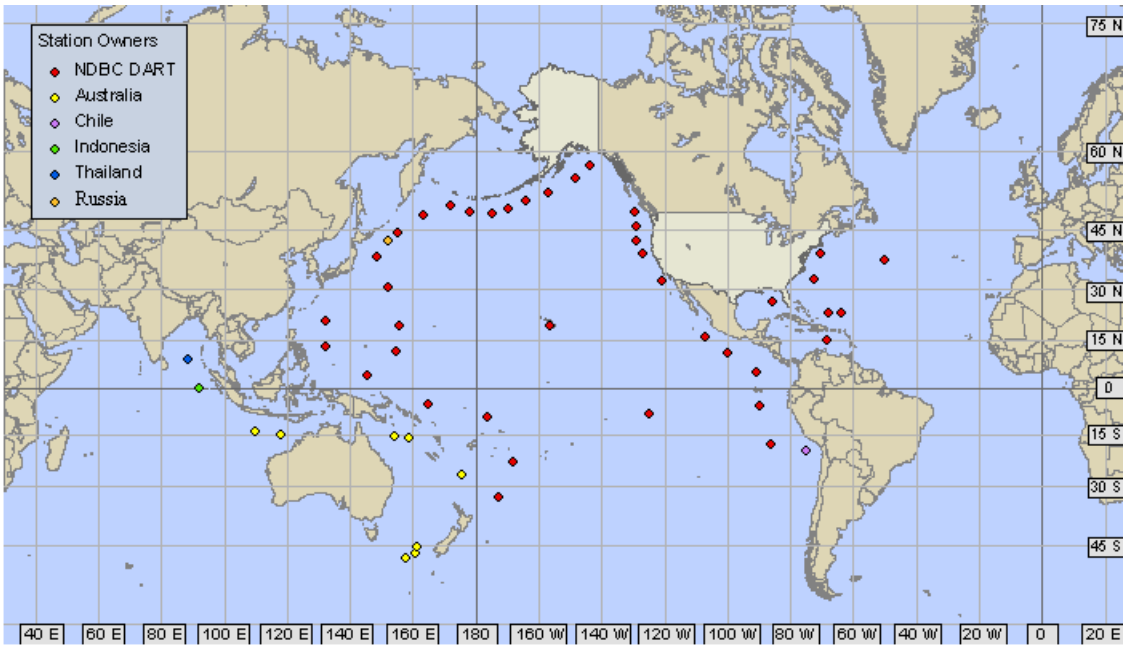


**Figure 2.9:** Deep-ocean Assessment and Reporting of Tsunamis Station Locations *(source: NOAA)*

[*Okal et al.* 2007]. However the availability of such kind of station is very limited because of their cost and high maintenance requirements. As an example, the cable connecting the sensor to the buoy is sometimes mixed up with fisher boats and gets destroyed. There is also a problem of acoustic interference with ships and biological noise [*Gonzalez et al.* 1998]. Figure 2.10 shows an example of different ambient noise recorded in Emerald Basin during an experiment conducted by *Osler et al.* (1998).

For any natural disaster, it is important to create an automated system of continuous observation in order to provide timely and reliable warning. In the history of tsunami warning, the system evolves gradually with the impact of destructive events and the progress of technology. Thomas Jaggar, founder of the Hawaiian Volcano Observatory (HVO), was the first person who issued a tsunami warning. He warned people of the possibility of big ocean wave in Hilo, Hawaii after the 1923 Kamchatka earthquake but very few people believed him. The tsunami warning became official only after the 1946 tsunami in the Aleutian

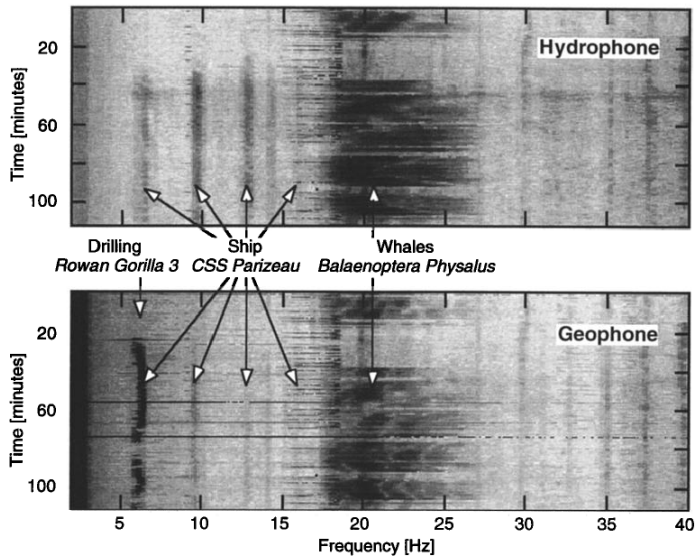


**Figure 2.10:** Oceanic ambient noise recorded by hydrophone and horizontal geophone. The time refers to the temporal position of the spectral frames in the sonogram. *(Osler et al., (1998)*

Islands. The center at Hawaii was established to watch the possibility of tsunami at the west coast of the US and Alaska. In 1960 the Chilean earthquake generated a tsunami and places as far away as Japan were devastated. This event increased the efforts by the center and cooperation was established between PTWS, USA and JMA, Japan [NOOA/PTWS].

The devastating Sumatra event in December 2004 showed that the role of the PTWC was limited. In 2005 the German and Indonesian governments agreed to coordinate efforts to build up an effective tsunami warning system in the Indian Ocean. The German Indonesian Tsunami Early Warning System (GITEWS) was established and the new system uses different variety of sensors like seismometers, GPS instruments, tide gauges and GPS-buoys as well as ocean bottom pressure sensors Figure 2.11. Because Indonesia is located along subduction zones the principal sources of tsunami in this region are local submarine earthquakes. Thus, the project aims to provide new procedures for the fast and reliable determination of strong earthquakes parameters by integrating available data from different sensors.

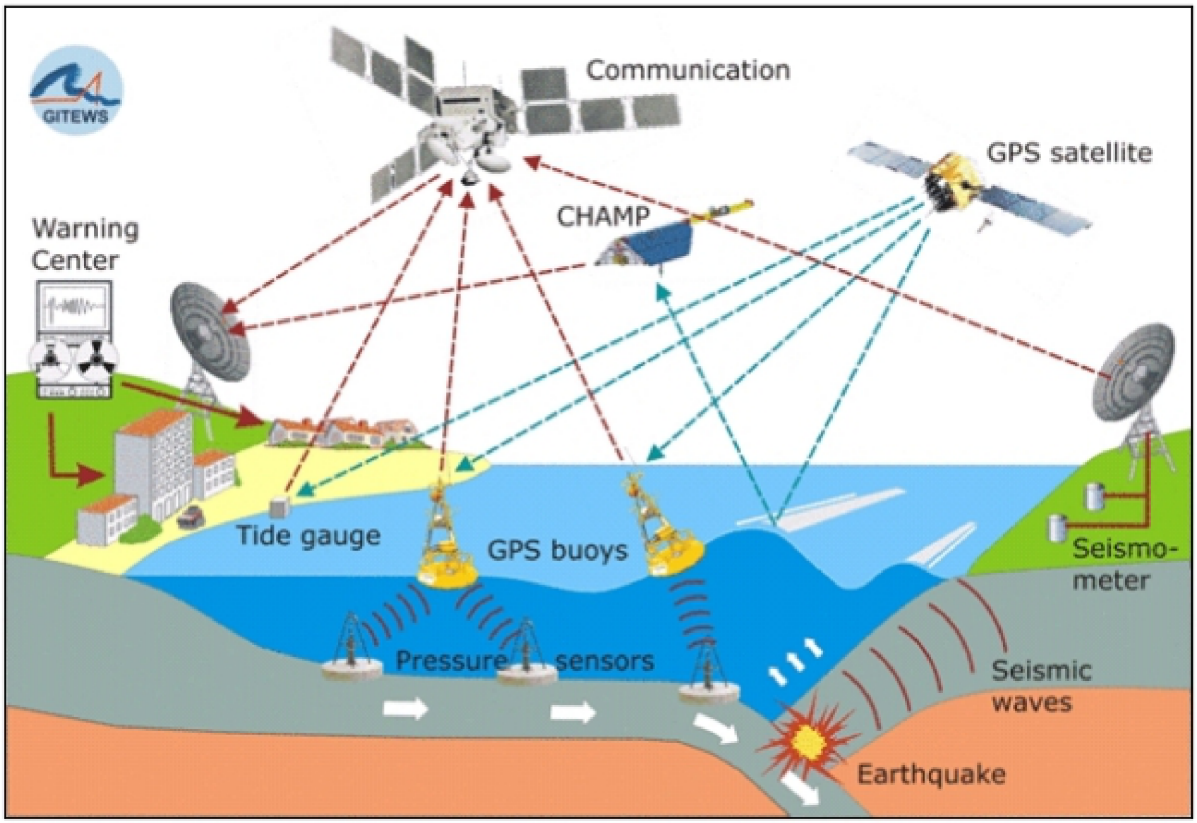


**Figure 2.11:** Different components of the German Indonesian Tsunami Early Warning System (GITEWS) *(Source: http://www.gitews.org)*

# Chapter 3

# Theory of Earth-Ocean-Atmosphere coupling

Frequently people assume for simplicity that the solid earth is decoupled from its atmosphere. Seismologists, for instance, consider the Earth's solid surface as a free surface whereas atmospheric scientists assume it as rigid surface. This is reasonably acceptable if we consider the high density contrast at the surface boundary. However, coupling does exist between these two media and provides many benefits which may include also the analysis of mechanisms involved in tsunami generation. On one hand the solid earth is excited continuously by its atmosphere with acceleration amplitude of about 0.3-0.5 nanogals in the fundamental modes between 2 and 7 mHz [*Nishida et al.* 2000; *Rhie et al.* 2004]. The atmosphere also vibrates due to an earthquake [*Lognonne et al.* 1998].

For the case of tsunamis, the water layer is excited by the dynamic seabed displacement caused by seismic faulting and transfers the energy to the sea surface. In turn, it generates an impulsive signal into the atmosphere and waves can propagate to a very long distance. Conversely, perturbation in the atmosphere generates a signal in the solid earth. *Harkrider*

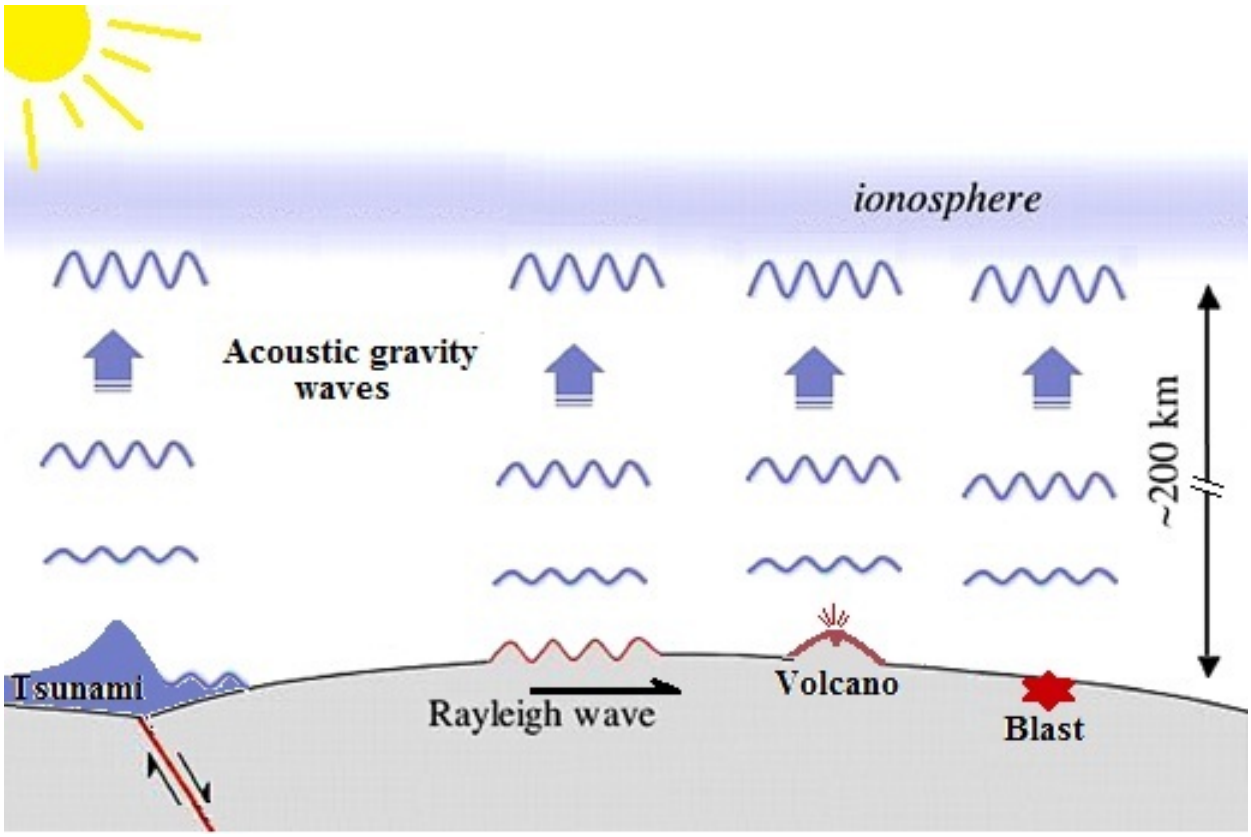


**Figure 3.1:** Schematic diagram showing the solid earth atmosphere coupling, adapted from *Calais*, (1998). Vertical displacement of Earth's surface excites the entire atmosphere up to the ionosphere, and propagate laterally [*Artru et al. 2005.*]

*and Press* (1967) reported that the energy produced by an explosion in the atmosphere can be transferred to the ocean in an efficient manner and can trigger long period seismic waves in the solid earth [see also *Widmer & Zurn*, 1992]. However the coupling is generally greater over continents than over oceans and the difference may reach the equivalent of 0.5 magnitude units [*Harkrider et al.* 1973]. Figure 3.1 illustrates different phenomena which interact with the atmosphere. As mentioned in the previous chapter, the main source of a tsunamis is an underwater earthquake. In this chapter, the first two sections will review the state-of-the-art regarding interaction between solid earth, ocean and atmosphere. Then we will emphasize the necessary condition for an earthquake to generate a tsunami and the last section will discuss the effect of tilting on seismometers.

## 3.1 Seabed-ocean coupling

In spite of the progress of science and technology, there are still many open questions in tsunami research. Since the last few decades theoretical-numerical techniques have become available to make the computation of tsunamis possible. This has much improved the understanding of the physical mechanism involved in tsunami generation. Tsunami modelers need to have detailed knowledge about the source generation which is one of the required initial conditions before the propagation of the wave in deep ocean and its run-up can be calculated [*Nosov* 1998].

For submarine earthquake an accurate prediction of tsunami heights depends on having a good estimation of the initial sea surface disturbance caused by a submarine earthquake. This mechanism is basically indicated as the coupling between seabed and the ocean.

In the past studies, different theories have been proposed. Initially *Kajiura* (1963) formu-

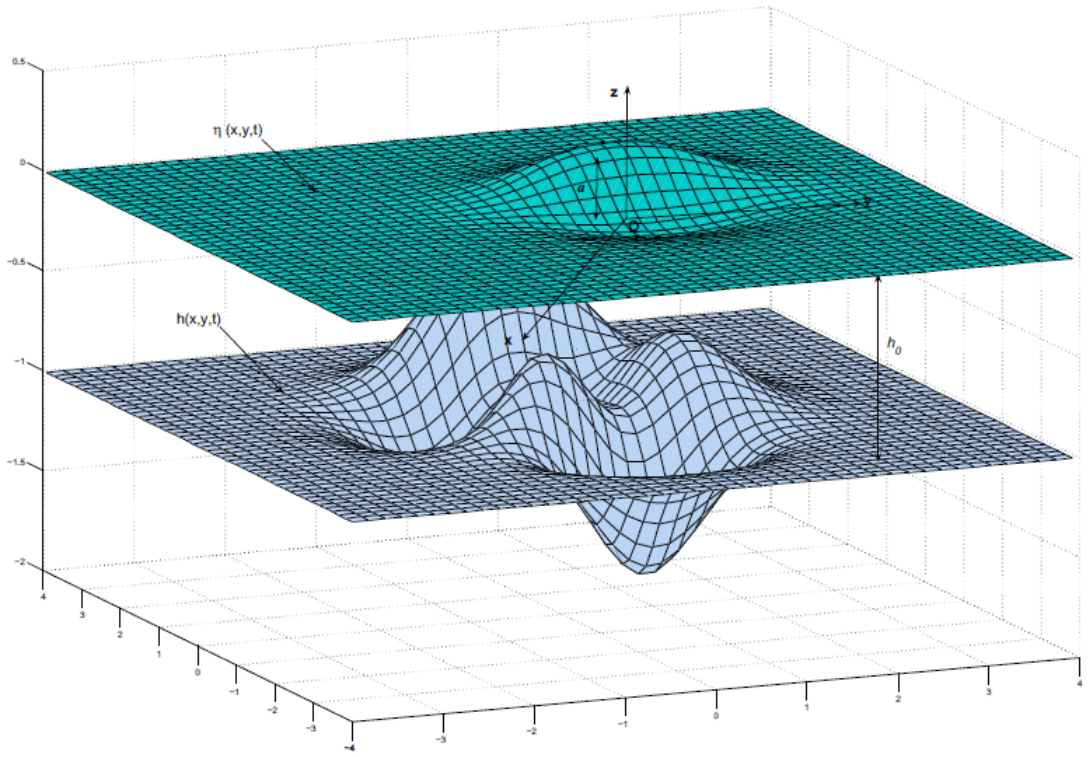


**Figure 3.2:** Physical interaction between seabed-ocean with horizontal displacement. Light blue represents the sea-bed excited vertically accompanied by horizontal displacement while the top layer (blue) shows the the sea-surface. The quantity $a$ is the corresponding response of the sea surface to the excitation from bottom and $h_0$ indicates the ocean depth. $h(x, y, t)$ and $\eta(x, y, t)$ indicate an arbitrary point at the sea bottom an on the sea surface respectively [*Dutykh et al.*, 2011].

lated that the water wave generation is caused by seabed deformation. *Kajiura*, (1970) discussed the energy exchange between seabed and the water. To study the tsunami generation *Yamashita and Sato*, (1974) evaluated effects of fault parameters on tsunami amplitude. In these studies only the static contribution of the seabed displacement is considered with a strong coupling between seabed and ocean. To overcome this problem *Omachi et al.* (2001) and *Wang et al.* (2004) demonstrate that seabed-wave coupling is weak. Consequently, the motion of sea water is influenced by that of the seabed, but the motion of the seabed can be assumed not to be influenced by that of the seawater. More recently, *Dutykh et al.* (2011) discussed the effect of the horizontal coseismic displacement on the tsunami generation, see Figure 3.2. Horizontal motion of the sea bottom is not very effective from the stand point of tsunami generation. When the sea bottom is inclined, due to the presence of topography, the effect can be assumed to be similar to the case of landslide. For the case of landslides the interaction seabed-ocean depends on the volume of sliding body. Only limited part of the potential energy released by the landslide is transferred to wave energy . The length of the landslide influences both the wavelength and the surface elevation while the thickness and acceleration of the landslide as well as the wave speed determine the surface elevation [*Harbitz et al.* 2006].

## 3.2 Earth-Atmosphere coupling

### 3.2.1 Solid Earth-Atmosphere coupling

Air-ground coupling phenomena have been among the routine observations of many researchers in geoscience. *Yuen et al.* (1969) and *Weaver et al.* (1969) reported atmospheric disturbances following a large earthquake. Several scientists have demonstrated that shallow events in the solid Earth can produce impulsive vertical displacements of the surface that changes the pressure in the atmosphere. *Afraimovich et al.* (2001) investigated the

acoustic shock waves in the atmosphere induced by earthquakes. *Calais, et al.*(1997) and *Fitzgerald* (1996) demonstrated that perturbations caused by mine blasts reach the ionospheric layer. *Blanc* (1985) and *Ducic et al.* (2003) studied an ionospheric impulsive anomaly associated with Rayleigh waves. Using normal modes approach used in seismology, *Watada* (1995) also mentioned that resonant coupling occurs between the solid Earth and the atmosphere when their modes overlap in frequency-wavenumber domain. Some observations of long period surface waves will be discussed later.

### 3.2.2 Ocean-Atmosphere coupling

Similarly to shallow earthquakes, ocean swelling also can be source of excitation of the atmosphere. However, the interaction of ocean waves with the atmosphere is not linear [*Arendt and Fritts 2000; Garces et al. 2002*] due to the temporal and spatial variation in the structure of the atmosphere [*Kulichkov et al. 2004*]. Since 1996, permanent observation of the atmosphere becomes possible thanks to the global infrasound network of the International Monitoring System (IMS) for the compliance of the Comprehensive Nuclear-Test-Ban Treaty (CTBT). Continuous monitoring of infrasonic waves at different IMS stations reveals the existence of atmospheric-ocean coupling. *Le Pichon et al.* (2004) and *Willis et al.* (2004), for instance, detected a dominant source of infrasonic waves caused by ocean swells. They concluded that the infrasonic waves generated by ocean surface waves are characterized by the quasi-permanent infrasonic spectral peak of 0.2 Hz. To explain the infrasonic signal called "microbaroms", which is generated by standing water waves associated with marine storms, *Posmentier* (1967) used the theory of the origin of microseisms developed by *Longuet-Higgins* (1950). This theory is based on the oscillations of the center of gravity of the air above the ocean surface on which the standing waves appear: *Posmentier* (1967) considers a model of incompressible air of density $\rho_0$ bounded below by a surface perturbed by two sinusoidal wave trains identical in period $T$, wave-

length $\lambda_0$, and amplitude $a$, but traveling in opposite directions . This movement creates a standing wave which excites the air above and the oscillation of the center of gravity of the vertical column of the air is similar to that of a pendulum (Figure 3.3). Therefore, the standing wave in the water produces a vertical propagating acoustic wave in the air above.

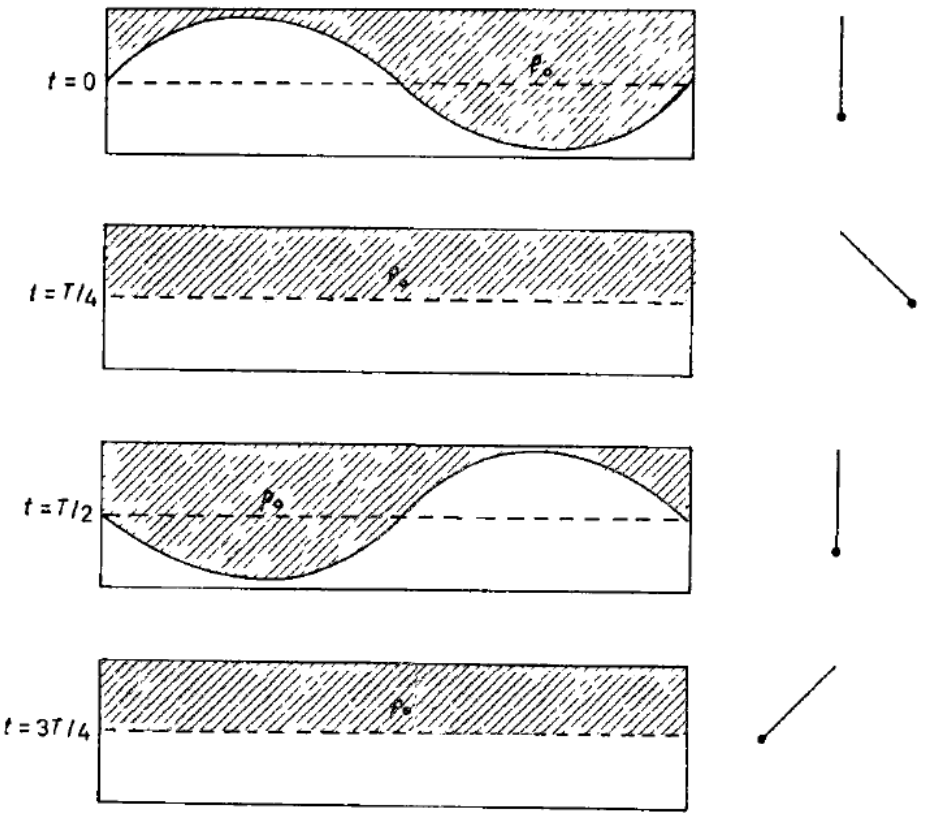


**Figure 3.3:** Comparison of the air (hatched area) above a standing water wave (left), with pendulum (right), both of period $T$. The height of the centre of gravity of a vertical column of the air oscillates similarly to the pendulum (right hand side). [*Posmentier* 1967].

The governing equation of the standing wave is:

$$\eta = 2a\,\cos(k_0 x)\,\cos(\omega t),\ \text{where } \omega = \frac{2\pi}{T} \text{ and } k_0 = \frac{2\pi}{\lambda_0} \text{ and } \eta \text{ is the surface height.} \quad (3.1)$$

The height of the center of gravity of the air in the hatched area is given by:

$$\epsilon = \frac{H}{2} - \frac{a^2}{H} cos^2(\omega t), \text{ where } H \text{ is the maximum water height.} \tag{3.2}$$

Using equation (3.1) and (3.2) and considering Newton's second law, the average pressure perturbation becomes:

$$\overline{p} = -2\rho_0 a^2 \omega^2 \cos 2\omega t \tag{3.3}$$

Equation 3.3 verifies that the centre of gravity coupling mechanism generates "micro-baroms" with one-half the ocean wave period.

Considering the above mentioned mechanism of the ocean-atmosphere coupling, *Daniel (1952)* attributed these atmospheric oscillations to a piston-like action of the ocean wave. Based upon this assumption, the mechanism of sound generated to the atmosphere would seems to be the result of the motion of the standing waves, supposedly to be similar to the motion of a big piston, set up by two superposed wave trains. In this matter, the target is to find the acoustic field due to small areas affected by equation 3.1 the standing wave discussed above, and by applying equation 3.2 to a single progressive wave trains. The results will be used to study the acoustic fields of the ocean whose surface is moving in randomly related patches of standing waves(see equation 3.1), and the ocean whose surface is moving in randomly related patches of progressive wave trains(see equation 3.2). We shall refer to the first as center of gravity coupling and the latter as off-resonant coupling.

For plane acoustic waves, the amplitude of the perturbation pressure is $\rho cv$, where $\rho$, $c$, $v$ are air density, acoustic velocity and vertical particle velocity, respectively. For hemispherical waves radiating outward from a piston of small area $S$ and maximum velocity $v$, the pressure amplitude will be, at large distances, $\rho cvkS/2\pi r$, where $k$ is the acoustic wave

number, and $r$ is distance from the source. The ratio of the latter pressure to the former is $kS/2\pi r$. If we multiply equation 3.3 by this ratio, the pressure perturbation due to a patch of standing waves has amplitude:

$$p = \frac{\rho a^2 v^2 K S}{\pi r} \tag{3.4}$$

Assuming that the patches are more or less coherent over a distance proportional to $n$ wavelengths $\lambda_0$ , then the contribution per unit area of generating surface to the square of the net pressure will be:

$$d(p^2) = \left( \frac{\rho a^2 v^2 K (n\lambda_0)^2}{\pi r} \right)^2 \tag{3.5}$$

The following assumptions can be applied to equation 3.4 and 3.5: perturbations of pressure, density, etc. are all small compared to their respective ambient values; the distance from source is larger than one acoustic wavelength; the size of the 'patches' is smaller than one acoustic wavelength; signals of one frequency whose phases are randomly related add incoherently,i.e. in power or in the square of the amplitudes.

In conclusion, the theory explains that the centre of gravity coupling mechanism will generate microbaroms if the ocean surface is affected by patches of standing waves. Detailed analysis of this mechanism has been demonstrated by *Posmentier* (1967).

## 3.3 Theoretical analysis of tsunami generation

### 3.3.1 Tsunami gravity wave

Consider a fluid bounded above by a free surface and below by a solid boundary and unbounded in the direction of propagation. Initially the fluid is at rest with the free surface and solid boundary defined by z=0 and z=-d, respectively (Figure: 3.4). For the case of

a tsunami, sea water is excited by a submarine earthquake and changes its equilibrium status which it strives to restore by its own gravity. Thus, the tsunami is assumed to be a gravity wave and Euler's equation will be written as:

$$\frac{D\boldsymbol{V}}{Dt} = -\boldsymbol{g} - \frac{1}{\rho}\boldsymbol{\nabla} p \tag{3.6}$$

where $\mathbf{V}$ is the velocity vector (whose $x$ and $z$ components are $u$ and $w$, respectively), $\mathbf{g}$ is the gravitational acceleration, $\rho$ and $p$ are water density and pressure, respectively and

$$\frac{D\boldsymbol{V}}{Dt} = \frac{\partial \boldsymbol{V}}{\partial t} + \boldsymbol{V}\boldsymbol{\nabla}\boldsymbol{V}, \text{a total derivative}$$

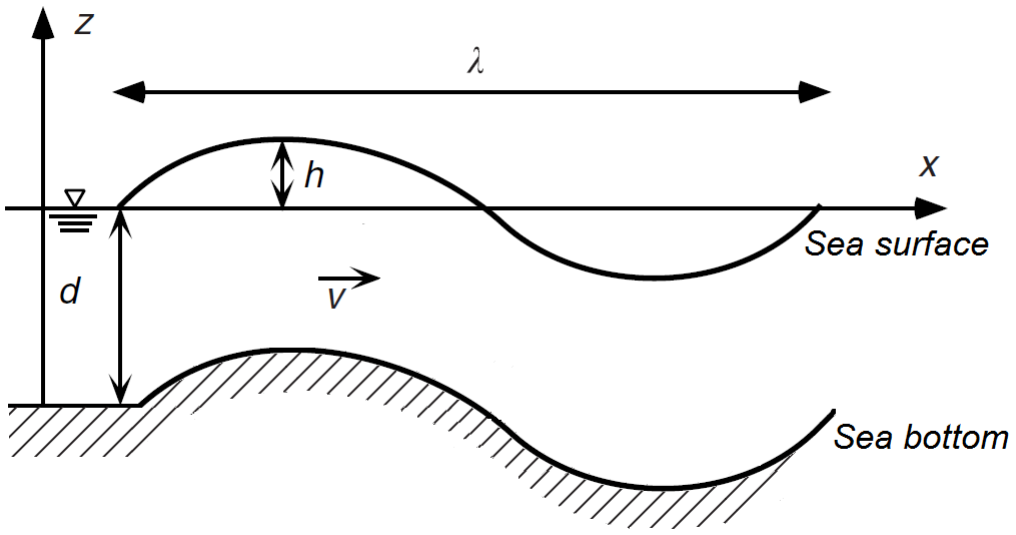


**Figure 3.4:** Ocean bottom and water surface displacement and coordinate system of tsunami (not to scale).

For a tsunami, the wavelength $\lambda$ (size of fault area) is much larger than the ocean depth $d$ ($\lambda \gg d$) so the vertical acceleration of water is negligible compared to gravity. Therefore the horizontal motion of tsunami is uniform from bottom to surface. The horizontal component

(on x axis) of equation 3.6 becomes:

$$\frac{D\boldsymbol{V}}{Dt} = \frac{\partial u}{\partial t} + u\frac{\partial u}{\partial x} \approx \frac{\partial u}{\partial t},$$

Because the nonlinear advective term is usually small for tsunami and can be therefore ignored. Thus the equation of motion can be written as:

$$\frac{\partial u}{\partial t} = -g\frac{\partial h}{\partial x} \tag{3.7}$$

In the deep ocean the amplitude of the tsunami is small compared to the water depth ($h \ll d$ ). The conservation of mass becomes:

$$\frac{\partial h}{\partial t} = -\frac{\partial (du)}{\partial x} \tag{3.8}$$

From equations 3.7 and 3.8 and considering that water depth is constant, the wave equation is given by:

$$\frac{\partial^2 h}{\partial t^2} = c^2\frac{\partial^2 h}{\partial x^2} \text{ where } c = \sqrt{gd} \tag{3.9}$$

The velocity is then determined only by the water depth.

### 3.3.2 Theory of tsunami generation

Analytically, the free surface elevation $h$ of a tsunami can be represented as a gravity wave which one wave component is given by $h$ (function of horizontal position x and time t):

$$h = a\cos(kx - wt) \tag{3.10}$$

where $a$ is amplitude, $k$ wave number and $\omega$ is angular frequency.

Considering a water depth $d$, the phase velocity is given by the following equation:

$$c = \frac{\omega}{k} = \left(\frac{g}{k}\tanh(kd)\right)^{1/2} = \left(\frac{g\lambda}{2\pi}\tanh\left(\frac{2\pi d}{\lambda}\right)\right)^{1/2} \tag{3.11}$$

as discussed before, in the case of tsunami, the water depth is much smaller than the wavelength ($d \ll \lambda$). Therefore, we can approximate $\tanh(2\pi d/\lambda) \approx 2\pi d/\lambda, \sinh(2\pi d/\lambda) \approx 2\pi d/\lambda, \cosh(\mathrm{k(z+d)}) \approx \cosh(\mathrm{kd}) \approx 1$. Then 3.11 goes to 3.9.

At an arbitrary height $z$ (the seabed is at $z = -d$) the horizontal and vertical particle velocities can be written as follows:

$$\begin{cases} u = a\omega\dfrac{\cosh(k(z+d))}{\sinh(kd)}\cos(kx-\omega t) & (3.12) \\ w = a\omega\dfrac{\sinh(k(z+d))}{\sinh(kd)}\sin(kx-\omega t) & (3.13) \end{cases}$$

under the same assumption mentioned previously, the velocity ratio of equation (3.12) to equation (3.13) is

$$\mid w \mid / \mid u \mid = 2\pi d/\lambda \tag{3.14}$$

This quantity is very small ($\frac{d}{\lambda} \ll 1$) and indicates that for the case of tsunami, the particle moves almost horizontally.

To get the analytical solutions of the gravity waves generated by any type of sources, *Kajiura* (1963) investigated the tsunami problem and introduced the Green′s functions for calculating sea-floor displacement ($\xi$) and the Green′s functions for calculating wave elevation at the sea surface ($\eta$). He showed that the initial condition given at the ocean

bottom and at the water surface differ by factor of 1/cosh(kd) (equation 3.15).

$$\eta = \xi * \left( \frac{1}{cosh(kd)} \right) = \xi * \left( \frac{1}{cosh(2\pi d/\lambda)} \right) \tag{3.15}$$

Equation 3.15 shows that when the wavelength $\lambda \sim 2d$ then cosh(kd) $\approx$ exp(kd) and consequently $\eta \ll \xi$. However, when $\lambda \gg d$ then cosh $\approx 1$. Therefore, it is theoretically proven that the sea surface just mirrors the bottom deformation if the wavelength (horizontal size of the tsunami at source) of ocean bottom deformation is much larger than the water depth.

*Kajiura* (1970) examined the energy exchange between the solid earth and ocean water for tsunami generated by bottom deformation with finite rise time. He showed that the efficiency of tsunami generation, defined as a ratio of dynamic tsunami energy to static energy, becomes nearly unity if the duration is short compared to time required for tsunami to travel through the source area.

## 3.4 The response of seismometer to tilt

It has been known that horizontal seismometers are sensitive not only to translation motion but also to tilt [*Simon et al.* 1967; *Gladwin et al.* 1987]. This is because a tilt motion generates a gravitational force which is equivalent to an inertial force due to a translational acceleration of the ground [*Rodgers* 1968]. On a very long period domain, broadband seismometer responds positively not only to the horizontal tilt motion but to the vertical translation motion as well but the second one has a very weak effect [*Hidayat et al. 2000*].

Traveling toward the coast, tsunamis move huge amounts of the water column with an homogeneous velocity from bottom to the surface. This wave induces signals recorded on seismometers and many scientists have observed its impact at local station and far field

stations. *Yanagisawa & Wakasugi* (1984), for instance, reported crustal tilt induced by the load of the 1983 Nihonkai-Chubu earthquake tsunami at local seismic stations. Similarly, *La Rocca et al.* (2004) observed low-frequency signals caused by the local tsunami generated by landslides at Stromboli in 2002. For regional scale, *Angenheister* (1920) observed a signal on the seismic horizontal components at the station in Apia on the arrival time of the tsunami generated by the earthquake on 17th September 1918 in the Kurils. *Yuan et al.* (2005) reported seismic signals recorded on the horizontal components of coastal seismometers in the region of Indian Ocean during the 2004 Sumatra tsunami. They interpreted their observations as the effect of tilt due to gravitational tsunami loading. *Okal* (2007) confirmed the previous observations and found additional worldwide signals. He proposed that these signals are the response of instruments to the combination of horizontal displacement, tilt and perturbation in gravity. In addition, he observed a small amplitude signal, caused by the tsunami, on the vertical seismometers component.

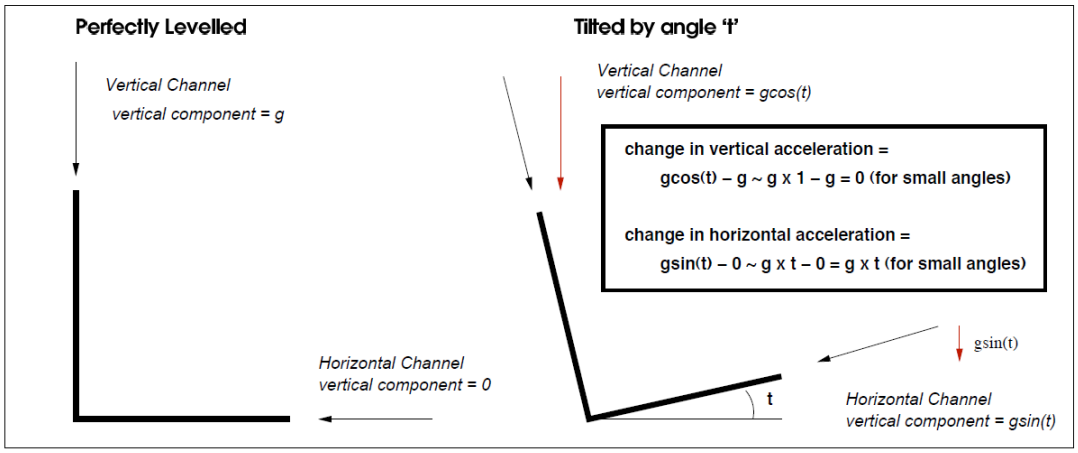


**Figure 3.5:** The effect of tilt on inertial seismometers [*Clinton*, (2004)].

# Chapter 4

# OBSERVATION OF TSUNAMIS

## 4.1 Seismic observation of tsunamis

### 4.1.1 Introduction

Tsunami are long period gravity waves in the sea caused by vertical displacements of large quantities of seawater. It is characterized by propagation through the whole water column and its velocity is uniformly distributed from bottom to sea surface which allow the wave to propagate to a very long distance. The speed of the tsunami depends on the ocean depth. When the tsunami travels toward a shallow water the wave speed decreases but the amplitude he wave grows up. Therefore the gravity loading of the wave propagating toward the shore induces seismic signal on the horizontal component of the seismometer. One of the mechanisms which may cause this signal is because the horizontal component of seismometers is very sensitive to tilt [*Gilbert* 1980]. The previous chapter explained the theory of coupling between ocean and continent as well as the response of the seismometer to tilt effect.

### 4.1.2 The Andaman-Sumatra, Indonesia 2004 tsunami

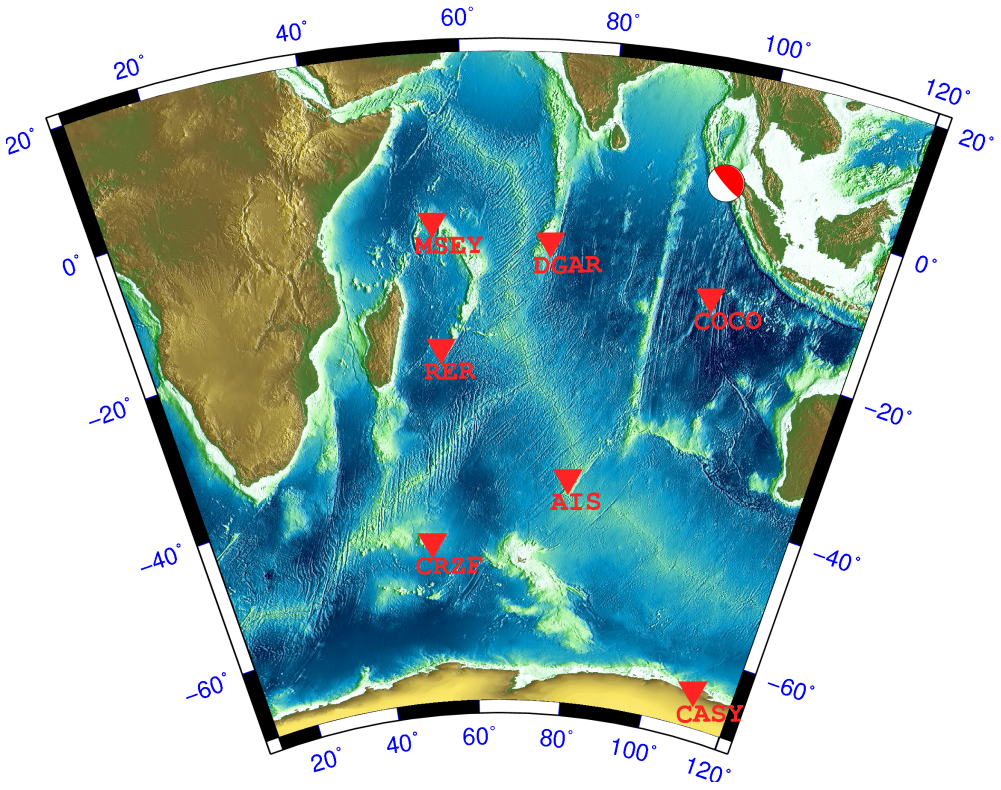


**Figure 4.1:** Location map of the seismic station used. The moment tensor solution of the Sumatra event indicates also its location.

Tide gauges are traditionally designed to monitor tsunamis. However, *Abe* (2007) reported that not only does the tide gauge respond too slowly to the sudden and abnormal change of sea level, like in the case of tsunami, but it also has a problem with the resonance of the harbor and even gets saturated for high water level. In addition, tide gauge station can also get damaged due to erosion caused by the rapid draw-down during flood drainage just after the first wave [*Isaac et al.* 2009]. These reasons motivated us to use seismic data for the purpose of tsunami monitoring. In this chapter, we analyze data from the horizontal component of seismic broad band sensor in order to determine the presence of a tsunami in the coastal area.

For the great Sumatra-Andaman earthquake of 26 December 2004, a vertical displacement of the seafloor of up to 10 m was estimated [*Bilham et al.* 2005, *Ji* 2005, *Fine et al.* 2005, *Song et al.* 2005 and *Heki et al.* 2006] and the rupture area extended over about 1500x200 km$^2$. The resulting vertical displacement of huge masses of water caused a catastrophic tsunami flooding many shores in the Indian Ocean.

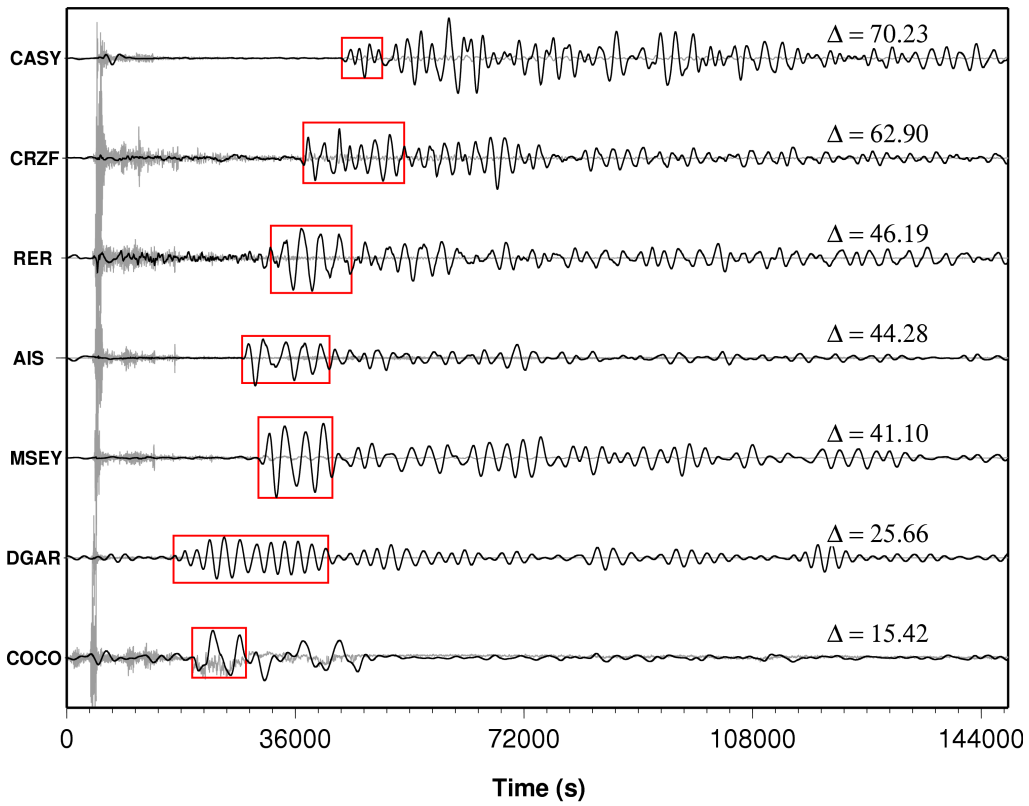


**Figure 4.2:** Seismic records of the Sumatra-Andaman earthquake of 26 December 2004 sorted by epicentral distance of the stations. Original unfiltered broadband records in gray ; long period low pass filtered in black ($F_c$=1000s). Red boxes indicate the first wave group of tsunami hitting the island. Zero seconds corresponds to March 11. 2011, 00:00:00.

During the inundation phase, the geomorphology of the coast at shores can drastically change the height of the tsunami. As explained in the previous study, ocean island and coastal stations of the global seismic network can be used for direct tsunami observations and local effects which influence tide gauges significantly are reduced since the tilting of

the island is an integral effect of a larger region. *Yuan et al.* (2005), *Hanson and Bowman* (2005) and *Okal* (2007) observed clear effects of the Sumatra-Andaman tsunami in seismic data. For this study, we analyze seven seismic stations in the Indian ocean [Figure 4.1] for the determination of the arrival time of tsunami.

#### 4.1.2.1 Observations

Very clear signals are observed in the seismic data. Figure 4.2 shows seismic signal detected at the arrival time of the tsunami. The starting time of the plot corresponds to the origin time of the earthquake. Gray traces are the original raw data and black are the long period filtered data. Data are sorted by the distance between the station and the epicenter of the earthquake indicated by $\Delta$ in the Figure 4.2. Red rectangle indicates the first wave group of the tsunami hitting the island. The end of the box is determined by the fact that the amplitude of the signal reduced to one-fourth of its maximun.

### 4.1.3 The Tohoku, Japan, tsunami 2011

The 11 March 2011 earthquake occurred at 05:46 UT with its epicenter at 28.231°N, 142.531°E (GEOFON Extended Virtual Network GEVN, Potsdam) approximately 373 km north-east of Tokyo and 130 km east of Sendai, Honshu in the Pacific Ocean near the Japan trench. The magnitude of this earthquake was initially estimated to be 8.9 ($M_w$), but later corrected by the United States Geological Survey (USGS) to 9.0 ($M_w$). Based on the earthquake/s location and magnitude, the Japan Meteorological Agency (JMA) issued a tsunami warning and ordered evacuations along the east coast of Japan. Besides, the West Coast and Alaska Tsunami Warning Center (WC/ATWC) in Alaska, USA issued also a tsunami watch for the entire Pacific coast. Considered to be the greatest event ever recorded in Japan, the earthquake triggered extremely destructive tsunamis of up to 24 meters high, recorded by the deep ocean gauge in Ofunato, Iwate (NGDC/NOAA Bul-

letin), traveling several kilometers inland. The tsunami generated by this earthquake was recorded by DART buoys and tide gauges in the Pacific Ocean.

In our observation, we infer signals detected on seismic stations caused by the average force applied on the whole island since the entire water column is moving during the propagation of the tsunami. Therefore, using this technique we can rule out the local effects of the beach and can obtain the true momentum of the tsunami wave. Further analysis of the available tide gauge data in the surrounding area close to the seismic station also allowed us to better understand the physical mechanism of the wave and its interaction with the land.

#### 4.1.3.1 Data

**Seismic data**

Seismic data recorded by broadband stations in the Pacific region were used in this study. These stations belong to the Global Seismographic Network (GSN) and data are provided by the Incorporated Research Institutions for Seismology (IRIS). The location of stations is shown in Figure 4.3 represented by triangles. We requested the available seismic data in the Pacific Ocean from the GSN/IRIS. Further examination of the data quality allows us to select 26 permanent seismic stations located on an island or on the continental shores. All stations analyzed in this study are listed in Table 4.1 with information about their respective distance from shores, arrival time of the tsunami detected at seismic station and its amplitude or ground velocity.

**Tide gauge data**

Tide gauge stations used in this study belong to the Center for Operational Oceanographic Products and Services (CO-OPS). Figure 4.3 shows the location of tide gauges station used

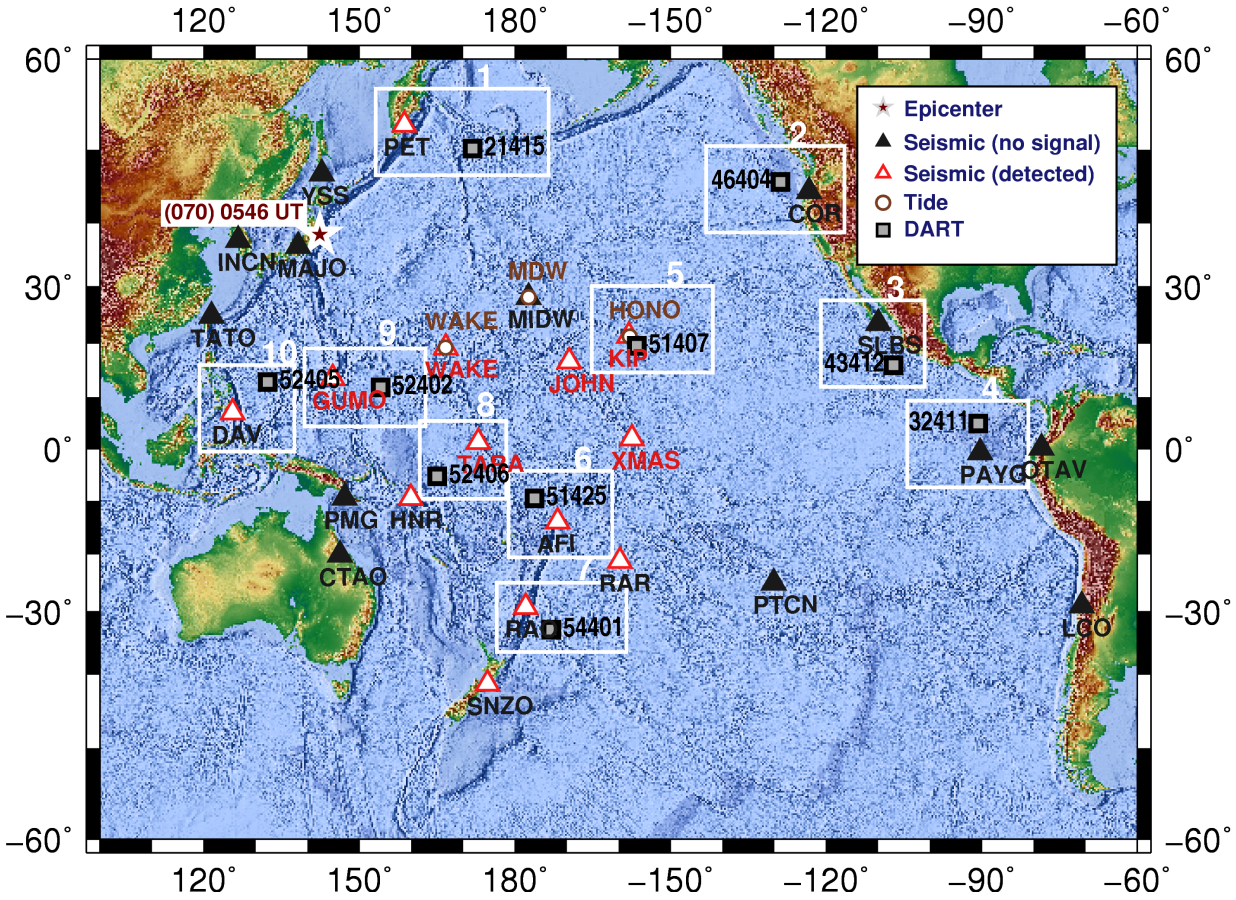


**Figure 4.3:** Location map of the stations used in this study. Star denotes epicenter of the Tohoku earthquake. Triangles represent seismic stations: black indicate the absence of a tsunami signal; empty red triangles represent the presence of signal. Tide gauge stations are indicated by empty brown circle and black squares represent DART stations. White rectangle with a numbering are the boxes discussed in the text.

in this study (brown circle). We selected three tide gauge stations collocated in the same Island with seismic station. However, only two of them are used here for comparison because at MIDW the seismometer had a problem few minutes after the earthquake. This does not allow us to analyze data from MIDW in the period when tsunami is expected to hit the island.

**DART gauge data**

In order to extend our observation, we look at the data from closest Deep-ocean Assessment and Reporting of Tsunami (DATA) to the seismic station. The area where both stations are available close to each other is marked by white rectangle on the figure 4.3. Therefore, we used data provided by the National Oceanic and Atmospheric Administrative (NOAA). Raw data are used from March, 11 2011.

#### 4.1.3.2 General descriptions and observations

Surrounded by a seismically active zone along the subduction system called "Ring of Fire", the Pacific basin is an home to an average number of two destructive tsunami per year [see *http://www.tulane.edu/ sanelson/geol204/tsunami.htm*]. About 80 percent of the world-wide tsunami occurs in the Pacific [*Kong* 2004] and one of the most vulnerable countries is Japan. The Tohoku-Oki earthquake occurred at the Japan trench on the interface of the Pacific and North American plates.

The Pacific plate moves approximately westwards with respect to the North America plate at a rate of 83 mm/yr (USGS), and begins its westward descent beneath Japan at the Japan Trench. The earthquake was caused by an abrupt release of stress which pushes the North American plate upward and this mechanism generated the devastating tsunami.

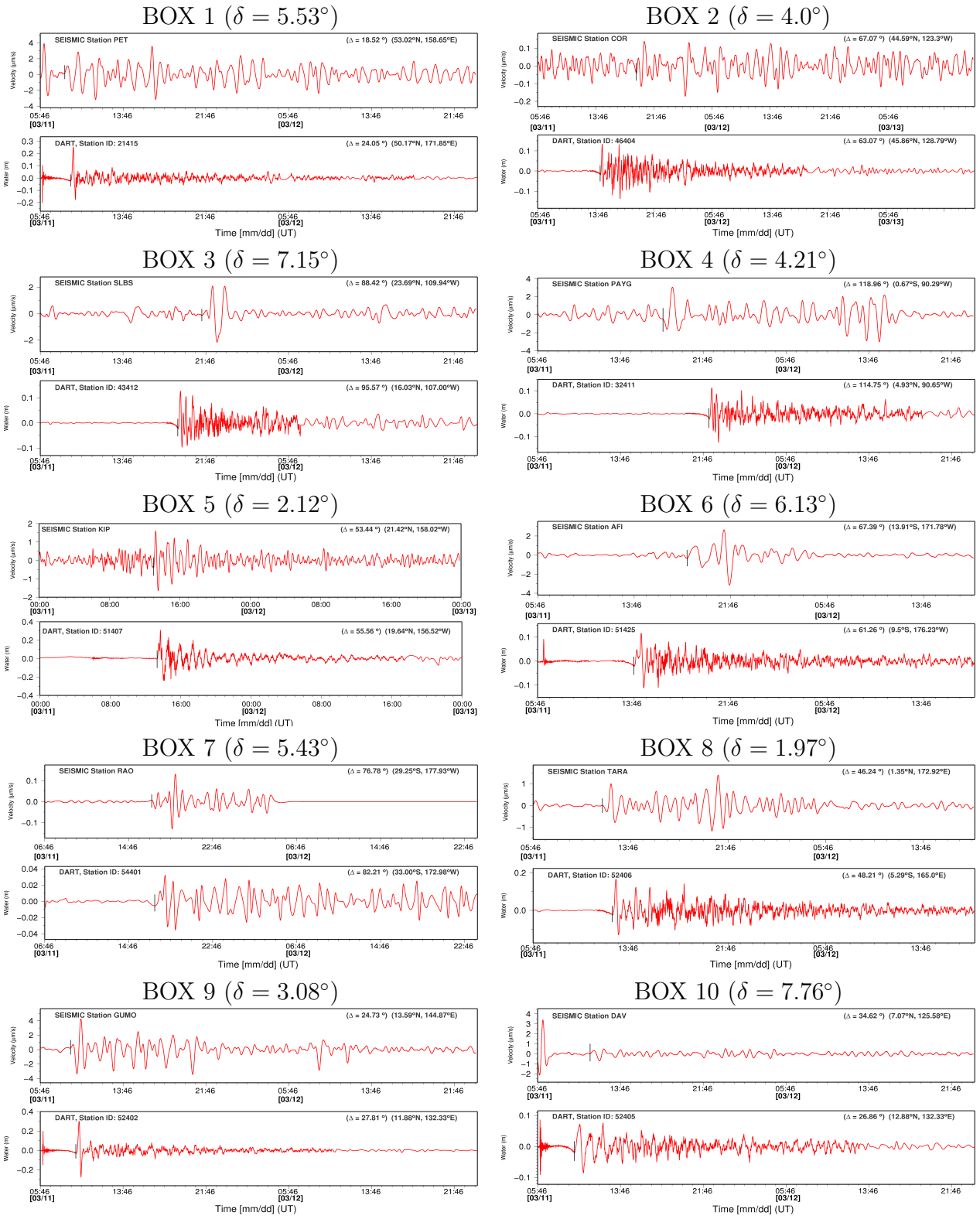


**Figure 4.4:** Comparison of seismic data band pass filtered in the frequency range of 1 mHz to 10 mHz with DART data. Location of boxes are shown in figure 4.3. Vertical black lines denote the picked arrival time of the tsunami. $\delta$ is the distance separating seismic and DART stations

**Table 4.1:** Observed properties of the tsunami waves generated by the Mw = 9 Japan earthquake in March 11, 2011. Time indicates the arrival time of the observed tsunami on seismic station. Coastal distance is the distance of the station from the shore and PGV stands for peak ground velocity i.e. the maximum amplitude of the first arrival.

| Name | Code | Lat | Long | Time (hh:mm:ss) | Coastal dist. (km) | PGV ($\mu$m/s) |
|---|---|---|---|---|---|---|
| Russia | PET | 53.02°N | 158.65°E | 08:07:59 | 0.61 | 0.96 |
| Philippines | DAV | 7.0697°N | 125.5791°E | 10:47:59 | 3.26 | 0.35 |
| Mariana Islands | GUMO | 13.59°N | 144.87°E | 08:59:08 | 3.46 | 5.84 |
| Wake Island | WAKE | 19.28°N | 166.65°E | 09:10:45 | 0.47 | 0.859 |
| Tarawa Island | TARA | 1.35°N | 172.92°E | 11:19:13 | 0.21 | 0.02 |
| Johnston Island | JOHN | 16.73°N | 169.53°W | 11:26:41 | 0.26 | 7.68 |
| Hawaii | KIP | 21.42°N | 158.02°W | 13:08:15 | 14 | 1.6 |
| Kiritimati Island | XMAS | 2.04°N | 157.45°W | 14:22:07 | 0.83 | 0.29 |
| Solomon Islands | HNR | 9.44°S | 159.95°E | 13:08:05 | 1.21 | 0.54 |
| Samoa | AFI | -13.91°S | 171.78°W | 17:30:37 | 9.38 | 3.09 |
| Kermadec Islands | RAO | 29.25°S | 171.78°W | 17:00:07 | 0.14 | 0.02 |
| Cook Islands | RAR | 21.21°S | 159.77°W | 17:54:36 | 0.58 | 2.03 |
| New Zealand | SNZO | 41.31°S | 174.7°E | 20:44:17 | 3.95 | 1.44 |

Many geophysical instruments located in the Pacific ocean have recorded the tsunami. The main energy of the tsunami propagates on the direction perpendicular to the fault zone [*Titov et al.* 1999; *Hébert et al.* 2001].

In our analysis, we took three days data in order to cover the complete excitation caused by the tsunami on the island. We then band pass filtered the date in the frequency range between 1 mHz to 10 mHz. The choice of the frequency band is based on previous work done by the above mentioned studies. Figure 4.5 shows the tsunami observation on the seismic record in the Pacific Ocean. The vertical dashed line represents the arrival time of the main earthquake. A clear signal are observed at 13 stations after filtering. Red rectangle shows the first group of tsunami detected at the seismic station after processing. After the box, a long wave train is still oscillating at the station. This can be an excitation caused by the water during the passage of the multiple waves following the tsunami main

energy plus the reflected waves from the surrounding coastal area. The signal can last for about one hour (Kiritimati Island, XMAS) but might oscillate for several hours and even days (New Zealand, SNZO). Tsunami signal are mainly observed on the same direction as the main lobe of potential energy dissipated by the tsunami. Note that the maximum energy of the tsunami generated by an earthquake on a fault zone is always perpendicular to the direction of the fault.

Figure 4.4 shows the comparison between low pass filtered seismic data and raw data obtained from the closest DART station. The distance $\delta$ between two stations varies from 1.97° (BOX 8) to 7.76° (BOX 10). In general, the observed signal on the seismic station corresponds to the arrival time of the tsunami on the DART station despite the difference in terms of frequency content between two data. This confirms that seismic station can be used as tsunameter even at some distance away from the shore line.
In box 2 we did not observed any signal on the seismic record because the SNR is very weak. In box 3 late arrival of the signal is observed on the seismic trace though seismic station is located closer to the source than the DART station. This might be a signal caused by waves which get trapped in the gulf of California after the passage of the heading tsunami and have grown-up and inundated the area. However, seismic signal on box 4 arrives earlier than the tsunami recorded on the DART station despite seismic station is farther from source than DART station. The signal observed on the seismic station can be caused by different source other than tsunami. In box 6, the late arrival of the signal is due to the ocean depth. Actually the tsunami travels at a speed of 50 m/s which correspond to shallow water similarly to the case here. At the seismic station DAV in box 10, a very weak signal is observed which travels as slow as the tsunami in box 6.

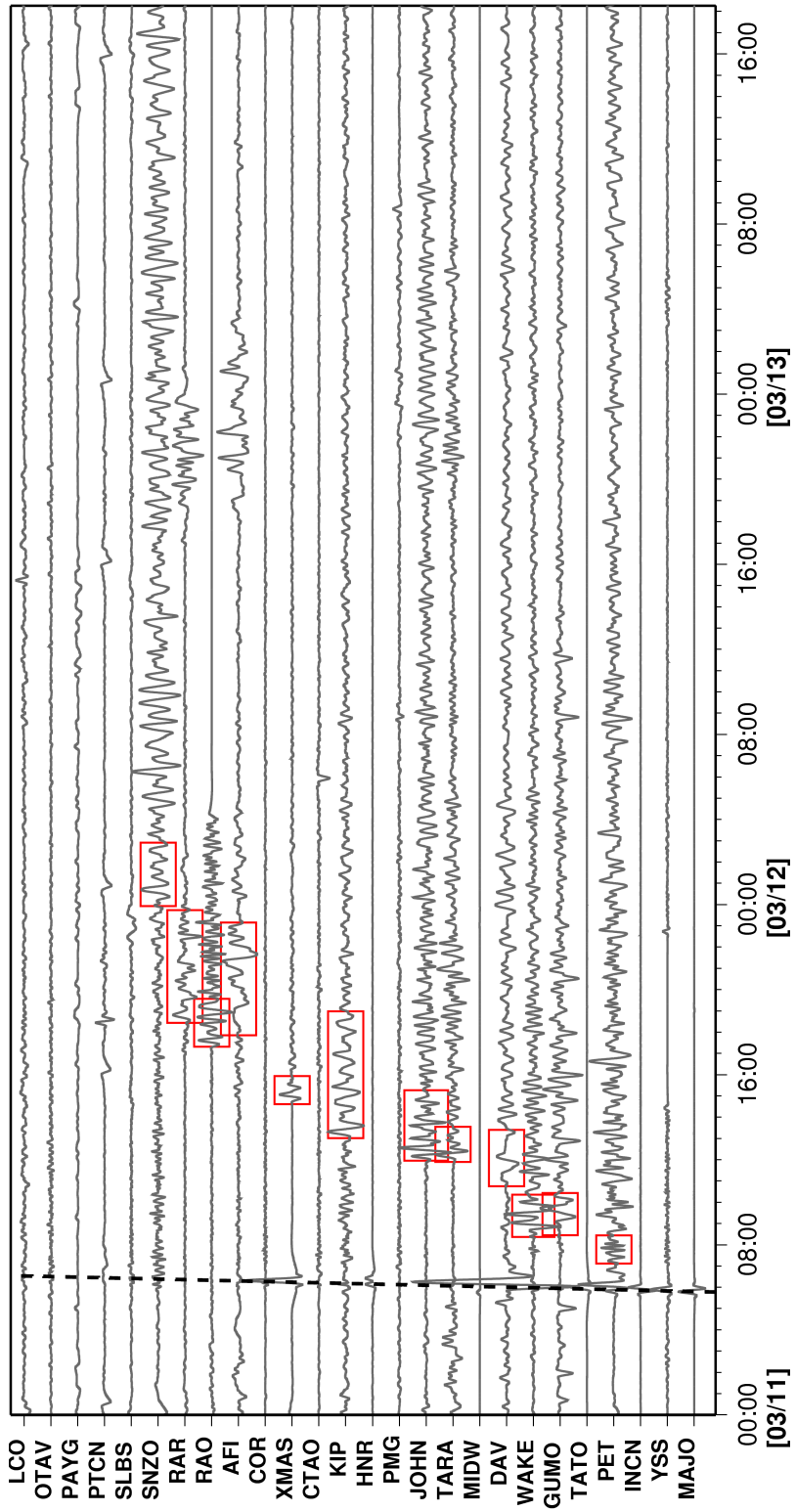


**Figure 4.5:** Seismic records band pass filtered in the frequency range of 1 mHz to 10 mHz. Dashed line denotes the time of the main seismic arrivals. Red rectangle represent the tsunami wave-group detected and the length is its estimated ringing times.

#### 4.1.3.3 Discussion

In this study, we tried to benefit from the existing global seismic network to detect the tsunami. We successfully identified tsunami signals on 13 seismic stations in the Pacific Ocean among the 26 stations analyzed. Table 4.1 shows that there is no direct connection between the amplitude of the observed signal and the distance between station and the coast. Seismometers located on an island in the ocean responded directly to the average deformation of the ocean floor due to the pressure of the ocean layer above.
This can be explained by the fact that located at few kilometers away from the shore, seismometers are sensitive to the passage of the tsunami. Tilt and gravitational potential can also be responsible of the excitation [*Okal*, 2007]. The red rectangle on Figure 4.5 can be interpreted as the first tsunami wave group striking the island. Multiple wave reflections from the continental boundary are also observed after the box. The duration of the ringing time varies from station to station. The length of the oscillation time might be controlled by many parameters but we suggested that the local topographic plays an important role. Note that the signal detected on the seismic station is still oscillating as long as the high frequency signal, due to tsunami, is present at the DART station.

Direct comparison between tide gauge and seismic data is also performed. Both, tide gauge and seismic stations, are co-located in the same oceanic island. The seismic data is band-pass filtered between 1 mHz and 10 mHz while the tide gauge data is just de-tided data i.e. the variation in the phase of the astronomic tide is removed from sea-level. This process is done by taking the difference between the measured sea level and the fitted prediction provided by NOAA. Two examples from two different island in the Pacific Ocean are analyzed in this study; the first station is located in Honolulu, Hawaii and the second one is on Wake Island.

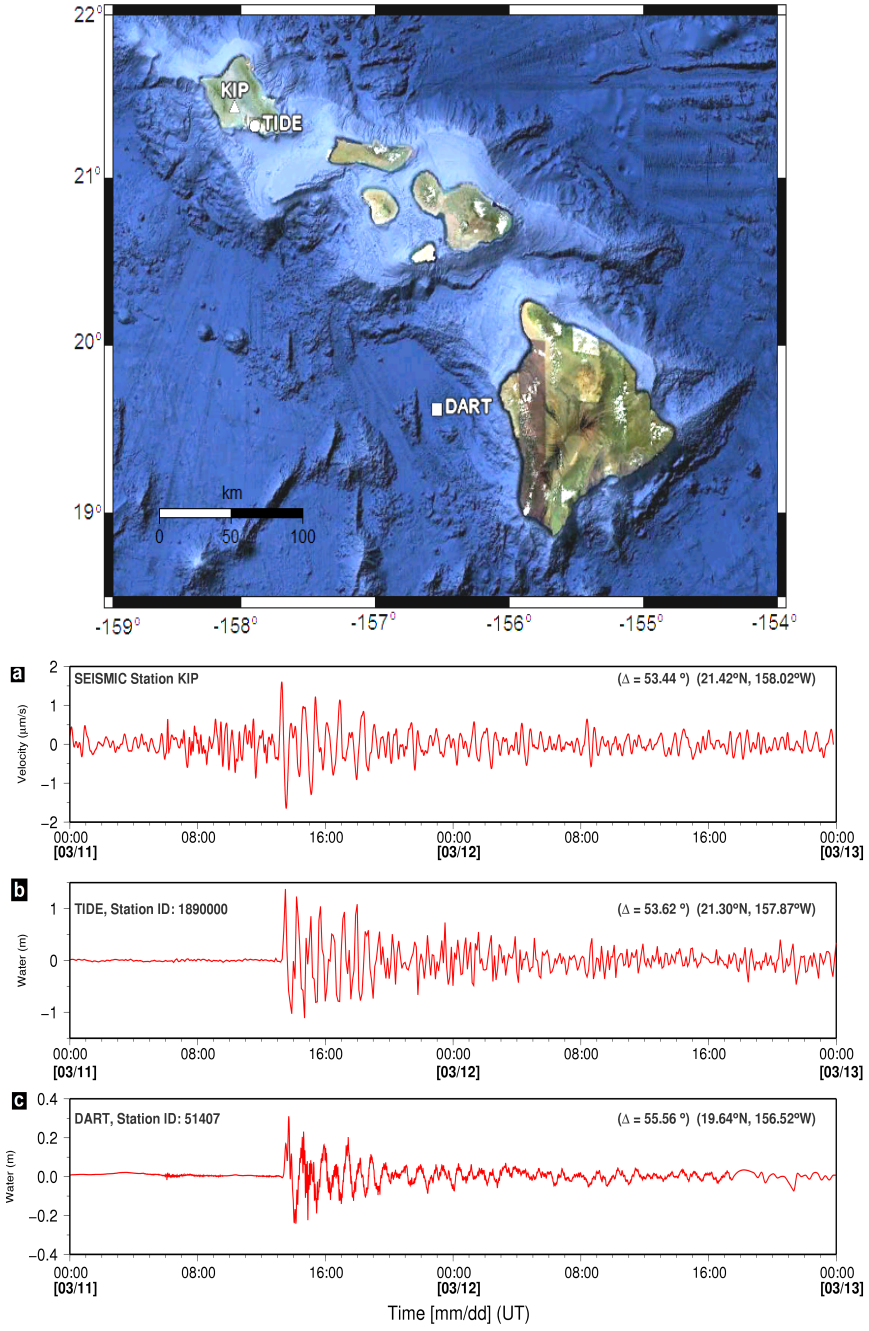


**Figure 4.6:** Comparison of seismic and tide gauge and DART data in Hawaii. Top: Map showing the location of seismic, tide gauge and DART stations. Bottom:(a) Seismic data bandpass filtered between 1mHz and 10 mHz.(b) de-tided tide gauge data.(c) DART data

On the first example of the Hawaii station in Figure 4.6 we noticed a perfect agreement between the two waveforms for about 10 hours from the moment when tsunami hits the Island. Despite the remarkable background oscillations, caused by the earthquake, before of the signal (red trace from 06:00 to 13:00) the SNR remains very good which allow us to see a very clear signal. Located at about 20 km away from the tide gauge station, a good correlation is observed between the seismic and the tide gauge signal. Note that the seismic signal arrived relatively earlier than the actual arrival time of the tsunami . However, the duration of ringing observed at both stations as well as the amplitude decay is relatively similar.

DART station located at about 200 km away from the two previous stations is also analyzed. It is confirmed that the signal observed on the seismic station is exactly caused by the excitation of tsunami. The late arrival is due to the distance and the water depth. For the second example, same procedure is used for the comparison of seismic and tide gauge data in Wake Island (Figure 4.7). Similarly to the previous example, the tsunami is observed on both records. However, one of the very remarkable observation is the polarity of the leading wave on both traces. If the seismic signal observed a negative leading wave, we note a positive amplitude on the first arrival on the tide gauge data. This should be an effect of the geometry of the island with respect to the location of the two stations. Wake island is "V"-shaped pointed towards the southeast surrounded by deep water and inside the two legs of the "V" is a lagoon. The seismic station (WAKE) is located at the east coast of the Island whereas the tide gauge is inside the two legs of the "V" (Figure 4.7). We noticed also the presence of high frequency signal on the tide gauge data. This is interpreted as the resonance of the tsunami wave trains in the channel between the two legs of that "V"; the tsunami came inside the two legs and gets trapped there. These high frequency wave trains are not observed in the seismic data (red trace). The energy decay

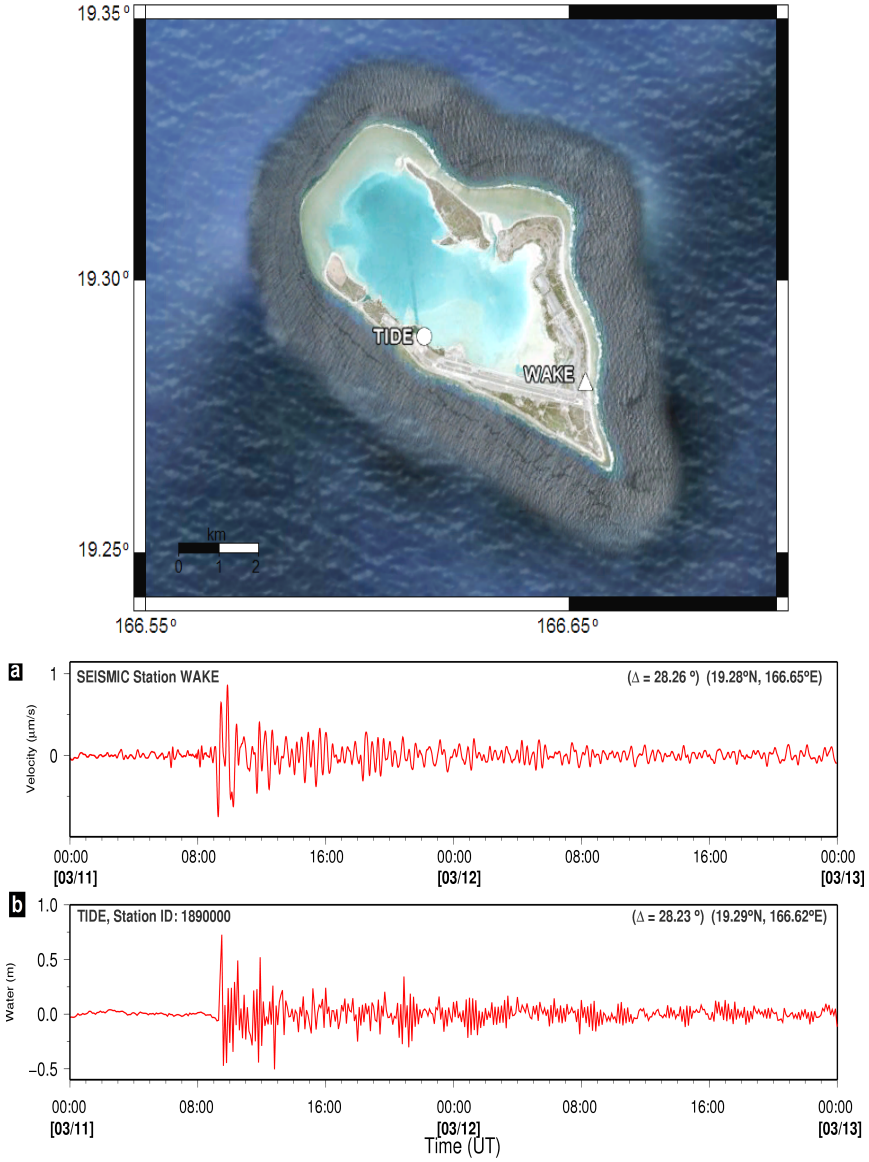


**Figure 4.7:** Comparison of seismic and tide gauge data in Wake Island. Top: Map showing the location of seismic and tide gauge stations. Bottom:(a) Seismic data bandpass filtered between 1mHz and 10 mHz.(b) de-tided tide gauge data.

is faster on the tide gauge than on seismic data.

On this second example, we can observed the effect of the local bathymetry on the arrival time of the signal. Even though the tide gauge station is located closer to the source than the seismic station, the tsunami arrived at the station only 20 minutes after the observed signal on the seismic data. This is caused by the effect of the geometry of the local harbor and the water depth. The station is located inside the two legs of the "V" shape in a shallow water. Therefore the wave propagated very slow to reach the station.

To calculate the expected arrival time of the tsunami at each station, a code developed by Dr A Babeyko (GFZ, Potsdam) is used. Figure 4.8 shows the comparison of the calculated marigram (red) and the long period [1 mHz $< F_c <$ 10mHz] seismic signal (black). In this comparison, imaginary tide gauge station are located at the closest harbor to the station. The distance $\delta$ separating the two stations varies from 0.01° to 0.2°. For the station located at the deep ocean, a very good estimation of the arrival time of the tsunami was observed. However, we observed a disagreement in the station WAKE. A weak signal was estimated to come at around 10:00 but the seismic station shows a very clear signal coming at 08:30. Same observation happened on HNR where the calculated arrival time came two hours later after the arrival time of the signal detected on the seismic data. For the station located on the shallow water along the continental border, a minor shift was observed i.e. observed seismic signal arrived earlier than the calculated. This might be due to the resolution of the bathymetry data used in the computation. For the station RAR, a very weak signal is observed at the expected arrival time of the tsunami but the big amplitude came 2 hours later. This signal can be interpreted as the combination of multiple reflected wave from the continental boundary. Exception is found at the station AFI where a very long period signal ($T \approx 2hours$) occurs at about three hours after the expected arrival time of tsunami. Based on its period, it cannot be interpreted as effect of

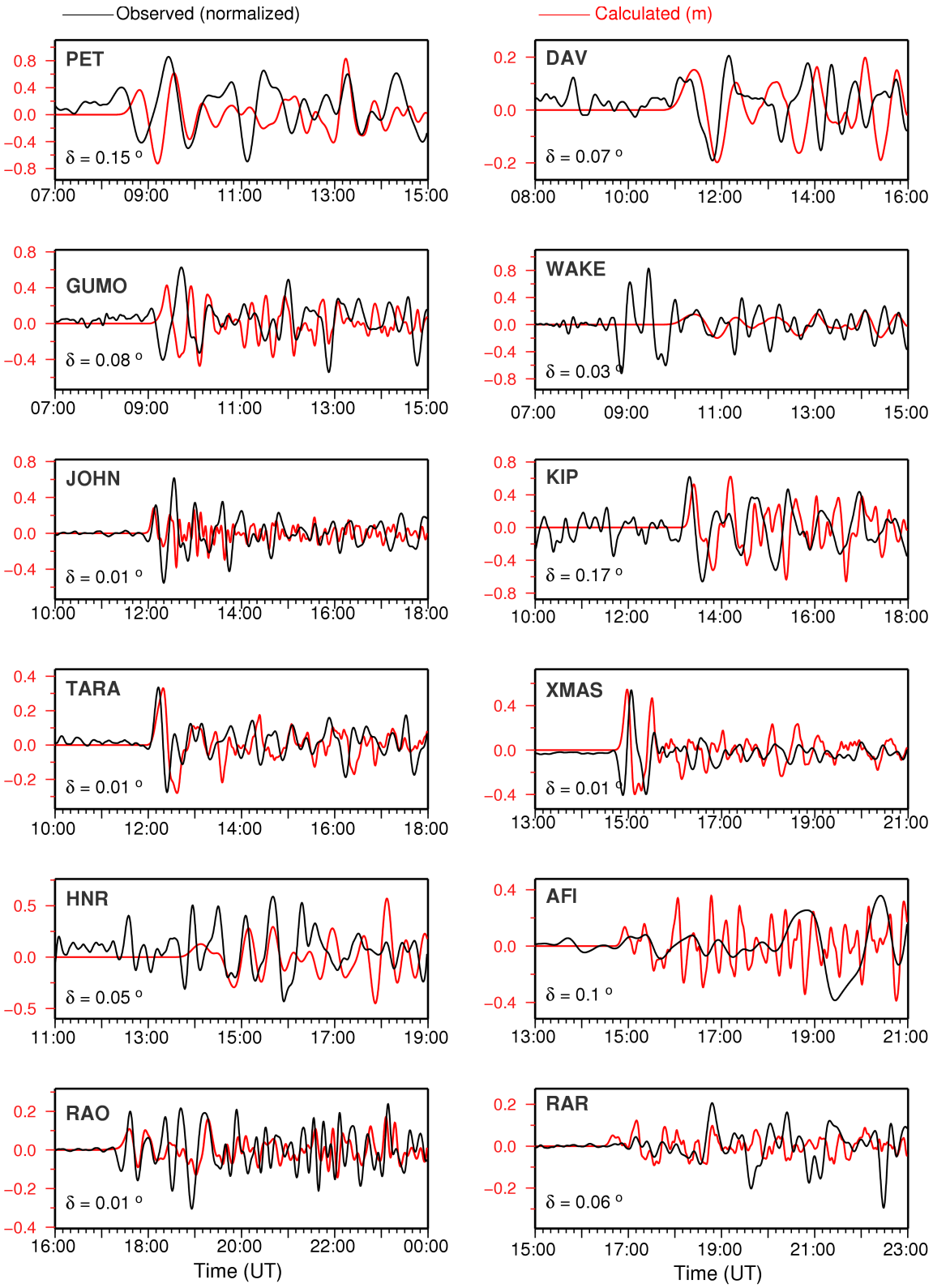


**Figure 4.8:** Seismic records (black) band pass filtered [1 to 10 mHz] and calculated marigram (red) located offshore. $\delta$ represents the distance between seismic station and the imaginary tide gauge station

tsunami.

#### 4.1.3.4 Conclusion

We have shown that for oceanic islands the distance of the seismic station from the shore does not affect much the amplitude of the ground velocity recorded caused by a tsunami. By doing a direct comparison of tide gauge and seismic data, we conclude that the seismic signal observed after filtering is comparable to the tsunami recorded by tide gauge because of the similarity between the filtered seismic wave shape and the de-tided tide gauge data as well as the good agreement with the tsunami arrival time. We suggest that broad band seismic stations on oceanic islands have the potential to contribute significant information for the purpose of tsunami monitoring. Expected arrival times of the tsunami, estimated from the theoretical marigrams, confirms that tsunami did generate signal which can be recorded by seismometer. Late arrival in some stations shows that the initial wave is not necessarily the largest and tsunamis can be dangerous for many hours after arrival. The signal observed at seismic stations during the tsunami is more consistent because it represents the average response of the whole island. Additionally, seismic stations are safe from damage due to erosion caused by the rapid draw down during flood drainage and free from the resonance of the harbor.

## 4.2 Infrasound observation of tsunamis

### 4.2.1 Introduction

Our motivation to analyze atmospheric data is based on the theory of the coupling mechanism existed between the ocean and the atmosphere explained in previous chapter. Note that there exist three main categories of sound waves in the atmosphere. The principal one

is the audible sound which is a wave traveling in the atmosphere with a frequency range of 20 to 20000 Hz. The next category of waves in the frequency range beyond 20000 Hz, the sound is known as an ultrasound and it is an inaudible sound. Animals like bats use such very high frequency wave as sonar for orientation. The third category is sound used by elephants for their communication over long distances by stomping their feet and sending vibration through the ground. This category of wave oscillates at a frequency lower than 20 Hz and cannot be heard by the human ears. It is known as "*infrasound*" and propagates at a speed of sound 343 m/s at 20 ° C in the air near the earth's surface. In this chapter, our attempt is to use infrasound data to detect signal generated by a tsunami into the atmosphere.

In the following paragraphs, the infrasound method refers to the measurement of the atmospheric pressure changes caused by different sources which disturb the equilibrium state of the air. Initially, the Allied forces used this technique during the World War I in order to locate artillery. This topic was considered as a top secret topic during the cold war period and very few people worked on infrasound data. In 1996, the general assembly of the Comprehensive Nuclear Test Ban Treaty Organization(CTBTO) required that a global network of infrasound station, composed of 60 stations, will be installed in order to detect and identify possible nuclear explosions. Since a few years ago, infrasound data is thus accessible for selected scientists. As a result, considerable progress has been made in atmospheric monitoring based on infrasound data analysis [Brachet et al. 2010].

### 4.2.2 Infrasound data

The infrasound data used in this study are from the network of the International Monitoring System (IMS) of the CTBTO in Vienna, Austria. Such an infrasound station consists of four to eight elements and the distance between elements varies from 1 to 3 km. Each

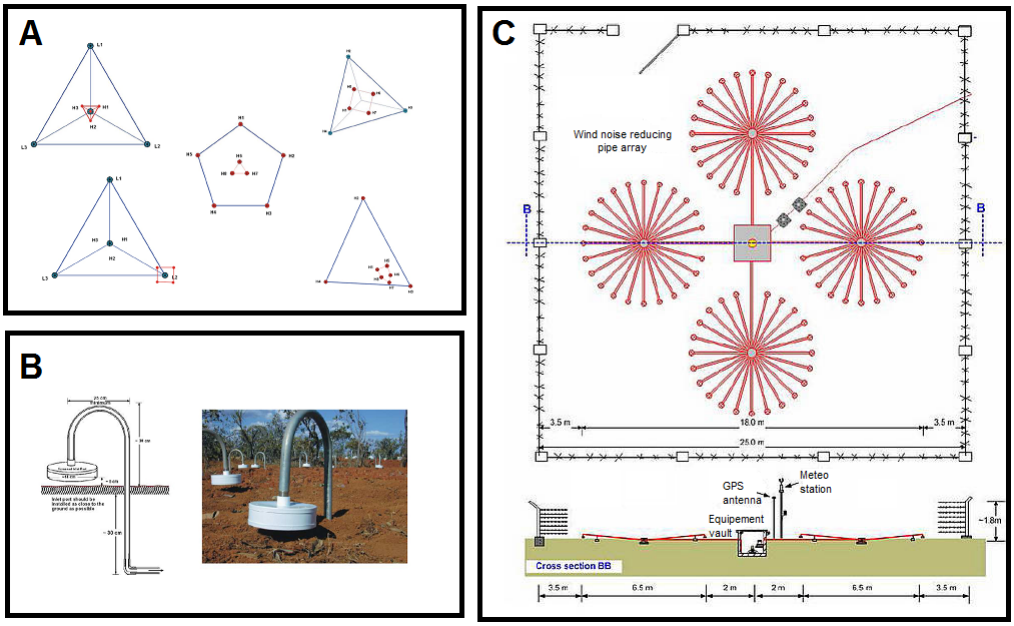


**Figure 4.9:** Infrasound station: (A) Different type of configuration of infrasound station, (B) End of the pipe (filtering system), (C) Prototype of one array element [*www.ctbto.org*].

array element includes pipe structures to reduce the surrounding noise and amplify the signals (Figure 4.9). When an acoustic wave reaches an infrasound station, the wave travels through these pipes to an infrasound sensor called a microbarometer. The sampling rate of the microbarometer is 20 Hz and it has a flat frequency response between 0.02 to 8 Hz [*Garces et al.*, 2005].

Since the microbarometer at the infrasound station measures the atmospheric pressure variation, the main source of noise is dominantly from the local condition of the meteorology like the wind. Therefore the ambient noise recorded at one element is normally uncorrelated with that of another element. Consequently, taking the direct summation of all traces will increase the quality of the data and reduce the noise level. Considering this specific configuration of the infrasound station, we take the summation of the array elements without any time shifts and this enable us to increase the signal to noise ratio. This is permissible because the wave length of the signal we are interested in is greater than the

size of the aperture of the array and the uncorrelated noises recorded at the station are short wavelength.

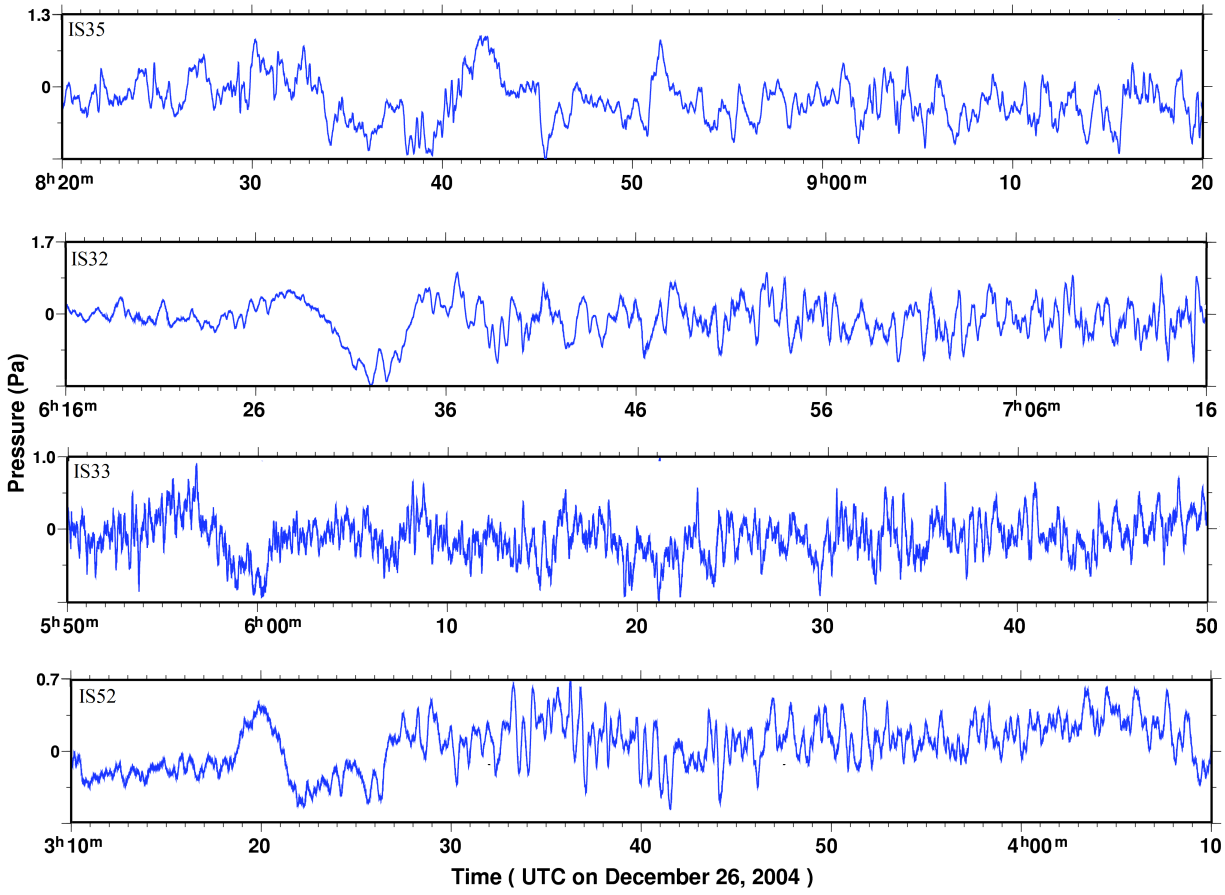


**Figure 4.10:** Recording of infrasound raw data from four IMS station after summation of all array elements.

### 4.2.3 The Andaman-Sumatra, Indonesia 2004 tsunami

#### 4.2.3.1 Observed data

**- Identification of the infrasound signal:**

The 2004 Sumatra-Andaman earthquake is still one of the most intensely studied events in the last decade. The giant earthquake had a huge humanitarian impact because not

only did it destroy local infrastructures but it also triggered a devastating tsunami along the coasts of most countries around the Indian Ocean which cost many lives In the realm of science the Sumatra-Andaman event was very interesting because it was recorded by many instruments, on the ground as high as in the ionosphere [*Artru et al.* 2005], even those which are not designed for tsunami monitoring like microbarometers deployed at an infrasound station. Therefore, four infrasound stations in the indian ocean rim detected signal from the tsunami. The summation of all raw data from each element of the station is presented in Figure 4.10. High frequency noises is eliminated in the first two top panels (IS35 and IS32). However, the station IS33, in the lower middle panel, is dominated by high frequencies which can be explained as other source of signal present in the whole array. The length of the time window used here is 60 minutes. The time windows at each station starts 10 min before the expected arrival time of the signal estimated from the average speed of tsunami in the deep ocean. For the detection of the event, we used all the data from each element of the array. In Figure 4.11, a second order Butterworth band-pass filter has been applied to the data with corner frequency of 1.19 and 4.16 mHz. The arrival time of signal caused by the tsunami are marked by vertical green lines which can be easily detected by the presence of coherent signals in at least three elements of the array. We used the elements where data is available. As an example, for the station IS35 only three elements (I35H2, I35H3, I35H4) of the array have data at the moment of the event. We observed also clear signal with good coherence arriving around 3:00 UT at the station IS52 prior to the arrival time of the tsunami air wave. These signals correspond to the pressure disturbance during the passage of large amplitude surface waves under the station circling the earth.

**- Location of infrasound source:**

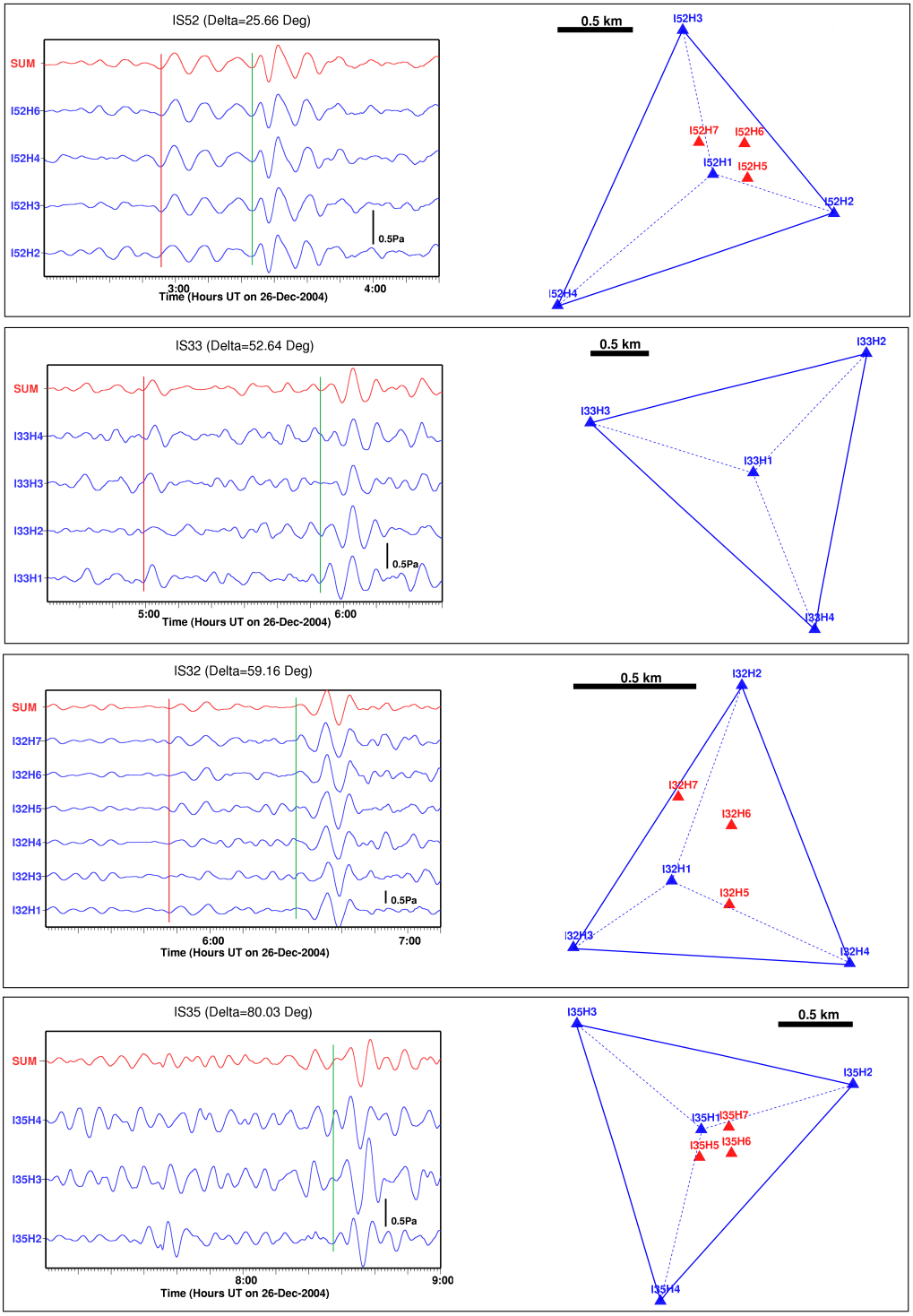


**Figure 4.11:** Left: Filtered data of each element of the infrasound array [BP: 4 - 14 min]. Name of the trace indicates the array element and SUM (red trace) stands for the summation of all traces. Vertical red line indicates the seismic surface wave circling the earth and green line are the arrival time of the tsunami. Right: Configuration of the array.

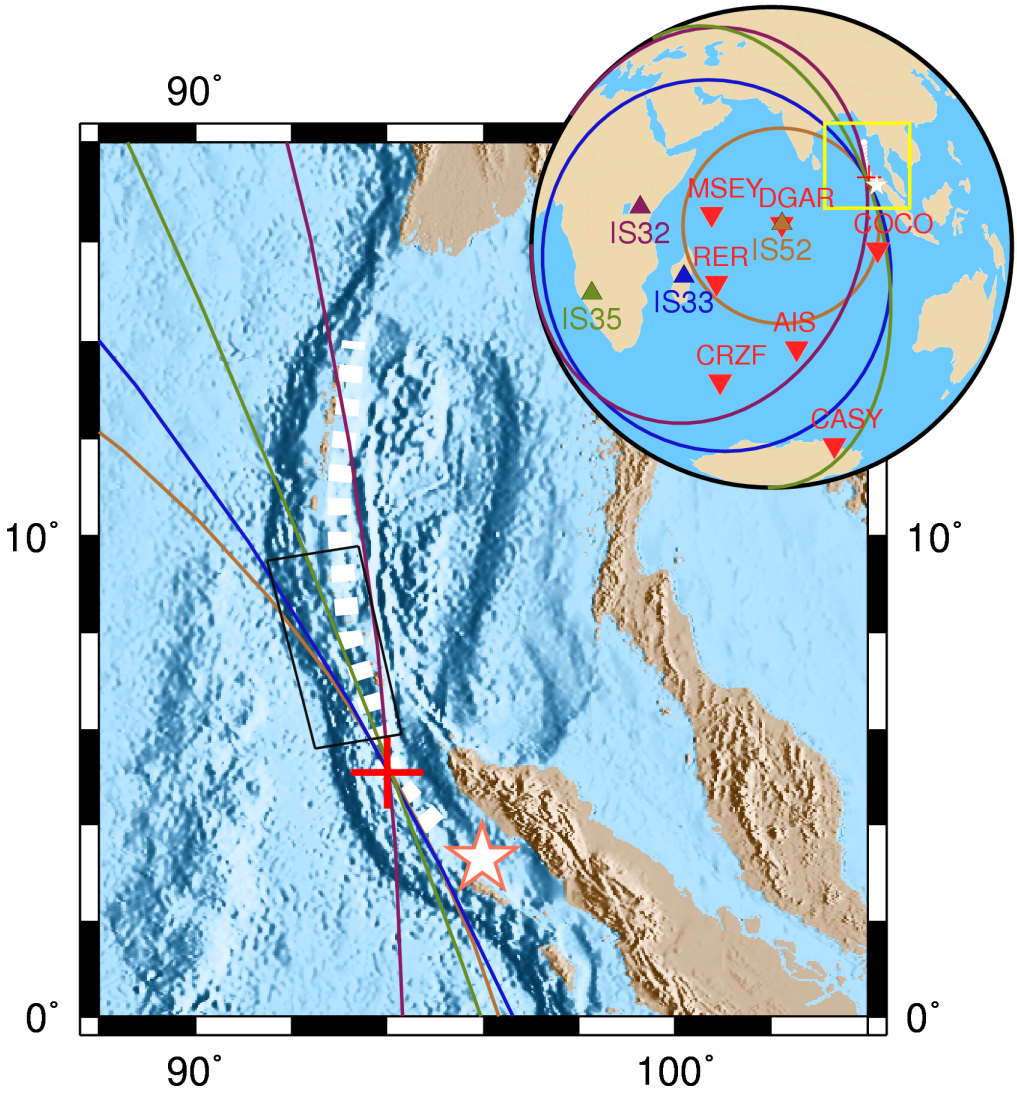


**Figure 4.12:** Inset: Red inverted triangles indicate seismic stations; infrasound stations are represented by color coded triangles; The star marks the earthquake epicenter and white dashed line represents the earthquake rupture track. The red + is the location of the source of the infrasound signals.

The star in Figure 4.12 shows the epicenter of the great earthquake from 26 December 2004 [USGS location: 3.316°N, 95.854 °E]. The approximate rupture propagation is indicated by the white dashed line. Accordingly, the circles centered at an infrasound station mark the possible source location according to the infrasound travel time to each station. At the very begining, origin time of the earthquake is used to locate the source of tsunami. The infrasound epicenter is located at the intersection of all circles indicated by the red cross.

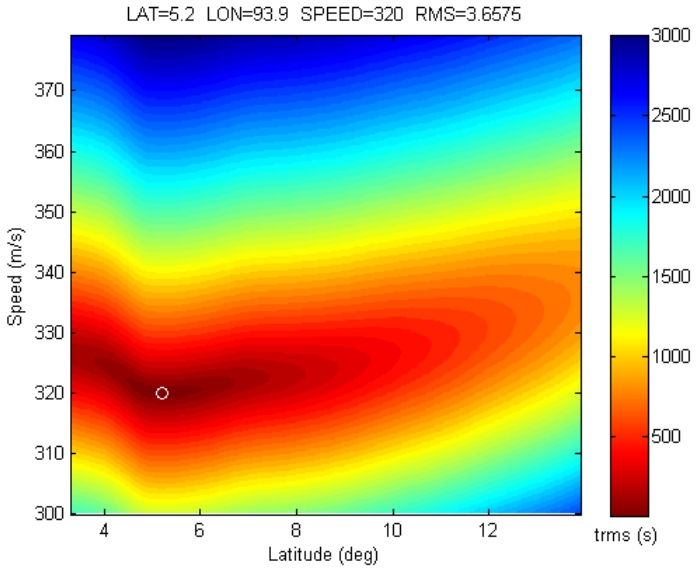


**Figure 4.13:** Time residual (rms) as a function of sound speed and the latitude along the rupture track. White circle indicates the solution of the grid search.

The location of the infrasound source was found by a grid search technique (over an area of 10x10 degrees with the infrasound speed, the source coordinates and tsunami origin time as free parameters. Since the location error was increasing when moving the source away from the rupture track, it seems sufficient to display as an example only the latitude and wave speed as free location parameter and move the source along the rupture track (Figure 4.13). We minimized the differences between observed and predicted arrival times at the four infrasound stations.

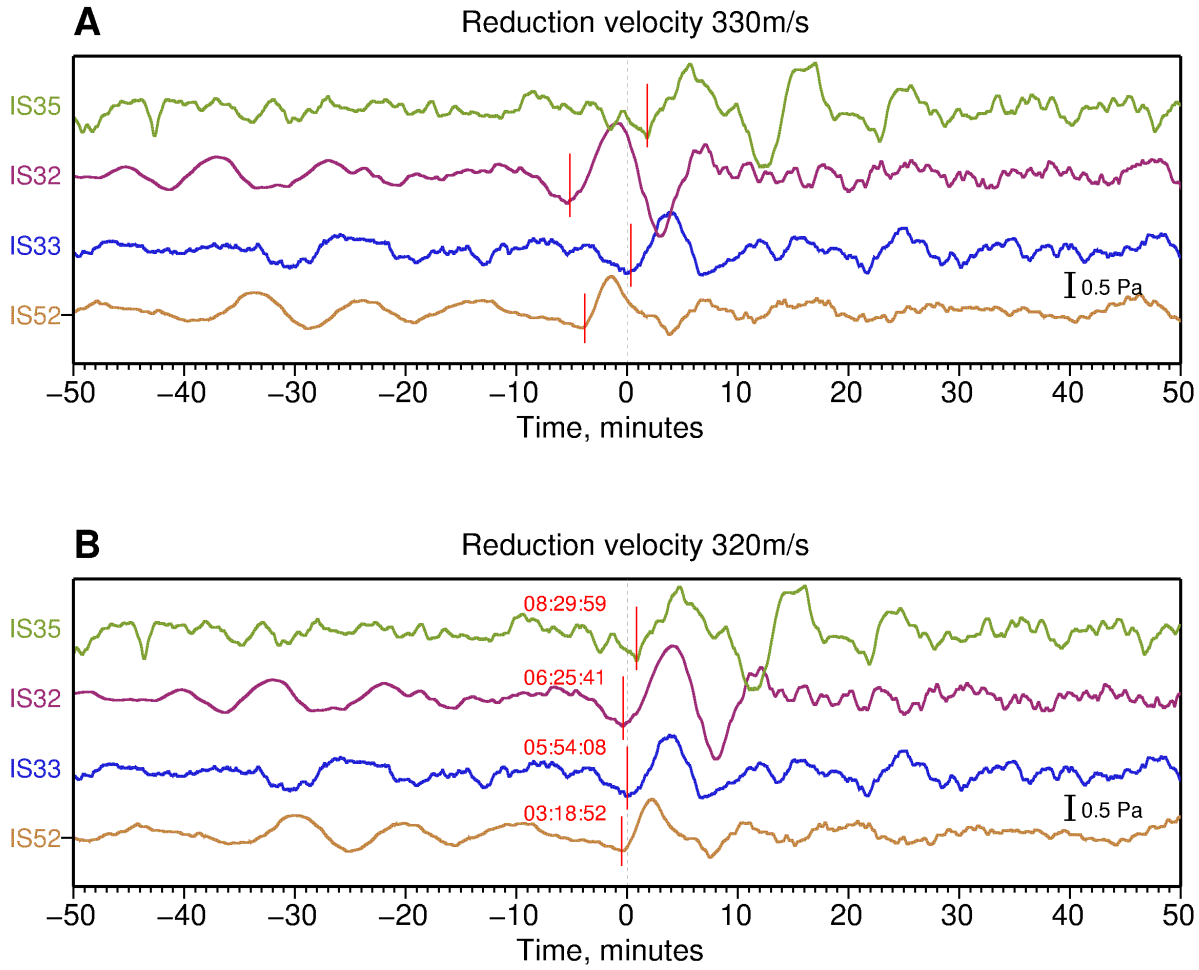


**Figure 4.14:** Summed infrasound records of each of the four infrasound arrays. The traces are filtered with an 800 s high pass filter. (A) Tsunami source is assumed at earthquake epicenter and origin time, traces are shifted according to a reduction velocity of 330 m/s (zero time). (B) Tsunami source parameters and infrasound velocity are taken from the caption of Fig. 4.12. Infrasound first arrival times are given at the traces.

The best solution was found for an infrasound speed of 320 m/s and a source location at 5°N latitude and 94°řE longitude (red cross in Figure 4.12A). A delay of 108 s of the tsunami origin time relative to the origin time of the earthquake was obtained. This fits well with the rupture velocity of 2.6 km/s obtained by Lay et al. (2005). Our infrasound source is located about 200 km to the south of the location by *Mikumo et al.* (2008), who derived their location from modeling of first arrival times and amplitudes of infrasound phases (black box in Figure 4.12A) with an extended source. Our location coincide to the maximum of co and post-seismic slip distribution on the Sunda megathrust estimated from inversion of geodetic data [*Subarya, et al.* 2006]

In Figure 4.14 infrasound waveforms are displayed with time shifts according to different source parameters. In Figure 4.14A the epicenter is assumed as source of the infrasound signal; in Figure 4.14B the source parameters determined by the grid search are used. The arrival times of the first infrasound signal are marked in Figure 4.14B. This figure also shows the good signal-to-noise ratio and the great similarity of the infrasound signals at all stations. Assuming the epicentral source and origin time of the earthquake to be the same as the source of infrasound fails to predict the arrival time.

#### 4.2.3.2 Synthetic data

In order to better understand the physical process of the interaction of the tsunami with the atmosphere and continent, we analyze theoretical data. The synthetics are calculated using code developed by *Wang* (1999) based on normal mode theory [*Gilbert and Backus* 1968, *Takeuchi and Saito* 1972] and the orthonormalized matrix algorithm of *Wang* (1999) for numerical stability. The seismic reference model PREM is used for the computations for the seismic response at the ocean bottom.

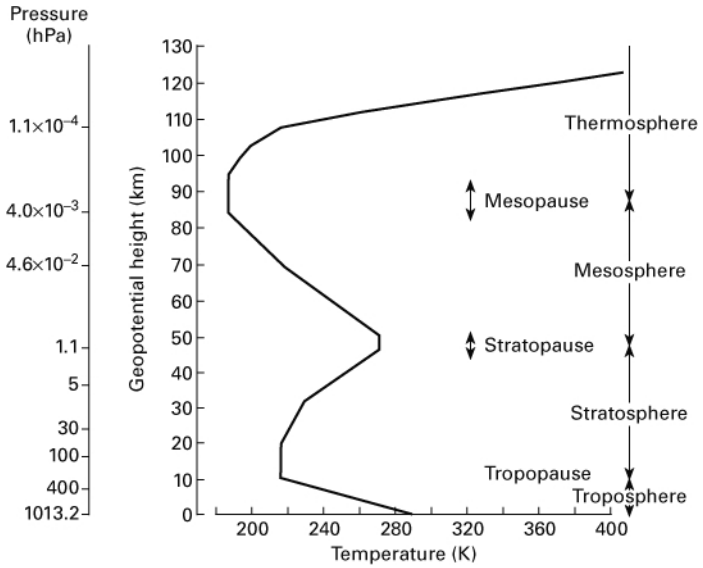


**Figure 4.15:** US Standard Atmosphere model.
(http://science.jrank.org/pages/65157/standard-atmosphere.html)

For a better fitting of the tsunami propagation velocity in the Indian Ocean, we changed the thickness of ocean layer in the original PREM model from 3 to 4 km and added a standard atmosphere above it (US Standard Atmosphere 1976, see Figure 4.15). Tilt effects due to gravitational tsunami loading are included in the calculation of seismic synthetics, but no instrumental effect is included.

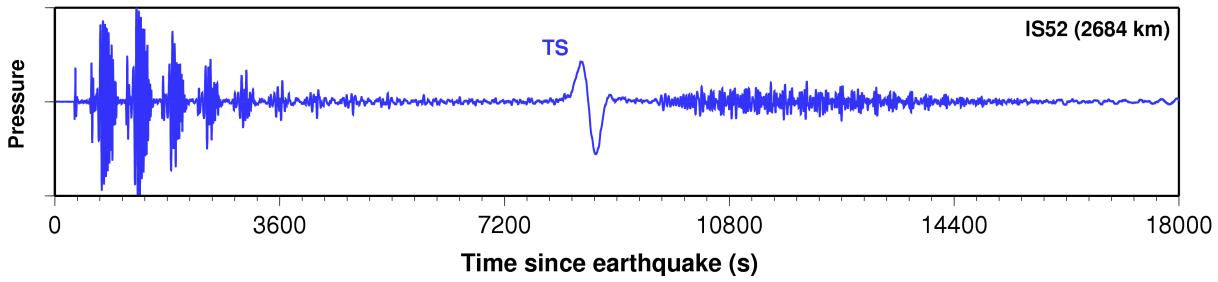


**Figure 4.16:** Example of synthetic infrasound trace of the great Sumatra-Andaman earthquake. TS indicates the arrival of tsunami air wave.
*(Source parameters: Harvard CMT Double-Couple solution - Earth model: PREM + US Standard Atmosphere)*

**Table 4.2:** Infrasound signal observed at IMS stations of the Andaman-Sumatra tsunami.

| Stations | Latitude | Longitude | Elevation (m) | Elements | Distance (°) | Amplitude (Pa) | Period (s) |
|---|---|---|---|---|---|---|---|
| IS32 | 1.242°S | 36.827°E | 1662.0 | 6 | 57.45 | 1.9 | 540 |
| IS33 | 19.011°S | 47.305°E | 1385.0 | 4 | 51.84 | 0.78 | 504 |
| IS35 | 19.191°S | 17.577°E | 1253.0 | 3 | 78.92 | 1.4 | 590 |
| IS52 | 7.378°S | 72.484°E | 1000.0 | 4 | 24.79 | 0.89 | 513 |

The theoretical infrasound trace (Figure 4.16) shows a clear signal of the tsunami air wave marked as TS. For the computation, the theory of coupling between the solid earth, ocean and atmosphere is basically involved. The ringing effect seen in the first hour of the trace is interpreted as a standing wave in the atmosphere being caused by the arriving seismic surface waves and being reflected between the Earth/s surface and the upper atmosphere. The high frequency coda occured after the infrasound signal is the response of the surface wave circling the earth. They are results of different seismic phases that couple into atmospheric acoustic waves propagating nearly vertically. The absence of wind in the model may increase the reflection effect of the wave at the atmospheric layer interface.

#### 4.2.3.3 Interpretation and discussion

Infrasound signals caused by a vertical displacement of sea surface during the generation of tsunami triggered by the great Sumatra-Andaman earthquake in 2004 are observed at four infrasound stations. The amplitude of the detected infrasound signal, measured after summation all traces of the array elements, varies from 0.7 to 1.9 Pa with a dominant period of 550 s [Table 4.2].

As discussed in the chapter 3 ocean swelling also can be a source of atmospheric excitation. The theory of coupling between solid earth, ocean and atmosphere indicates that the excitation from the sea bottom due to the earthquake can be transferred to the upper

atmosphere though the ocean layer. Equation 3.3 indicates that the air wave above the sea surface oscillates about the double of the frequency of the sea surface waves. While analyzing tide-gauge data from the Indian subcontinent and surrounding area, *Nagarajan* (2006) shows that 20 minutes is the prominent periodicity of the tsunami. The period of the observed infrasound signal is therefore consistent with the theory. Based on the theory of the leading wave of tsunami by *Kajiura* (1963) different tsunami simulators also have demonstrated that the initial tsunami distribution is identical to the sea bottom deformation caused by the submarine earthquake [*Tanioka et al.* 2001; *Piatanesi et al.* 2007; *Saito et al.* 2009].

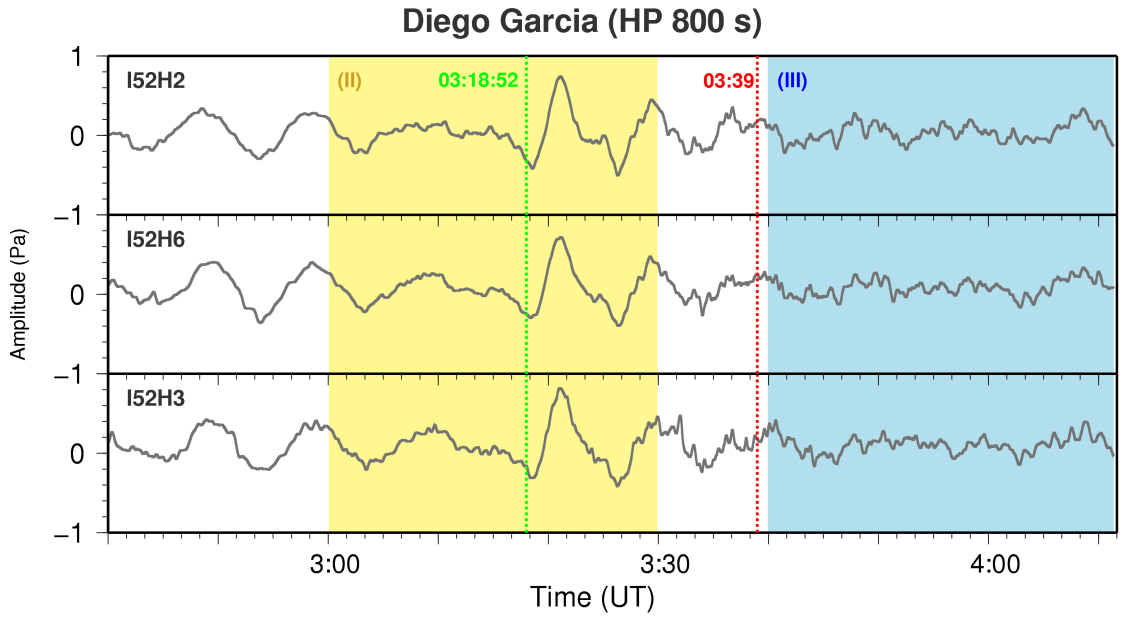


**Figure 4.17:** Three individual components of the infrasound array at Diego Garcia

Figure 4.17 shows the infrasound records of the three individual components of the infrasound array at Diego Garcia filtered with an 800 s high pass filter. *Le Pichon et al.* (2005) located the source of the signals in group II (yellow) in the extended area of the seismic source but did not conclude that the infrasound waves have been caused by coseismic uplift and subsidence of the sea bottom and associated swelling and depression of the sea surface.

They located the sources of the secondary signals in group III (blue) in the area between Sumatra and the Bay of Bengal. *Mikumo et al.* (2008) concluded that the first arriving signals have been caused by sea level changes in the open seas at the seismic source area. However, they gave partly questionable arrival times of the first signals. In a personal communication, they confirm that the mistake comes from the automatic picking. In the case of Diego Garcia their first arrival time (03:39, see vertical red line) is about 20 minutes later than ours (03:18:52, see vertical green line). We compared the infrasound time scale with the seismic time scale at Diego Garcia and found no error in our time determination.

### 4.2.4 The Tohoku, Japan, tsunami 2011

The Mw 9.0 earthquake in Japan, which caused triple serious disaster for the Japanese people, has been subject of several investigations. A part from the severe damage of the nuclear power plant, estimated to create a long term danger for the population, the shaking of the earthquake itself followed by the tsunami produced an immediate damage to Japan's infrastructures and thousands of casualties. Located at triple trenches junction, Japan is one of the countries vulnerable not only to an earthquake with large magnitude but also to tsunami. Therefore, Japanese government has deployed different kind of instrument to monitor any kind of hazards which may reach Japan. Seismic stations are used for monitoring earthquake whereas tsunami is traditionally monitored by numbers of tide gauge stations deployed not only at the shoreline of the Island but also in some other continents. For the same purpose, Japan uses Ocean bottom pressure gauges. The tsunami was recorded by many instruments of different technologies because of its size. Due to the coupling of oceanic disturbance with the atmosphere, the tsunami is also detected by infrasound stations. These observations are explained in the following paragraph.

#### 4.2.4.1 Identification of the infrasound signal

We searched through the infrasound network station of the IMS/CTBTO in Vienna for the very long-period signal of the Tohoku-Oki tsunami. As described in the previous paragraph, an infrasound station is composed of small array with four to eight elements. To identify the signal caused by the tsunami, we summed up good traces (without spikes) from all elements to increase the signal to noise ratio. Then a second order Butterworth high-pass filter with a corner frequency of 800 s is applied. Clear signals were found up to thousands of kilometers from the source in Continental Asia and in Alaska. These signals are shown in Figure 4.18.

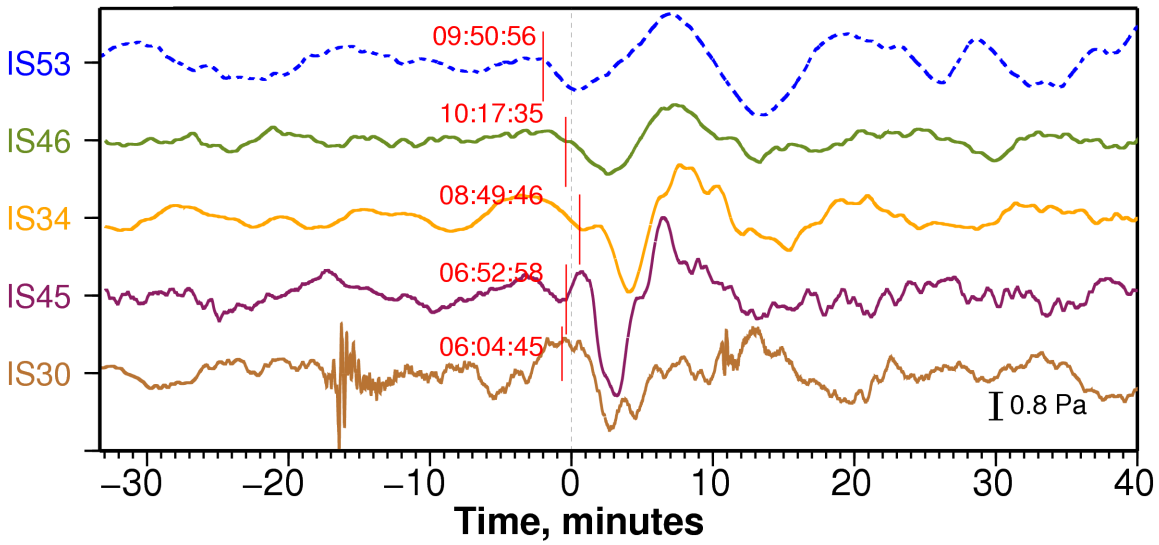


**Figure 4.18:** Each trace corresponds to the sum of traces in each array at the indicated station name on the left. Infrasound traces are filtered with a 800s high pass filter. Arrival times of the signal at each station is indicated on each trace. Zero time on the plot corresponds to the speed of 290 m/s except for IS53 (dashed line)traveling with a speed of 356 m/s.

On Figure 4.18 traces are sorted by the distance from the earthquake source location. Vertical red lines denote the arrival time of the tsunami signal. The actual arrival time (in

UT) is mentioned next to these line. The period of the detected signals varies from500 s to 800 s and the signal travels with a speed of 290 m/s for the Asian stations and 356 m/s for the station in Alaska [see table 4.3].

#### 4.2.4.2 Location of the infrasound source

During the tsunamigenic earthquake in Tohoku-Oki, Japan the sea floor is displaced vertically. These displacements are shown in Figure 4.19 -A by red arrows computed by using GPS/acoustic combination techniques. These values are the difference between the sea floor depth observed before (2010) and after (2011)the event [*Sato, et al.*, 2011]. As explained in the previous chapter, the energy released during that vertical displacement is transferred into the ocean which in turn produces a vertical displacement on the sea surface above the hypocenter of the earthquake. The sudden vertical displacement of the sea surface generates an acoustic gravity wave in the atmosphere which was detectable by infrasound stations. We used these detected signals to locate the source of the tsunami.

The location of the tsunami source is done by a grid search over the coordinates of the tsunami source location and the sound speed. The search is done within area of 4X4degrees around the epicenter of the earthquake. By knowing the arrival time of the signal, we choose one arbitrary speed and consider it as zero time. Then we align all the signal to the zero line by doing reduction speed and we keep on changing the speed until we find a location where the time difference between the zero line and the arrival time is very small.

The origin time of the earthquake was used as the tsunami origin time. Figure 4.20 shows the large view of the whole station. Here, similar technique formally used in seismology for locating earthquake is used. In each station, we draw a circle centered at the station itself and the radius of the circle is equal to the product of the propagation speed and the

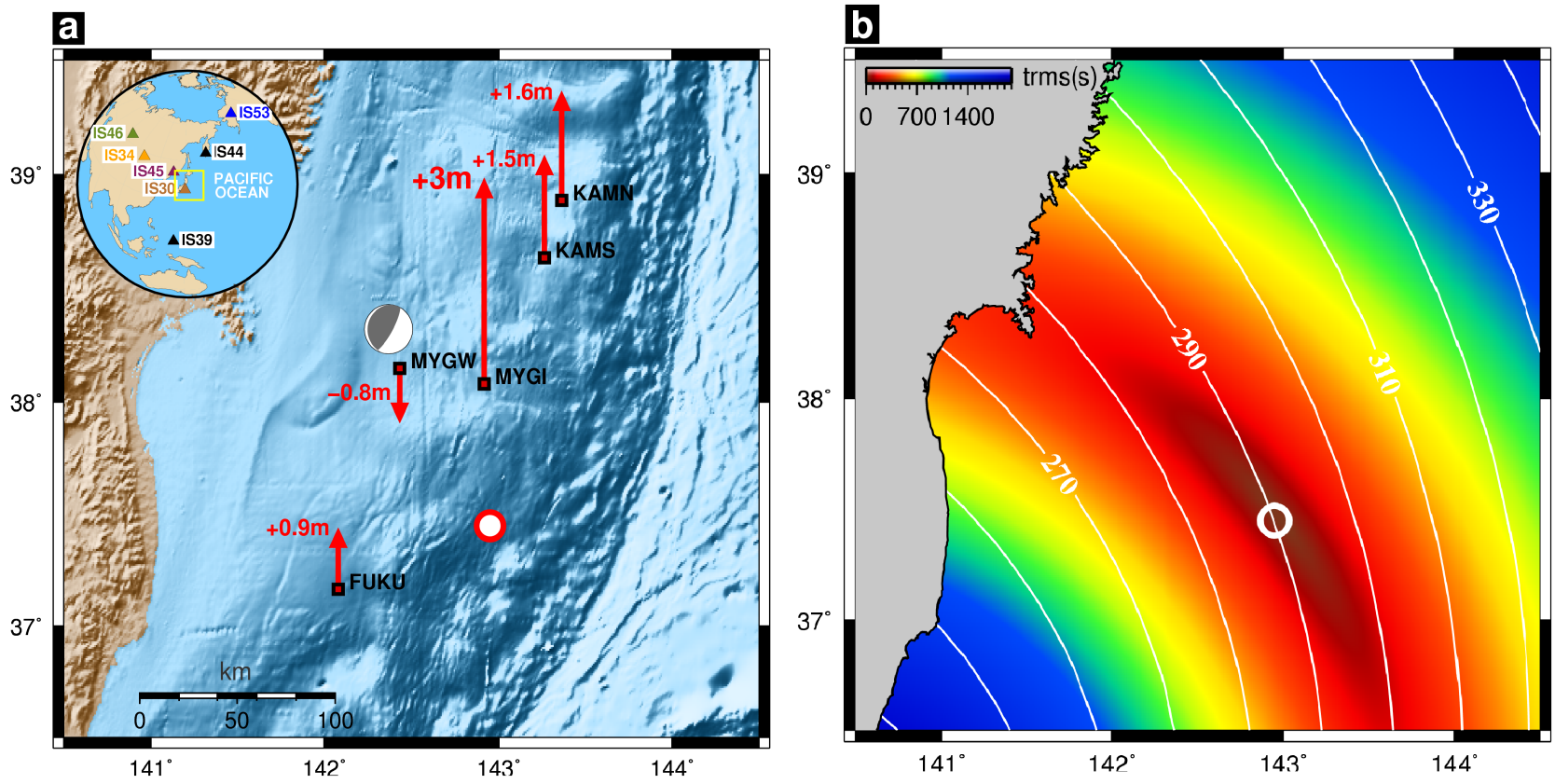


**Figure 4.19:** Grid search technique for the location of the 2011 Tohoku-Oki tsunami.(A) Inset figure shows the location of the Infrasound array: two black triangles show the station where signal is absent or very weak wheras colored triangles are the place where signals are detected.The source of the tsunami obtained from calculation is shown as a red-white sphere. The seismic epicenter according to the US Geological Survey is shown as a grey-white beach ball marking the fault orientation. Arrows indicates the vertical displacement of the sea-floor observed by using GPS/acoustic combination technique [*Sato, et al.*, 2011]. (B) Grid seach method. White circle corresponds to the location of the tsunami source, isolines indicate the calculated sound speed in each grid point and the color shows the time residual between the zero line and the arrival time of the signal.

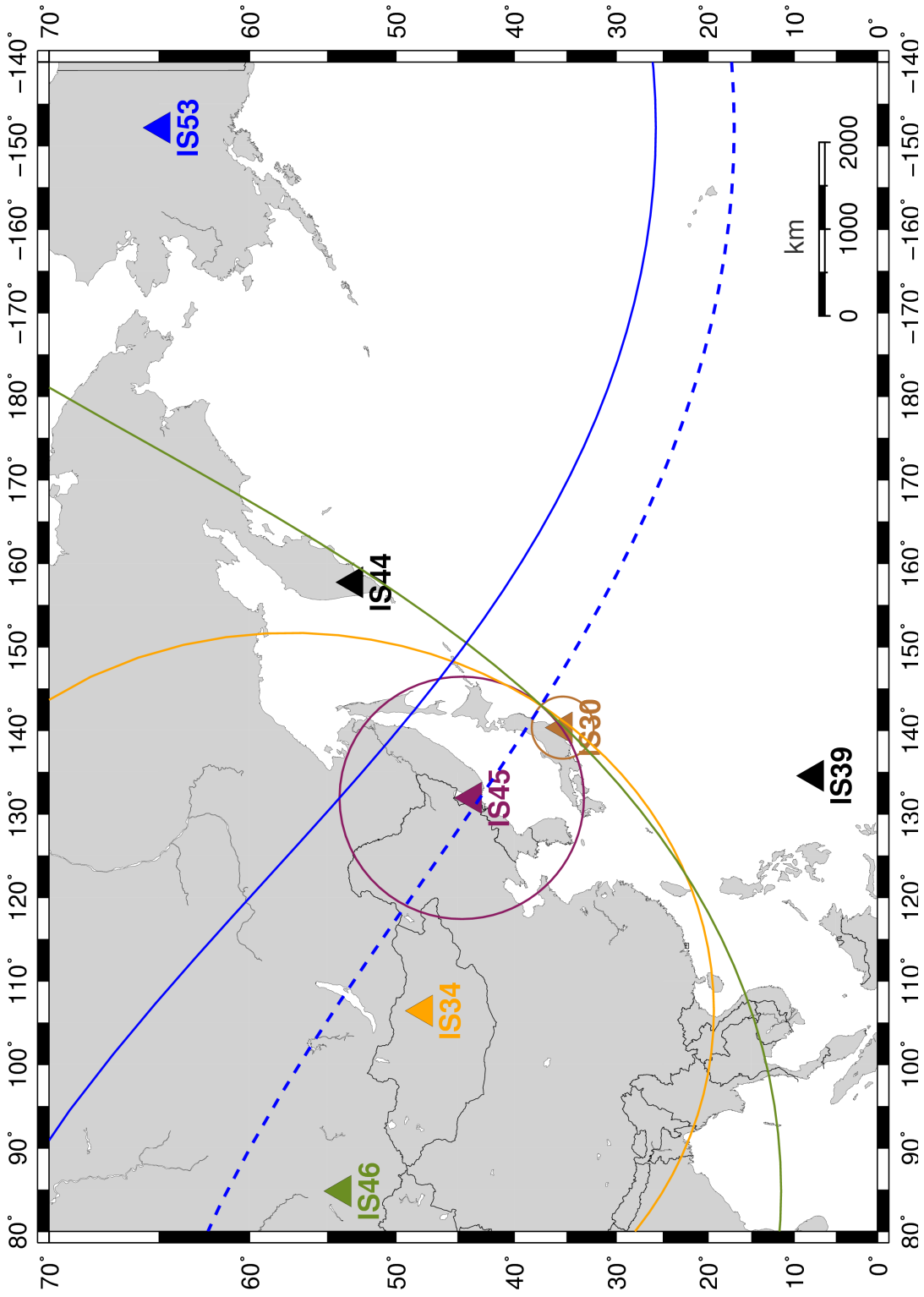


**Figure 4.20:** Enlarged location map of infrasound stations. Circles indicate the possible source of the tsunami for each station. Coordinates of the tsunami source and average wave speed of the tsunami are the free parameters in the grid search. The tsunami source is estimated to be at the intersection of all circles. Solid blue line indicates the arrival time of the signal recorded at Alaskan station with a speed of 290 m/s whereas dashed blue line is the same signal with a speed of 356 m/s.

**Table 4.3:** Infrasound signal observed at IMS stations for the 2011 Tohoku-Oki tsunami.

| Stations | Latitude | Longitude | Elevation (m) | Distance (°) | Speed (m/s) | Period (s) |
|---|---|---|---|---|---|---|
| IS30 | 35.31°N | 140.31°E | 52.0 | 3.02 | 288 | 604 |
| IS45 | 43.7°N | 131.9°E | NaN | 10.46 | 290 | 560 |
| IS34 | 47.8°N | 106.41°E | 1288.0 | 28.56 | 290 | 516 |
| IS46 | 53.95°N | 84.82°E | NaN | 42.54 | 290 | 628 |
| IS53 | 64.87°N | 147.86°W | 200.0 | 48.06 | 356 | 848 |

traveling time. The location of the source will be the area where circular zone of three or more stations intersect at the same location. As a result, the Asian station intersects at 37.45 °N, 142.95 °E with a speed of 290 m/s whereas the Alaskan needs 356 m/s to reach the same location (dashed blue line). Delays of the tsunami origin time relative to the earthquake origin time by up to 100s changed the location of the tsunami source by less than 50km.

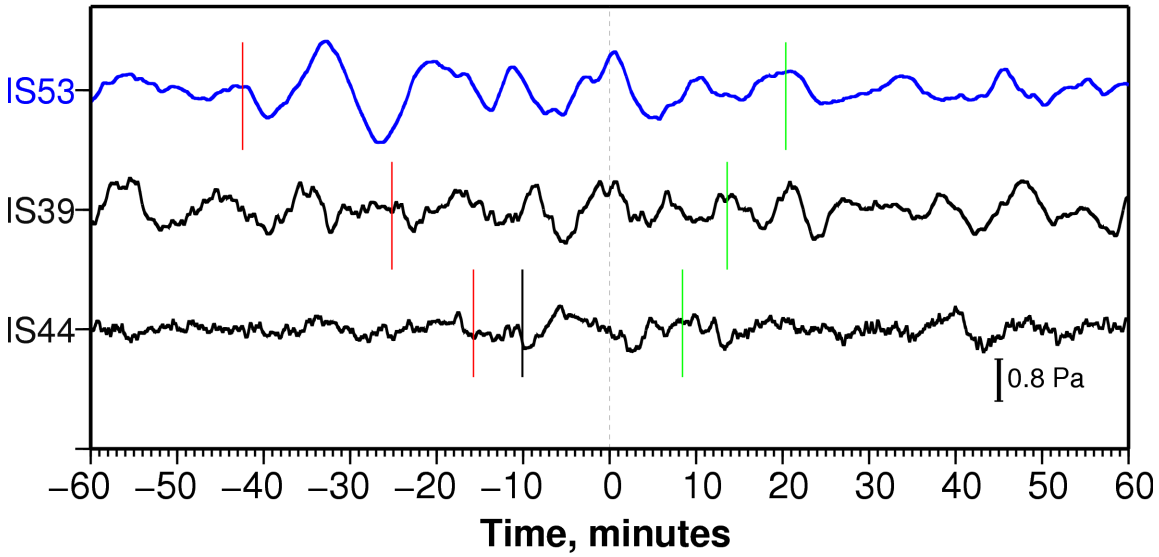


**Figure 4.21:** Black trace shows station where there was no signal. Alaskan station (blue) is taken as reference. The red and green marks indicate speeds of 356 and 290m/sec, respectively. Zero time corresponds to a speed of 310m/sec. A weak indication for a signal traveling with a speed of 330m/sec is marked in black at station IS44.

Figure 4.21 shows the infrasound records of the stations IS39 and IS44 in comparison with the station IS53 in Alaska. Zero time of the traces indicates the arrival time of a possible

signal traveling with a speed of 310m/sec. In our search, we fail to detect signal traveling with a speed of 356 and 290m/sec indicated by red an green marks respectively. A very weak signal traveling with a speed of 330 m/s may be detected at station IS44, which has a similar backazimuth like the Alaskan station. No signal is detectable above the noise level at station IS39 in the western Pacific, which has a backazimuth nearly opposite to the Alaskan station. This might be an effect of source directivity.

#### 4.2.4.3 Discussion

The location of the tsunami source obtained by using this technique is reasonably acceptable. Note that the largest observed GPS ground displacement and the tsunami source are all located within about 100km of each other and the seismic epicenter is also within the same area. It indicates that the Tohoku-Oki earthquake has generated dislocations of the sea surface in the epicentral region of the earthquake, which acted as source of ultra long period infrasound signals. Thus, infrasound source region is also the source region of the tsunami and the region with largest vertical displacements of the sea bottom. The common velocities of infrasound are near 300m/s with variations of ±50m/s due to wind speed [*Arrowsmith et al* 2010]. Here we observe for the Asian stations 290m/s and for the Alaskan station 356m/s. This could be explained by a strong wind component blowing in the opposite direction of the propagating infrasound to all Asian stations. For the Alaskan station a wind of about the same speed but in the same direction as the infrasound would increase its infrasound speed. Data from a larger number of better distributed and closer infrasound stations would certainly increase the accuracy of the location of the infrasound source. Therefore, real-time processing of infrasound observations may improve tsunami modeling for early warning purposes. Assuming an average water depth of 1000m, the speed of the tsunami is about three times less than the speed of infrasound. This means a tsunami needs about 15 minutes to reach a coast 100km away from the epicenter. The

infrasound signal of the tsunami already indicates 5 minutes after the origin time that a tsunami is definitely coming. From the size and the regional distribution of the infrasound signals a better modeling of the tsunami arriving at the shores may be obtained.

# Chapter 5

# DISCUSSION

It has been known for a long time that tsunamis induce seismic signals on the horizontal components of seismometers [*Angenheister* 1920; *Yuan et al.* 2005; *Hanson and Bowman* 2005] in the near field as well as regional and far field [*Okal* 2007]. The signal detected at the seismic station is the result of the tsunami reaching the shore and arrives nearly at the same time as the tsunami measured by tide gauge. The great Sumatra-Andaman earthquake of the 26 December 2004 caused seismic waves propagating through the solid Earth, tsunami waves propagating through the ocean and infrasound or acoustic-gravity waves propagating through the atmosphere. In this chapter, we compare infrasound data with data recorded at seismic station in order to explain the coupling mechanism between the ocean and the atmosphere.

## 5.1 Observed data

Figure 5.1 shows the direct comparison between the seismic data recorded at station DGAR and infrasound data recorded at station IS52 both on the island of Diego Garcia. The tsunami is well recorded on the long period seismic horizontal components [*Yuan et al.*

2005].

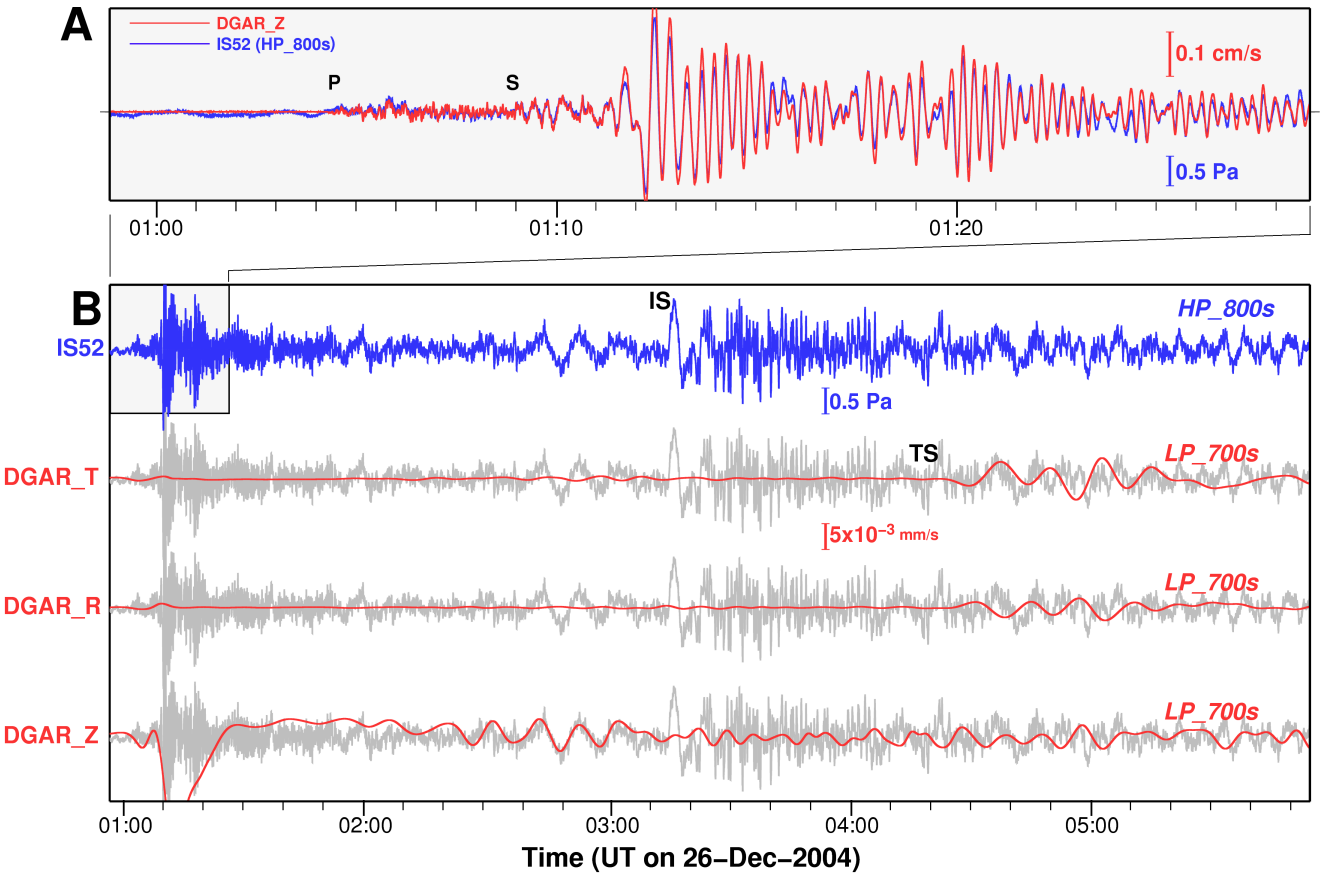


**Figure 5.1:** Comparison of seismic and infrasound records at Diego Garcia.(Filter used are written above the trace)
**A**(top): Seismic (red) and infrasound (blue) data zoomed between the first 30 min. **B**(bottom): (red) Long period filtered three-component seismic data. TS indicates the tsunami arrival and IS marks the infrasound arrival, (blue) Filtered infrasound data, gray traces are the duplicate of the infrasound blue trace.

By comparing the two traces recorded from two different types of instruments, the seismic and infrasound data in Figure 5.1-A show a nearly one to one agreement for the first half hour after the origin time of the Sumatra-Andaman earthquake. *Watada et al.* (2006) showed similar observations while analyzing the M8.3 Tokachi-Oki, Japan earthquake in 2003. This is an indication of the existing coupling between solid earth and the atmosphere. However, the coupling is not a total and the system where the phenomenon occurs is very complex. Therefore, we initially assumed that the good correlation between two traces in

the first half an hour could be partially caused by mechanical effect of the ground shaking during the passage of the seismic wave on the instrument.

Figure 5.1B shows different long period signal detectable not only on infrasound data (blue) but also on the three (vertical, radial and transversal) components of the seismic data (red). Therefore different type of filters are applied to each component. For the infrasound data, a second order high-pass Butterworth filter with a corner frequency of 800s is applied. The small box on the infrasound trace indicates the seismic phase which is zoomed on Figure 5.1A. The arrival of the infrasound caused by the tsunami is marked "IS".

We applied different filters for the seismic data. The vertical component is band-pass filtered by second order Butterworth with corner frequencies 200 s and 600 s. The Rayleigh wave groups traveling around the globe is observed on the filtered vertical component which starts nearly at 02:20 (UT) and stops at 04:30 (UT). An indication of long period signal is observed on infrasound trace which may correspond to this passage. No clear infrasound signal is identified at the arrival time of the tsunami. However, on the two horizontal components, a very clear signal related to the tsunami arrival time is observed and marked "TS". This is a confirmation of several similar observations, as mentioned in chapter 3, that seismometer horizontal components respond to the loading effect of the tsunami.

## 5.2 Synthetic data

Similarly to the comparison done with the observed data, Figure 5.2 shows the theoretical trace of both seismic and infrasound data. Thus, we compared a waveform of about 30 minutes length [Figure 5.2A]. The zero time of the trace corresponds to the origin time of the earthquake. A perfect agreement between both types of data is noticed up to

about 01:17 UT. This good correlation confirms that the near-perfect agreement between observed seismic and infrasound signals in Figure 5.1A is largely caused by coupling of solid Earth to atmosphere. Note that no instrument effect is introduced on the calculation of the theoretical trace. The amplitude scale of the signal does not have any physical meaning however we noticed that the ratio of the two traces is 5 Pa/(cm/s) which is exactly similar to what is observed data in Figure 5.1A. This indicates that the entire observed infrasound signal (Figure 5.1A) is indeed caused by leaking of seismic energy into pressure changes in the atmosphere. Shaking of the microbarograph does not contribute much to the infrasound record.

The theoretical seismic and infrasound records up to 01:17 UT agree very well. After that time we obtain strong infrasound signals predicted by the model but we do not observed similar signal in the recorded data. We interpret this signal as a vertical reflection of the waves, generated by the passage of seismic surface wave at the infrasound station, in the atmosphere and do not propagate horizontally. Their amplification may be caused by insufficient attenuation in the atmosphere of our model. We used in the atmosphere a quality factor Q of 100. Test computations with larger Q values increased the ringing effects drastically. The Q factor used here must be understood not necessarily as the usual Q caused by friction. It also represents attenuations caused by lateral heterogeneities and has therefore no physical meaning.

In Figure 5.2B the infrasound signal of the tsunami and also the tsunami effect on the seismometers is relatively well reproduced. The absence of any signal on the transverse component of the theoretical seismograms is due to the fact that the calculation is done for a point source. However, the radial component detects well the arrival of the tsunami at shore.

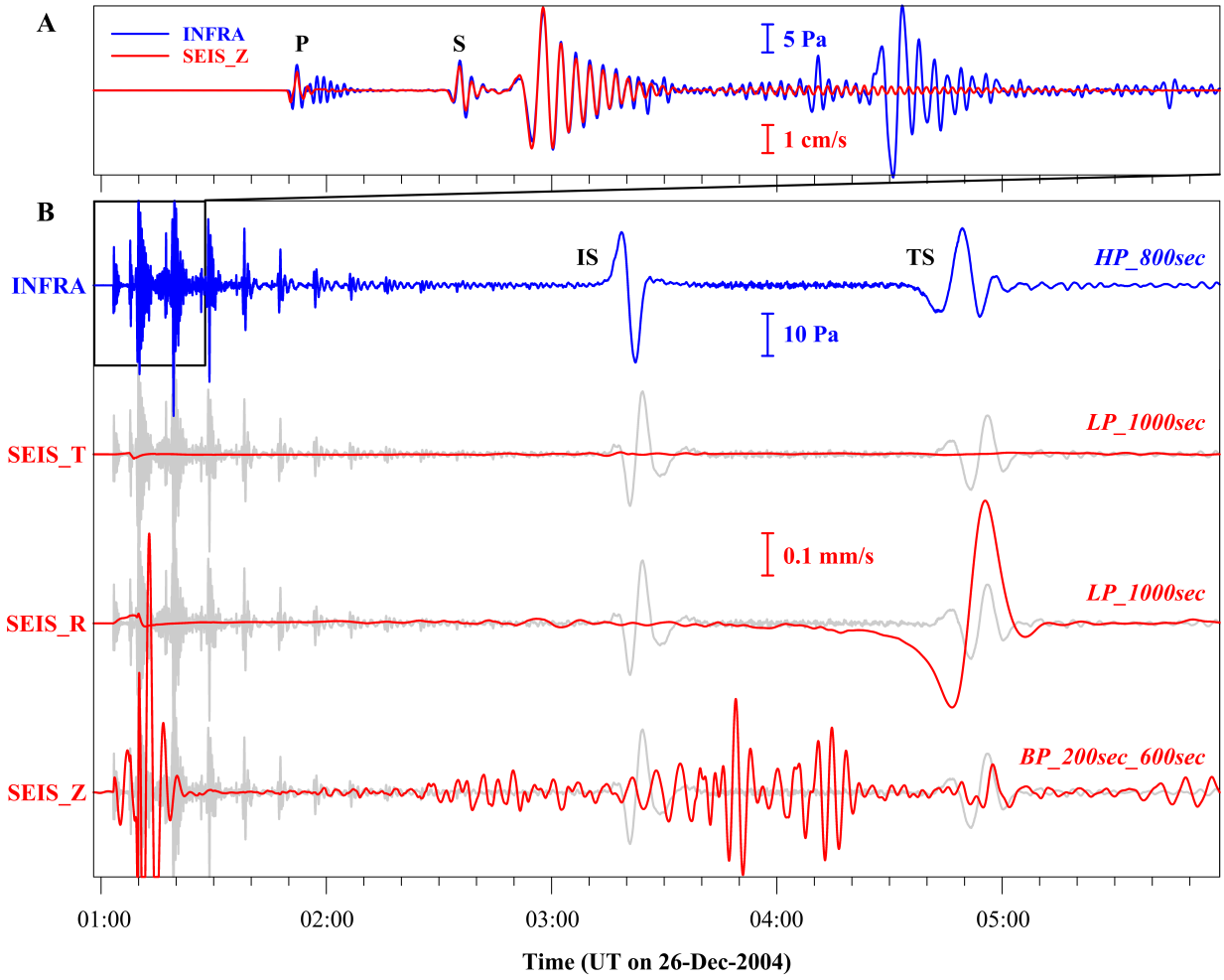


**Figure 5.2:** : Comparison of theoretical infrasound and seismic traces for the stations at Diego Garcia.
**A**: Zoom in of the synthetic data of seismic (red) and infrasound (blue). **B**:(blue) Filtered synthetic infrasound trace, gray traces are the duplicate of the blue. (red) Theoretical three component (vertical, radial and transverse) seismic signals for a point source

## 5.3 Infrasound generating seismic signal

It has been known for a long time that infrasound may also cause seismic signals [*Kanamori et al.*, 1991; *Neumann & Zürn* 1999]. Therefore we checked the seismic signals at the arrival time of the infrasound signals at Diego Garcia. Figure 5.3 shows a direct comparison between seismic and co-located infrasound trace. Blue traces named as SUM_IS52 are the summation trace from elements of the infrasound station array. A second order Butterworth high pass filter with a corner frequency of 800 s is applied to the result. An equivalent trace is computed and low-pass filtered with corner frequency of 200 s named INFRA. The seismic signals are in red: the observed vertical, radial and transverse components are called DGAR_Z, DGAR_R and DGAR_T respectively. Similarly, computed seismic signal are called SEIS_Z, SEIS_R and SEIS_T.

The zero time on the Figure 5.3, marked by vertical dashed line, corresponds to the arrival time of the infrasound signal caused by the sudden vertical displacement of the sea surface at the tsunami source. We marked the maximum amplitude of the signal and notice the time shift variation within the three components. We found a relatively clear correlation of all three seismic components with the first arriving acoustic-gravity signal. Figure 5.3 shows the comparison between theoretical and observed of the acoustic and seismic signals in Diego Garcia. There are an indications of a similarity between the calculated and observed trace. Thus, we align all three components of the seismic data on the arrival time of the infrasound and compare each component to the corresponding infrasound signal. Therefore, we observed that the vertical component of the seismic and the infrasound signal are completely in phase, in the observed traces as well as in the theoretical traces whereas the radial and transverse component are not. The theoretical traces behave nearly the same as the signal in the observation. Therefore we conclude that these observations are good evidence for infrasound signals producing seismic signals while passing at a seismic

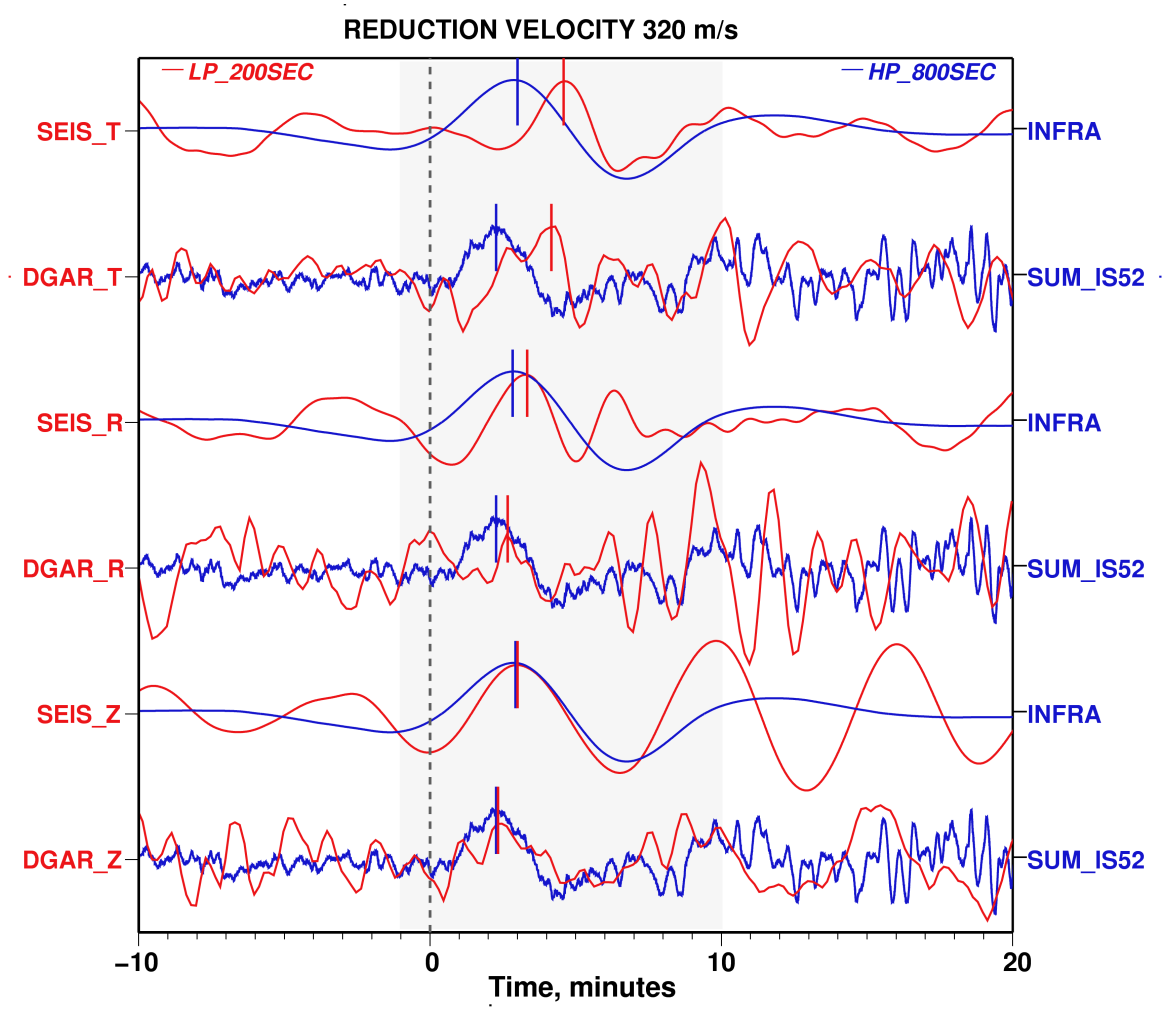


**Figure 5.3:** : Comparison of theoretical and observed infrasound and seismic signals at the arrival time of the infrasound signal at Diego Garcia.

station. However, the energy radiated on a seismic station is relatively small.

## 5.4 Conclusion

In Figure 5.4 the direct comparison of seismic and infrasound data is shown. Both types of data are displayed as a function of the distance to the earthquake epicenter [USGS: latitude 3.30°N, longitude 95.98°E on 26DEC2004 at 00:58:53.45]. The difference in the location of the epicenter of the earthquake and the source of the infrasound signal is not

considered in this figure. The seismic data show clearly a wave traveling with a velocity of about 203 m/s, which is a tsunami velocity. These waves have been observed by *Yuan et al.* (2005) and interpreted as effect of tilted ocean islands or ocean shores caused by the tsunami. The infrasound data shows a phase traveling with a velocity of about 320 m/s. The usual seismic phases are traveling with much faster velocity.

We have confirmed that the first arriving acoustic-gravity signal may originate from the tsunami source region that is the region of great changes of the sea level caused by changes of the sea floor due to the earthquake. Therefore these signals can be used for tsunami early warning purposes. Acoustic-gravity waves are usually recorded at microbarograph stations. We have shown that acoustic-gravity waves may also be recorded at seismic broadband stations. There exist usually more seismic stations than infrasound stations, therefore such stations may be supplemented by the large number of seismic stations in tsunami warning systems. It is known that seismic stations at ocean islands or coastal regions behave similarly to tide gauges or DART buoys and record tsunami. Now it seems useful to develop technique of scanning seismic data in order to identify an indications of infrasound signals radiated from the tsunami source region which arrive earlier than the tsunami and to use this information for early warning purposes.

The observation made for Tohoku-Oki event in Japan confirms that the sudden vertical displacement of the sea surface at the tsunami source produces a very long period acoustic gravity signal in the atmosphere. Infrasound station, designed to detect nuclear explosion in the atmosphere, can clearly detect such signal. The solution from our grid search of the minimum value of the residual time demonstrated the possible location of the tsunami source in an ellipse nearly perpendicular to the direction of the trench.

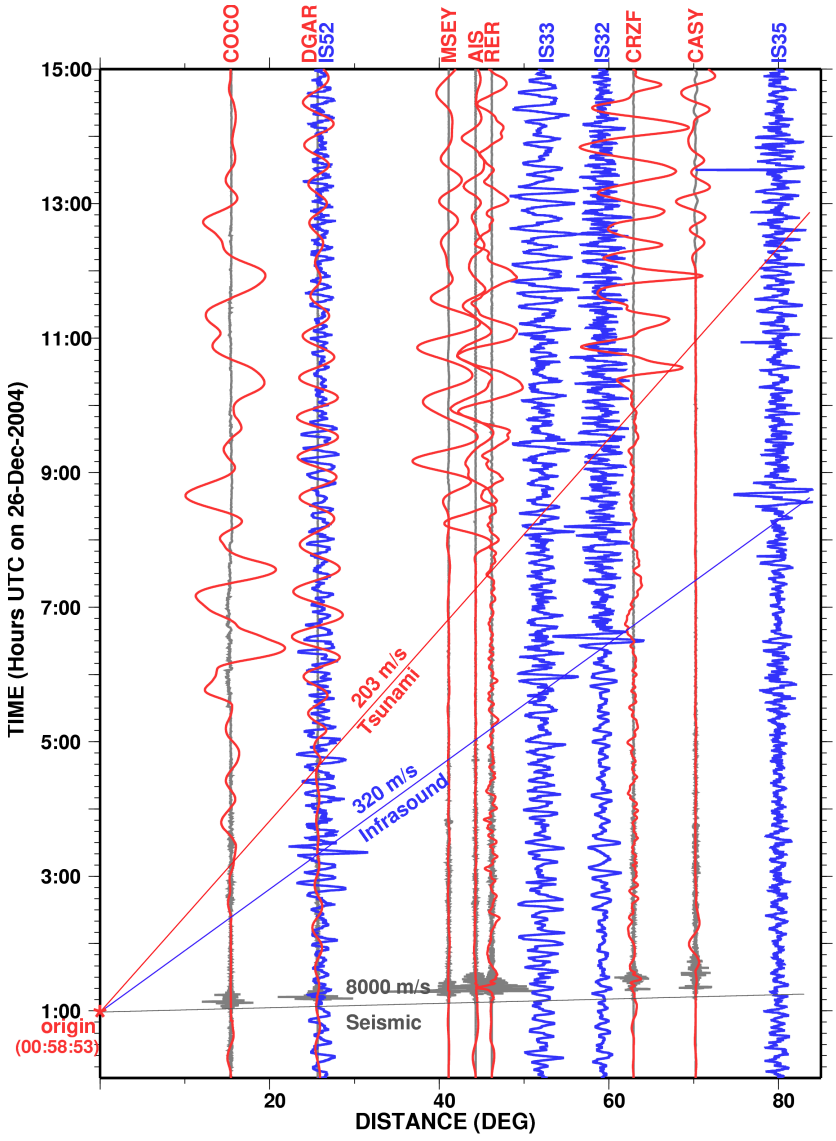


**Figure 5.4:** C: Seismic and infrasound records of the Sumatra-Andaman earthquake of 26 December 2004 sorted by epicentral distance of the stations. black: Original unfiltered seismic records; red: long period filtered seismic records; blue: long period filtered infrasound data. Straight lines with velocity indications for the different wave types are also given.

# Chapter 6

# Summary and Outlook

The aim of this work was to find an additional set of data which can provide additional information of evidence of tsunami following a great earthquake. This work demonstrates that seismometers can be very sensitive to the passage of tsunami for seismic stations deployed on oceanic island within distance less than 100km away from the shore line. Therefore, by applying a third order band pass Butterworth filter with a corner frequency between 1 mHz and 10 mHz, a very clear evidence of tsunami (large SNR) with a period of $\approx 30min$ was observed on the horizontal component of the seismometer. The seismic data show clearly a wave traveling with a velocity of about 203 m/s, which corresponds to the average velocity of a tsunami. For the station located on an island close to close to a continental boundary, combination of the multiple wave reflected from the continent and the effect of the shallow bathymetry are involved in the signal and the speed of the wave decreased. Comparison of signal observed on seismometer with data form nearby DART and tide gage stations demonstrate that seismometers respond to tsunami and can be used as a tsunameter. This can be advantageous for tsunami monitoring because seismic stations are located inland i.e. safe from any damage caused by the tsunami itself and free from local effect of the geometry of the local harbor.

The second dataset analyzed for tsunami detection in this study is infrasound. Initially, infrasound station installed by CTBTO, Vienna are designed to detect nuclear explosion in the atmosphere but since tsunami can excite the atmosphere due to the coupling effect, we were motivated to investigate tsunami signals on infrasound data. In this part, we focused on infrasound signals generated by a tsunami around the source itself. After analysis of data from IMS/CTBTO we have confirmed that the sudden vertical displacement of the sea surface at the tsunami source produces a very long period acoustic gravity signal in the atmosphere. The first arriving acoustic-gravity signal recorded at an infrasound station originates from the tsunami source region that is the region of great changes of the sea level caused by changes of the sea floor due to the earthquake. This location of the tsunami source obtained by using infrasound data corresponds to the largest coseismic slip obtained from GPS data analysis. It is somewhat located within about 100km from the maximal vertical displacement. In this study, we deducted that the velocity of the acoustic-gravity wave detected in the infrasound data travels near 300m/s with variations of $\pm$50m/s.

In chapter 5, we compare the seismic and infrasound data fro the Sumatra-Andaman event. For the first half an hour after the earthquake, a good agreement is found between these two data set. This might be caused by a mechanical effect of the shaking on the instrument. Besides, the same correlation between seismic and infrasound data was also found by doing comparison of theoretical data in which no instrument effect was introduced. The second observation from synthetic data demonstrates that earth-atmosphere coupling is also involved. Data from Diego Garcia shows an evidence of acoustic-gravity waves recorded at seismic station.

We have shown also that the infrasound signal travels faster than the seismic so infrasound

can not only be used for tsunami early warning purposes but it can be used for tsunami source location which might help tsunami modelers for the initial condition of their run.

As explained in this thesis, infrasound station can detect long period signal generated by tsunami. Therefore, in order to get a good coverage of data, it might be a task of future work to increase a number of infrasound station in the area close to a potential source of tsunami. As described before, location of the tsunami source was based on the empirical method of circle intersection used by seismologist. This implies that many simplification was applied during this study which need to be corrected. This may improve not only the location of the tsunami source but also a better estimation of the acoustic gravity wave speed.

Observation from one station indicated the presence of an acoustic gravity wave on seismic broadband station. Therefore, it might also be important to investigate more in detail these signal on seismic broadband station since there exist more seismic station than infrasound station deployed all around the world. Infrasound would be supplemented by the large number of seismic station in tsunami warning system.

# Bibliography


Abe, K. (1973). Size of great earthquakes of 1873 - 1974 inferred from tsunami data. *J. Geophys. Res.*, **84**, 1561 - 1568.

Abe, K. (1973). Tsunami and mechanism of great earthquakes, *Phys. Earth. Planet. Inter.* **7**, 143 – 153.

Abe, K. (1988). Tsunami magnitude and the quantification of earthquakes tsunamis around Japan. *Bull. Earthquake Res. Inst. Univ. Tokyo.* **63**,289 - 303.

Abe, K. (2007). Phases representing source Lengths of tsunami in Tide gauge records. *Pure appl.geophys..* **164**,453-463.

Afraimovich E.L., et al. (2001). The shock-acoustic waves generated by earthquakes, *Annales Geophysicae*,**19** 395-409.

Angenheister, G. (1920). Vier Erdbeben und Flutwellen im Pazifischen Ozean, beobachtet am Samoa- Observatorium, 1917-1919. *Nachrichten von der Gesellschaft der Wissenschaften zu Göttingen*, **201-204**.

Arendt, S., & Fritts, D. (2000). Acoustic radiation by ocean surface waves, *J. Fluid. Mech.*,**415**, 1-21.

Artru, J., V. Ducic, H. Kanamori, Ph. Lognonne and M. Murakami (2005), Ionospheric detection of gravity waves induced by tsunamis, *Geophys. J. Int.*, **160**, 840 - 848.

Arrowsmith, S. J., J. B. Johnson, D. P. Drob, and M. A. H. Hedlin (2010), The seismoacoustic wavefield: a new paradigm in studying geophysical phenomena, *Rev. Geophys.*,**48** RG4003.

Bilham, R., E .R. Engdahl, N. Feldl and S. P. Satyabala (2005), Partial and complete rupture of the Indo-Andaman plate boundary 1847- 2004, *Seismol. Res. Lett.*, **76**, 299-311.

Blanc, E. (1985). Observations in the upper atmosphere of infrasonic waves from natural or artificial sources: A summary, *Ann. Geophys.*, **3**, 673-688.

Boris, L., & Mikhail, N. (2009). Physics of tsunamis. *Springer, Netherlands.*

Brachet N., Brown D., Le Bras R., Mialle P., Coyne J. (2010). *Monitoring the earth's atmosphere with the global IMS infrasound network. Atmospheric variability and infrasound monitoring, Springer*,**73 – 114.**

Calais, E., Minster J.B., Michelle A.H. & Hedlin, M.(1998). Ionospheric signature of surface mine blasts from Global. Positioning System measurements. *Geophys. J. Int.*,**132**, 191-202.

Clinton, John F. (2004) Modern digital seismology - instrumentation, and small amplitude studies in the engineering world. *Dissertation (Ph.D.), California Institute of Technology.*

Comer, R.P. (1980). Tsunami height and earthquake magnitude: theoretical basis of an empirical relation. *Geophys. Res. lett.*, **7**, 445 - 448.

Daniels, Fred B.(1952). Acoustical Energy Generated by the Ocean Waves, *J. Acoust. Soc.*

*Am.*, **24**, 83-83 .

Degg, M. and Doornkamp, J.C. (1994). Earthquake hazard Atlas: 7 Iberia (Portugal and Spain) including the Azores: Balearics, Canary and Madeira Islands. *London: London Insurance and Reinsurance Market Association.*

Dotsenko, S.F., Kuzin, I.P., Levin, B.V., Solov'eva O.N. (2000). Tsunami in the Caspian sea: Seismic sources and features of propagation. *Oceanology*, **40**. 474 - 482.

Ducic, V., Artru, J. & Lognonné P.(2003)Ionospheric remote sensing of the Denali Earthquake Rayleigh surface waves. *Geophys. Res. Lett.*,**30**, 1951.

Dutykh, D., Dimitrios, D., Chubarov, L.,Shokin, Y. (2011) The contribution of horizontal sea-bed displacements into tsunami generation processes.
*http://arxiv.org/abs/1002.3019.*,**12**.

Eric, B. K., Joost, A. B. (1994). Atmosphere-Ocean Interaction, Second Edition, *Oxford monographs on geology and geophysics N 27*, **ISBN 019 506618 9** Earl, E.G., William H. (1975). Wave in the atmosphere: Atmospheric Infrasound and Gravity waves. Their generation and propagation, *Library of Congress Card Number: 73 89155*, **0 444 41196 8** Fine, I. V., Rabinovich A. B. & Thomson R. E. (2005), The dual source region for the 2004 Sumatra tsunami, *Geophys. Res. Lett.*, **32**, L16602.

Fitzgerald, T.J. (1997). Observations of total electron content perturbations on GPS signals caused by a ground level explosion. *J. of Atm. & Solar-Terrestrial Phys.* **59**, 829-834 .

Francis, P. W.(1985). The origin of the 1883 Krakatau tsunamis. *J. Volcanol.Geotherm. Res.*, **25**, 349 369.

Garces, M.,Hetzer, Claus., Businger, S., & Willis M. (2002). Modeling of microbarom signals in the Pacific. *paper presented at the 24th Seismic Research Review Nuclear Explosion Monitoring: Innovation and Integration.*

Garces, M., P. Caron, C. Hetzer, A. Le Pichon, H. Bass, D. Drob & Bhattacharyya J. (2005). Deep Infrasound Radiated by the Sumatra Earthquake and Tsunami. *Eos Trans. AGU*, **86**, 317-319.

Geller, R.J. (1976). Sacling relations for earthquake source parameters and magnitudes. *Bull. Seismol. Soc. Am.*, **66**, 1501 - 1523.

Gilbert, F. (1980) An introduction to low-frequency seismology. *In Proc. Intl. School Phys. "Enrico Fermi", (eds. A.M. Dziewonski and E. Boschi)*, **78**, 41 81 (North Holland, Amsterdam, 1980).

Gilbert, F. & Backus G. (1968). Elastic-gravitational vibrations of a radially stratified sphere, in Dynamics of Stratified Solids. *American Society of Mechanical Engineers, New York*, **82-95**.

Gladwin, M.T., Gwyther, R.L., Hart, R., Francis, M., Johnston, M.J.S. (1987). Borehole tensor strain measurements in California. *J. Geophys. Res.*, **92**, 7981 7988.

Gonzalez, F.I., Milburn, H.M., Bernard, E.N. and Newman, J.C. (1998). Deep-ocean Assessment and Reporting of Tsunamis (DART): Brief Overview and Status Report. *In Proceedings of the International Workshop on Tsunami Disaster Mitigation, 19-22 January 1998, Tokyo, Japan. Retrieved September 20, 2005.*
*http://www.pmel.noaa.gov/tsunami/dart_report1998.html*

Hanson, J.A. & Bowman, J., R. (2005). Dispersive and reflected tsunami signals from the

2004 Indian Ocean tsunami observed on hydrophones and seismic stations. *Geophys. Res. Lett*__17__, L17606.

Harbitz, C.B., Lovholt, F., Pedersen, G., & Masson, D.G. (2006). Mechanisms of tsunami generation by submarine landslides: a short review. *Norwegian Journal of Geology*, **86**, 255-264.

Hakrider, D., Press, F. (1967). The krakatoa Air-Sea Waves: an example of pulse propagation in coupled systems. *Geophys. J. R. astr. Soc.*, **13**, 149-159.

Harkrider,David G., Newton,Carl A. & Flinn,Edward A. (1974). Theoretical Effect of Yield and Burst Height of Atmospheric Explosions on Rayleigh Wave Amplitudes. *Geophys. J. R. astr. Soc.*, **36**, 191-225.

Hatori, T. (1979). Relation between tsunami magnitude and wave energy. *Bull. Earthq. Res. Inst. Univ. Tokyo*, **54**, 131 - 541.

Hébert, H., Heinrich, P., Schindelé, F., and Piatanesi, A. (2001). Far-field simulation of tsunami propagation in the Pacific Ocean: impact on the Marquesas Islands (French Polynesia). *J. Geophys. Res.*, **9161 - 9177.**

Heki, K.,Otsuka Y. , Choosakul N., Hemmakorn N., Komolmis T. & Maruyama T. (2006) Detection of ruptures of Andaman fault segments in the 2004 great Sumatra earthquake with coseismic ionospheric disturbances. *J. Geophys. Res.*, **111**, B09313.

Hidayat, D., Voight, B., Langston, C., Ratdomopurbo, A. & Ebeling, C. (2000). Broadband seismic experiment at Merapi Volcano, Java, Indonesia: very-long-period pulses embedded in multiphase earthquakes, *J. Volc. Geotherm. Res.*, **100**, 215 231.

Iida K., Cox, D.C., Pararas-Carayannis, G. (1967). Preliminary catalog of tsunami occurring in the Pacific Ocean. *Data Report No. 5, HIG-67-10. University of Hawaii, Hnolulu.*

Isaac V. Fine, Josef Y. Cherniawsky, Alexander B. Rabinovich, Stephenson F.(2009). Numerical modeling and observations of tsunami waves in Alberni Inlet and Barkley Sound, British Columbia. *Pure appl. geophys.*, **165**, 2019 2044.

Jacques, V. M. and Soloviev,S. L. (1971). Distant registration of small waves of tsunami type on the shelf of the Kuril. *Islands, Dok. Akad. Nauk USSR*, **198**, 816-817.

Ji, C. (2005), Magnitude 9.0 earthquake off the west coast of northern Sumatra: Preliminary rupture model, *report, U.S. Geol. Surv., Denver, Colo.*
*http://neic.usgs.gov/neis/eq_depot/2004/eq_041226/neic_slav_ff.html.*

Kajiura, K. (1963). The leading wave of a tsunami. *Bull. Earthquake Res. Inst.*, **41**, 535 571.

Kajiura, K. (1970). Tsunami source, energy and the directivity of wave radiation. *Bull. Earthquake Res. Inst.*, **48**, 835 869.

Kanamori, H. (1972). Mechanism of tsunami earthquakes, *Phys. Earth Planet. Int.*, **6**, 246 259.

Kanamori, H. J. Mori, D.L. Anderson & T.H. Heaton (1991). Seismic excitation by the space shuttle Columbia. *Nature*, **349**, 781 782.

Kulichkov, S., N. (2004). Long-range propagation and scattering of low-frequency sound pulses in the middle atmosphere. *Meteorol. Atmos. Phys.*, **85**, 47 60.

Kulichkov, S. N., Chunchuzov, I. P., Bush, G. A., & Perepelkin, V. G. (2008). Physical

modeling of long-range infrasonic propagation in the atmosphere. *Izvestiya Atmospheric and Oceanic Physics*, **44**, 175 186.

Kong, L. (2004).Scientists hope to save more lives by learning better ways to predict the approach of killer waves.*SCIENCE YEAR, The World Book Annual Science Supplement*(http://ioc3.unesco.org/itic/files/worldbook_tsunami.pdf)

Lander, J.F., Whiteside, L.S., Lockridge, P.A. (2002). A brief history of tsunami in the Caribbean Sea. *Sci. Tsunami Hazards*, **20**.

La Rocca, M., Galluzzo, D., Saccorotti, G., Tinti, S., Cimini, G.B., and Del Pezzo E. (2004), Seismic signals associated with landslides and with a tsunami at Stromboli Volcano, Italy. *Bull. Seismol. Soc. Amer.*, **94**, 1850 1867.

Lay T., H. Kanamori, C.J. Ammon, M. Nettles, S.N. Ward, R.C. Aster, S.L. Beck, S.L. Bilek, M.R. Brudzinski, R. Butler, H.R. DeShon, G. Ekstrom, K. Satake & Sipkin S. (2005). The great Sumatra-Andaman earthquake of 26 December 2004. *Science*, **308**, 1127-1133.

Le Pichon, A., Maurer, V., Raymond, D., & Hyvernaud, O. (2004). Infrasound from ocean waves observed in Tahiti. *Geophys. Res. Lett.*,**31**, L19103.

Le Pichon, A., P. Herry, P. Mialle, J. Vergoz, J. Brachet, N. Garces, D. Drob & Ceranna L. (2005), Infrasound associated with 2004-2005 large Sumatra earthquakes and tsunami. *Geophys. Res. Lett.*, **19**, L19802.

Longuet-Higgins, M. (1950). A theory of the origin of microseisms. *Phil, Trans. Royal Soc. London, Series A., Mathematical and Physical Sciences*,**243**,1-35.

Lognonné, P., Clévédé C., & Kanamori H. (1998). Normal mode summation of seismo-

grams and barograms in an spherical Earth with realistic atmosphere. *Geophys. J. Int., Geophys. J. Int.*, **135**, 388-406.

Meltzner, A. J. et al. (2006) Uplift and subsidence associated with the great Aceh-Andaman earthquake of 2004. *J. Geophys. Res.*,**111**, 02407

Mikumo, T., T. Shibutani, A. Le Pichon, M. Garces, D. Fee, T. Tsuyuki, S. Watad & Morii W.(2008), Low-frequency acoustic-gravity waves from coseismic vertical deformation associated with the 2004 Sumatra-Andaman earthquake (M-w=9.2), *J. Geophys. Res.*, **113**, B12402.

Nagarajan, B., Suresh, I., Sundar D., Sharma R., Lal, A. K., Neetu, S. , Shenoi, C., Shetye, S., R. and Shankar, D. (2006). The Great Tsunami of 26 December 2004: A description based on tide-gauge data from the Indian subcontinent and surrounding areas. *Earth Planets Space*, **58**, 211 215.

Neumann, U. & Zürn W. (1999). Gravity signals from atmospheric waves and their modeling, *Bull. Inf. Marees Terr.*, **131**, 10,139-10,152.

Nishida, K., Kobayashi, N., & Fukao Y.(2000). Resonant Oscillations Between the Solid Earth and the Atmosphere.*Science*, **287**, 2244.

Nikonov, A.A. (1997). Tsunami occurrence on the coasts of the Black Sea and the Sea of Azov. *Izv.Phys.Solid Earth*, **33**, 72 - 87.

Nosov M. A. (1998). Tsunami generation in compressible ocean.*Phys. Chem. Earth (B)*,**24**, 437-441.

Ohmachi, T., Inoue, S., Matsumoto, H., Tsukiyama, H. (2001). Tsunami simulation tech-

nique considering dynamic seabed displacement and acoustic effects of water. *Int. Tsunami Symp.*, **session 7**, 7-8.

Okal, E.A., and Titov, V. (2007). MTSU: Recovering seismic moments from tsunameter records. *Pure Appl. Geophys.*,**164**, 355 - 378.

Okal E. A. (2007). Seismic Records of the 2004 Sumatra and Other Tsunamis: A Quantitative Study. *Pure appl. geophys.*, **64**, 325 353 .

Osler, J. C., & Chapman, D. M. F. (1998). Quantifying the interaction of an ocean bottom seismometer with the seabed. *J. Geophys. Res.*, **103(B5)**, 9879 9894.

Posmentier, E. (1967). A Theory of Microbaroms. *Geophys. J. R. Astr. Soc.*, **13**, 487-501.

Piatanesi, A., & Lorito S. (2007), Rupture process of the 2004 Sumatra-Andaman Earthquake from Tsunami waveform inversion, *Bull. Seismol. Soc. Am.*, **97**, 223 231.

Rabinovich, A., & RICHARD, E. (2007).The 26 December 2004 Sumatra Tsunami: Analysis of Tide Gauge Data from the World Ocean Part 1. Indian Ocean and South Africa. *Pure appl. geophys.*, **164**, 261 308

Rhie J., & Romanowicz B. (2004). Excitation of Earth's continuous free oscillations by atmosphere ocean seafloor coupling. *Nature*, **431**, 552-556.

Rodgers P. W. (1968). The response of the horizontal pendulum seismometer to Rayleigh waves, Love waves, tilt, and free oscillations of the Earth, *Bull. Seism. Soc. Am.*, **58**, 1384-1406.

Saito, T., & Furumura T. (2009), Three-dimensional simulation of tsunami generation and propagation: Application to intraplate events, *J. Geophys. Res.*, **114**.

Sato M.,Ishikawa T.,Ujihara N., Yoshida S., Fujita M., Mochizuki M., Asada A.(2011). Displacement Above the Hypocenter of the 2011 Tohoku-Oki Earthquake. *Science*, **332**, 1395.

Song, Y. T., C. Ji, L.-L. Fu, V. Zlotnicki, C. K. Shum, Y. Yi, & Hjorleifsdottir V. (2005), The 26 December 2004 tsunami source estimated from satellite radar altimetry and seismic waves, *Geophys. Res. Lett.*, **32**, L20601.

Self, S., & Rampint,M., R. (1981) The 1883 eruption of Krakatau, *Nature*,**294**, 699-704.

Sigurdsson, H.; Carey, S.; Mandeville, C.; Bronto, S. (1991). Pyroclastic flows of the 1883 Krakatau eruption. *EOS 72*, **36**, 377-381.

Simon, D., Schneider, M.M. (1967). Zum Auftreten luftdruckbedingter Storungen in Horizontalpendelaufzeichnungen auf drei verschiedenen Erdgezeitenstationen. *B.I.M.*, **49**, 2218 2225.

Soloviev, S.L., Go C.N., Kim Kh.S. (1986). Catalogue of tsunamis in the Pacific ocean, 1969-1982. *Izd. MGK, USSR AS, Moscow.*

Soloviev, S.L. (1970). Recurrence of tsunamis in the Pacific. *In: "Tsunamis in the Pacific Ocean", East-West Center Press, Honolulu*, 149 - 164.

Subarya C., Chlieh M., Prawirodirdjo L., Avouac J.P., Bock Y., Sieh K., Meltzner A. J., Natawidjaja D. H. & McCaffrey R. (2006).Plate-boundary deformation associated with the great Sumatra Andaman earthquake.*nature*, **440**, doi:10.1038/04522 Takeuchi, H. & Saito M. (1972), Seismic surface waves, in Methods in Computational Physics, pp. 217-295, ed. Bolt, B. A., Academic Press, New York.

Tanioka, Y., & Seno T. (2001), Sediment effect on tsunami generation of the 1896 Sanriku tsunami earthquake, *Geophys. Res. Lett.*, **28**, 3389 3392.

Tinti, S., Bortolucci, E. & Chiavettieri, C. (2001). Tsunami Excitation by Submarine Slides in Shallow-water Approximation. *Pure Appl.Geophys.*, **158**, 759 797.

Tinti, S., Maramai A., and Graziani L.. (2004). The New Catalogue of Italian Tsunamis . *Nat. Haz.*, **33**, 439-465.

Titov, V. V, Mofjeld, H. O., Gonzalez, F. I., and Newman, J. C. (1999). Offshore forecasting of Alaska-Aleutian subduction zone tsunamis in Hawaii. *NOAA Tech. Memorandum, ERL PMEL-114, PMEL, Seattle, WA, 22*

Yamashita, T., & Sato R. (1974). Generation of tsunami by a fault model. *J. Phys. Earth*, **22**, 415 440.

Yanagisawa, M., and T. Wakasugi (1984). Observations of crustal tilt and strain indeced by the load of the 1983 Nihonkai-Chubu Earthquake tsunami. *J. Geod. Soc. Jpn.30* , **3**,204 212.

Yokoyama, I. (1981) A geophysical interpretation of the 1883 Krakatau eruption, *J. Volcanol. Geotherm. Res.*,**9**, 359-378.

Yokoyama, I. (1987) A scenario of the 1883. Krakatau tsunami, *J. Volcanol. Geotherm. Res.*,**34**, 123-132.

Yuan, X. H., R. Kind & Pedersen H. A. (2005). Seismic monitoring of the Indian Ocean tsunami.*Geophys. Res. Lett.*, **15**, L15308.

Yuen, P.C., Weaver, P.F., Suzuki, R.K. & Furumoto, A.S. (1969). Continuous traveling

coupling between seismic waves and the ionosphere evident in May 1968 Japan earthquake data. *J. Geophys. Res.*, **74**, 2256 2264.

Verbeek, R.D.M.(1885) Krakatau, *Govt. Press Batavia*,**495**.

Van Dorn, W G, LeMehaute, B, & Hwang, Li-San. (1968). *Final Report : Handbook of Explosion-Generated Water Waves.*

Wang J.G.,Nogami, T., Dasari, G.R.,Lin, P.Z.(2004). A weak coupling algorithm for seabed wave interaction analysis. *Comput. Methods Appl. Mech. Engrg.*, **193**, 3935 3956.

Wang, R., (1999). A simple orthonormalization method for stable and efficient computation of Green's functions. *Bull. Seism. Soc. Am.*, **89**, 733-741.

Watada, S.(1995). Part I: Near- source Acoustic Coupling Between the Atmosphere and the Solid Earth During Volcanic Eruptions, *PhD Thesis, California Institute of Technology.*

Watts, P., (2001). Potential landslides tsunami near Aitape, Papua New Guinea,*ITS 2001 Proceedings, Session 2, Number 2-11.* **425**

Wessel, P. & Smith, W. H. F. (1998). New, improved version of Generic Mapping Tools released.*Eos Trans. Amer. Geophys. Un.*,**79**, 47-579.

Widmer, R. & Zürn,W. (1992). Bichromatic excitation of long-period Rayleigh and air waves by the Mount Pinatubo and El Chichon volcanic eruptions. *Geophys. Res. Lett.*, **19**, 765-768.

Willis, M.,Garces M., Hetzer, C., & Businger, S. (2004). Infrasonic observations of open ocean swells in the Pacific: Deciphering the song of the sea. *Geophys. Res. Lett.*, **31**,

L19303.

# ACKNOWLEDGEMENT

I am deeply grateful to my supervisor, Prof. Dr. Rainer Kind from the Freie Universität Berlin, for his guidance, stimulating suggestions, patience, motivation and support. I consider myself very fortunate for being able to work with a very considerate and encouraging professor like him; I appreciated much his pragmatic approach to my research project which helps and motivates me to finish my study.

I wish to express my warm and sincere thanks to Prof. Dr. Frederik Tilman, Head of the Section seismology (2.4) at the German Research Centre for Geosciences (GFZ) Potsdam, for his valuable advice and friendly help. His extensive discussions around my work and perspective comment has improved chapters of this work.

I would like to express my gratitude to the committee members of my thesis for taking their precious time to consider my work.

I am grateful to Dr Rongjiang Wang, GeoForschungsZentrum (GFZ) Potsdam, for providing the synthetic infrasound data used in this study; he is always open for questions and discussions aspect about theoretical aspect. My sincere thanks also goes to Dr. Andrey Babeyko, GFZ Potsdam, for the theoretical marigram data for the Tohoku-Aki event.

I want to thank the GFZ, Helmholtz Centre Potsdam, for allowing me to carry my research work at the department of seismology and for giving me the permission to use all available facilities at the department. I would like to express my gratitude to the United Nation University in Bonn, Germany for the financial support during my stay in Germany and for giving grant to attend any scientific meeting which allows me to optimally carry out my research. I would like furthermore to thank Ms Evalyne Katabaro, PhD program Asso-

ciate for her indispensable help dealing with travel funds, administration and bureaucratic matters since my arrival to Germany until the end of my contract.

Collective and individual acknowledgments are also owed to my colleagues at GFZ whose present somehow perpetually refreshed, helpful, and memorable. I also want to thank you for the very good working environment we have shared together withing last few years. I would like to thank Dr Forough Sodoudi for giving me an effective introduction to seismic handler program and its application. Many thanks go in particular to Mrs Liane Lauterjung who persuaded me to follow a German class. That helped me a lot to deal with daily life problem here in Germany.

I convey special acknowledgment to my former professors, specifically Prof Gerard Rambolamanana, Head of the Institut et Observatoire de Geophysique d'Antananarivo without their prior teachings, I could never have embarked and started doing research work in geophysics. Thank you all.

Last but not the least, I would like to thank my brothers and sisters. Without their encouragement and understanding it would have been impossible for me to finish my research work abroad. My parents deserve special mention for their endless support.

# APPENDIX

**A1) Manuscript submitted Geophysical Journal International**

**Seismic and Acoustic-Gravity Signals from the Source of the 2004 Indian Ocean Tsunami**

A. Raveloson [1], W. Wang[1], R. Kind [1,2,*], L. Ceranna[3], X. Yuan[1]

[1] GFZ Deutsches GeoForschungsZentrum, 14473 Potsdam, Germany

[2] Freie Universität, Institut für Geologische Wissenschaften, 12249 Berlin, Germany

[3] Bundesanstalt für Geowissenschaften & Rohstoffe, 30655 Hannover,Germany

*Corresponding Author, email: *kind@gfz-potsdam.de*

## Abstract

The great Sumatra-Andaman earthquake of the 26 December 2004 caused seismic waves propagating through the solid Earth, tsunami waves propagating through the ocean and infrasound or acoustic-gravity waves propagating through the atmosphere. Since the infrasound wave is travelling faster than the tsunami, it is for warning purposes very intriguing to study the possibility of infrasound generation directly at the earthquake source. *Garces et al.* (2005) and *Le Pichon et al.* (2005) emphasized that infrasound was generated by mountainous islands near the epicenter and by tsunami propagation along the continental shelf to the Bay of Bengal. *Mikumo et al.* (2008) concluded from the analysis of travel times and amplitudes of first arriving acoustic-gravity waves with periods of about 400-700 s that these waves are caused by coseismic motion of the sea surface mainly to the west of the Nicobar islands in the open seas. We reanalyzed the acoustic-gravity waves and corrected the first arrival times of *Mikumo et al.* (2008) by up to 20 minutes. We found the source of the first arriving acoustic-gravity wave about 300 km to the north of the earthquake epicenter. This still confirms the result of *Mikumo et al.* (2008) that sea level changes at the earthquake source may cause long period acoustic-gravity waves.

Seismic and infrasound stations have been collocated in 2004 on the island of Diego Garcia. The infrasound signal from the tsunami preceded the actual tsunami (observed at the seismic station, see *Yuan et al.* 2005) by more than one hour. We have also found that the acoustic-gravity waves from the tsunami are visible in the seismic record at Diego Garcia. This opens the possibility to use the great number of seismic broadband stations in tsunami early warning systems for the detection of in the earthquake epicenter region generated acoustic-gravity waves before the actual tsunami arrives.

## Introduction

Tsunamis are long period gravity waves in the sea caused by vertical displacements of large quantities of seawater. For example, for the great Sumatra-Andaman earthquake of 26 December 2004, a vertical displacement of the seafloor of up to 10 m was estimated (*Bilham et al.* 2005, *Ji* 2005, *Fine et al.* 2005, *Song et al.* 2005 or *Heki et al.* 2006). The rupture area extended over about $1500x200km^2$. The resulting vertical displacement of huge masses of water caused a catastrophic tsunami flooding many shores of the Indian Ocean. Tsunamis are an oceanographic phenomenon and they are traditionally monitored with tide gauges or by sea floor pressure recorders (e.g. DART). The great Sumatra-Andaman tsunami has also been recorded by satellites, which might be a promising future perspective (*Fujii and Satake* 2007). However, it may also be possible to use ocean island and coastal stations of the global seismic network for direct tsunami observations. *Angenheister* (1920) already pointed out that on Samoa at the arrival time of the tsunami of the 17 September 1918 Kurils earthquake a signal was observed on the horizontal components at the seismic station Apia. *Yuan et al.* (2005), *Hanson and Bowman* (2005) and *Okal* (2007) observed clear effects of the Sumatra-Andaman tsunami in seismic data. Very similar effects of acoustic-gravity waves on seismic records are known (Neumann and Zürn 1999).

Vertical displacements of the Earth's surface, sea or land, may cause infrasound or acoustic-gravity waves in the atmosphere. There are reports of observations of such waves caused by the Sumatra-Andaman tsunami. *Le Pichon et al.* (2005) and *Mikumo et al.* (2008) used infrasound arrays of the International Monitoring System (IMS, http://www.ctbto.org/) and barograph stations in Japan for such observations. *LePichon et al.* (2005) located the source of their first arriving infrasound observations (dominant period  50 s) in the epicentral region of the earthquake. They also identified in the later parts of the records signals originating even from the northern part of the Bay of Bengal. *Mikumo et al.* (2008) identified 500 s acoustic-gravity waves caused by the tsunami and travelling with a speed of about 300 m/s. They used waveform modeling for determining the region of larges displacements of the seafloor. *Heki et al.* (2006) used GPS data to observe ionospheric disturbances caused by acoustic-gravity waves from the tsunami source region for estimations of the vertical displacement of the surface of the sea. Already *Bolt* (1964) observed dispersive acoustic-gravity waves from the great 1964 Alaska earthquake at the Berkeley station with periods of about 10 min and a velocity of about 310 m/s. He suggested using such observations for tsunami warnings. *Mikumo* (1968) reported additional barograph observations of the same earthquake and modeled their dispersion curves based on a theoretical development by *Harkrider* (1964). There are also many observations of infrasound signal caused by earthquakes that have occurred on land or at volcanoes which are not related to a tsunami [see *LePichon et al.* 2006, *Arrowsmith et al.* 2009 or *Wiens et al.* 2005].

## Data

Figure 1A shows the locations of the infrasound arrays and seismic stations used in this study. The seismic stations belong to the IRIS and GEOSCOPE networks; the infrasound

arrays to the IMS, Vienna. Each infrasound array consists of four to eight array elements with an aperture of about 2 km. In our study ultra longperiod data of the array elements have been summed without any time shifts to improve the signal-to-noise ratio.

The star in figure 1A shows the epicenter of the great Sumatra-Andaman earthquake from 26 December 2004 (according to the USGS). The rupture propagation is indicated by white dashed line. The location of the infrasound source was found by a grid search technique over an area of 10x10 degrees with the infrasound speed, the source coordinates and tsunami origin time as free parameters. Since the location error was increasing when moving the source away from the rupture track, it seems sufficient to display as an example (see figure 1B) only the latitude and wave speed as free location parameter and move the source along the rupture track. We minimized the differences between observed and predicted arrival times at the four infrasound stations (figure 2B). The best solution was found for an infrasound speed of 320 m/s and a source location at 5°N latitude and 94°E longitude (red cross in figure 1A). A delay of 108 s of the tsunami origin time relative to the origin time of the earthquake was obtained. This is fitting well the rupture velocity of 2.6 km/s obtained by *Lay et al.* (2005). Our infrasound source is located about 200 km to the south of the location by *Mikumo et al.* (2008), who derived their location from modeling of first arrival times and amplitudes of infrasound phases. Their arrival times at the stations IS32, IS33 and IS52 are 8, 7 and 20 min later than ours, respectively (see Fig. 1C and Table 1 by *Mikumo et al.* 2008). *Mikumo et al.* (2008) observed similar wind speeds in easterly and westerly directions which indicate that the wind speed was not very influential at that time. In figure 2 infrasound waveforms are displayed with time shifts according to different source parameters. In figure 2A source parameters of the earthquake are used; in figure 2B the new source parameters are used. The arrival times of the first infrasound signal are marked in figure 2B. This figure also shows the good signal-to-noise

ratio and the great similarity of the infrasound signals at all stations.

Figure 3 shows the records of the individual array components at the infrasound station at Diego Garcia (IS52 or I52). The travel times or time intervals used by *Le Pichon et al.* (2005) and Mikumo et al. (2008) are marked. The first arrival time given by *Mikumo et al.* (2008) seems astonishing.

Figure 4 shows the direct comparison between the seismic (station DGAR) and infrasound (station IS52) records on the island of Diego Garcia. The tsunami is well recorded on the longperiod seismic horizontal components (*Yuan et al.*, 2005). There is a nearly one to one agreement of the waveforms in the first half hour between seismic and infrasound traces (figure 4A). Similar observations have been made by *Watada et al.* (2006). Coupling between solid Earth and atmosphere and also between sea surface and atmosphere is well known and may be observed with GPS due to the coupling atmosphere-ionosphere (*Heki et al.* 2006, *Artru et al.* 2005). Shaking of the barograph by the seismic waves may also contribute to the sgnals. No clear infrasound signal is identified at the arrival time of the tsunami. The longperiod vertical seismic component in Figure 4B shows mainly Rayleigh wave groups travelling around the globe.

Figure 5 shows theoretical seismic and infrasound traces. The synthetics are calculated using a self-developed code based on normal mode theory (*Gilbert and Backus* 1968, *Takeuchi and Saito* 1972) and the orthonormalized matrix algorithm of *Wang* (1999) for numerical stability. The seismic reference model PREM is used for the computations for the seismic response at the ocean bottom. For a better fitting to the tsunami propagation velocity in the Indian Ocean, we changed the thickness of ocean layer in the original PREM model from 3 to 4 km. Infrasound traces are computed for a modified PREM model without

the ocean layer but with a standard atmosphere added (US Standard Atmosphere 1976). Tilt effects due to gravitational tsunami loading are included in the calculation of seismic synthetics, but no instrument effect is included. The theoretical seismic and infrasound records up to 01:17 UT agree very well. After that time we obtain strong infrasound signals but no according seismic signal. We interpret this signal as a standing wave in the atmosphere being caused by the arriving seismic surface waves and being reflected between the Earth's surface and the upper atmosphere. We used in the atmosphere a quality factor Q of 100. Test computations with larger Q values increased the ringing effects drastically. The Q factor used here must be understood not necessarily as the intrinsic Q caused by friction. It also represents attenuation caused by lateral heterogeneities, i.e. the scattering Q, and has therefore no real physical meaning. The good agreement in Figure 5A during the first 17 minutes between the theoretical seismic and infrasound traces confirms that the near-perfect agreement in Figure 4A between observed seismic and infrasound signals is largely caused by coupling of solid Earth to atmosphere. The infrasound signal of the tsunami and also the tsunami effect on the seismometers is relatively well reproduced. The theoretical seismograms in Figure 5B are calculated for a point source. There is therefore no signal on the transverse component caused by the tsunami loading.

It is known since a long time that infrasound may also cause seismic signals (e.g. Kanamori et al. 1991or Neumann and Zürn 1999). Therefore we checked the seismic signals at the arrival time of the infrasound signals at Diego Garcia (see figure 6). We found a relatively clear correlation of all three seismic components with the first arriving acoustic-gravity signal. The comparison with theoretical acoustic and seismic signals confirms this observation.

In Figure 7 the direct comparison of seismic and infrasound data is shown. Both types of data are displayed as a function of the distance to the earthquake epicenter (US Geological

Survey: latitude 3.30°N, longitude 95.98°E, 26DEC2004, 00:58:53.45). The relatively slight difference in the location of the epicenter of the earthquake and the source of the infrasound signal is not considered in this figure. The seismic data show clearly a wave traveling with a velocity of about 203 m/s, which is a tsunami velocity. These waves have been observed by *Yuan et al.* (2005) and interpreted as effect of tilted ocean islands or ocean shores caused by the tsunami (even much smaller tsunamis from landslides have been observed in seismic records, *La Rocca et al.* 2004). The infrasound data show a phase travelling with a velocity of about 320 m/s. The usual seismic phases are travelling with much faster velocity.

## Discussion and Conclusions

We have confirmed that the first arriving acoustic-gravity signal may originate from the tsunami source region that is the region of great changes of the sea level caused by changes of the sea floor due to the earthquake. Therefore these signals may be used for tsunami early warning purposes. Acoustic-gravity waves are usually recorded at microbarograph stations. We have shown that acoustic-gravity waves may also be recorded at seismic broadband stations. There exist usually more seismic stations than infrasound stations, therefore such stations may be supplemented by the large number of seismic stations in tsunami warning systems. It is known that seismic stations at ocean islands or coastal regions are also recording the tsunami (similar to tide gauges or DART buoys). Now it seems useful to scan these seismic data also for indications of infrasound signals radiated from the tsunami source region which arrive earlier than the tsunami and to use this information for early warning purposes.

## Acknowledgements

We wish to thank Emile Okal for pointing out the Angenheister observations and Frederik Tilmann for reading the manuscript and for discussions. This research was supported by

the GITEWS project of the German Federal Ministry for Education and Research and by the United Nations University, Bonn.

## References

Angenheister, G. (1920), Vier Erdbeben und Flutwellen im Pazifischen Ozean, beobachtet am Samoa- Observatorium, 1917–1919. *Nachrichten von der Gesellschaft der Wissenschaften zu Göttingen*, **201-204**.

Arrowsmith, S. J., R. Burlacu, R. Whitaker and G. Randall (2009), A repeating secondary source of infrasound from the Wells, Nevada, earthquake sequence, *Geophys. Res. Lett.*, **36**.

Artru, J., V. Ducic, H. Kanamori, Ph. Lognonne and M. Murakami (2005), Ionospheric detection of gravity waves induced by tsunamis, *Geophys. J. Int.*, **160**, 840-848.

Bilham, R., E .R. Engdahl, N. Feldl and S. P. Satyabala (2005), Partial and complete rupture of the Indo-Andaman plate boundary 1847- 2004, *Seismol. Res. Lett.*, **76**, 299–311.

Bolt, B. A. (1964), Seismic air waves from the great 1964 Alaskan earthquake, *Nature*, **202**, 1095– 1096.

Fine, I. V., A. B. Rabinovich, and R. E. Thomson (2005), The dual source region for the 2004 Sumatra tsunami, *Geophys. Res. Lett.*,**32**.

Fujii, Y. and K. Satake (2007), Tsunami Source of the 2004 Sumatra-Andaman Earthquake Inferred from Tide Gauge and Satellite Data, *Bull. Seism. Soc. Am.*, **97**, S192-S207.

Garces, M., P. Caron, C. Hetzer, A. Le Pichon, H. Bass, D. Drop and J. Bhattacharyya (2005), Deep infrasound radiated by the Sumatra earthquake and tsunami, *EOS Trans.*

*AGU*, **86(35)**, 317-319.

Gilbert, F. and G. Backus (1968), Elastic-gravitational vibrations of a radially stratified sphere, in Dynamics of Stratified Solids, pp. 82-95, ed. G. Herrmann, American Society of Mechanical Engineers, New York.

Hanson, J.A. and J. R. Bowman (2005) Dispersive and reflected tsunami signals from the 2004 Indian Ocean tsunami observed on hydrophones and seismic stations. *Geophys. Res. Lett*, **17**.

Harkrider, D. G. (1964), Theoretical and observed acoustic-gravity waves from explosive sources in the atmosphere, **J. Geophys. Res.**, **69**, 5295- 5321.

Heki, K., Y. Otsuka, N. Choosakul, N. Hemmakorn, T. Komolmis, and T. Maruyama (2006) Detection of ruptures of Andaman fault segments in the 2004 great Sumatra earthquake with coseismic ionospheric disturbances, J. Geophys. Res., 111, B09313.

Ji, C. (2005), Magnitude 9.0 earthquake off the west coast of northern Sumatra: Preliminary rupture model, *report, U.S. Geol. Surv., Denver, Colo.* (Available at emphhttp://www.pmel.noaa.gov/tsunami/dart_report1998.html

Kanamori, H., J. Mori, D.L. Anderson and T.H. Heaton (1991) Seismic excitation by the space shuttle Columbia. *Nature* **349**, 781-782.

La Rocca, M., D. Galluzzo, G. Saccorotti, S. Tinti, G.B. Cimini and E. Del Pezzo (2004) Seismic signals associated with landslides and with a tsunami at Stromboli volcano, Italy. Bull. *Seism. Soc. Am.* **94**, 1850-1867.

Lay T., H. Kanamori, C.J. Ammon, M. Nettles, S.N. Ward, R.C. Aster, S.L. Beck, S.L.

Bilek, M.R. Brudzinski, R. Butler, H.R. DeShon, G. Ekstrom, K. Satake and S. Sipkin (2005) The great Sumatra-Andaman earthquake of 26 December 2004. *Science* **308**, 1127-1133.

Le Pichon, A., P. Herry, P. Mialle, J. Vergoz, J. Brachet, N. Garces, D. Drob and L. Ceranna (2005), Infrasound associated with 2004-2005 large Sumatra earthquakes and tsunami, *Geophys. Res. Lett.*, **19**.

Le Pichon, A., P. Mialle, J. Guilbert and J. Vergoz (2006), Multistation infrasonic observations of the Chilean earthquake of 2005 June 13, *Geophys. J. Int.*, **167**, 838-844.

Mikumo, T. (1968), Atmospheric pressure waves and tectonic deformation associated with the Alaskan earthquake of March 28, 1964, *J. Geophys. Res.*, **73**, 2009- 2025.

Mikumo, T., T. Shibutani, A. Le Pichon, M. Garces, D. Fee, T. Tsuyuki, S. Watad and W. Morii (2008), Low-frequency acoustic-gravity waves from coseismic vertical deformation associated with the 2004 Sumatra-Andaman earthquake (M-w=9.2), *J. Geophys. Res.*, **113**.

Neumann, U. and W. Zürn (1999), Gravity signals from atmospheric waves and their modeling, *Bull. Inf. Marees Terr.*, **131**, 10,139-10,152.

Okal, E. A. (2007), Seismic records of the 2004 Sumatra and other tsunamis: A quantitative study, *Pure and Applied Geophysics*, **164**, 325-353.

Song, Y. T., C. Ji, L.-L. Fu, V. Zlotnicki, C. K. Shum, Y. Yi, and V. Hjorleifsdottir (2005), The 26 December 2004 tsunami source estimated from satellite radar altimetry and seismic waves, *Geophys. Res. Lett.*, **32**.

Takeuchi, H. and M. Saito (1972), Seismic surface waves, in Methods in Computational Physics, pp. 217-295, ed. Bolt, B. A., Academic Press, New York.

U.S. Standard Atmosphere, 1976, U.S. Government Printing Office, Washington, D.C., 1976.

Watada, S., T. Kunugi, K. Hirata, H. Sugioka, K. Nishida, S. Sekiguchi, J. Oikawa, Y. Tsuji and H. Kanamori (2006), Atmospheric pressure change associated with the 2003 Tokachi-Oki earthquake, *Geophys. Res. Lett.*, **33**.

Wang, R.J. (1999), A simple orthonormalization method for stable and efficient computation of Green's functions, *Bull. Seism. Soc. Am.*, *89*, 733-741.

Wiens, D.A., S.H. Pozgay, A.W. Sauter and R.A. White (2005) Tilt recorded by a portable broadband seismograph: The 2003 eruption of Anatahan Volcano, Mariana Islands, *Geophys. Res. Lett.*, **32**.

Yuan, X. H., R. Kind and H. A. Pedersen (2005), Seismic monitoring of the Indian Ocean tsunami, *Geophys. Res. Lett.*, **15**.

## Figures

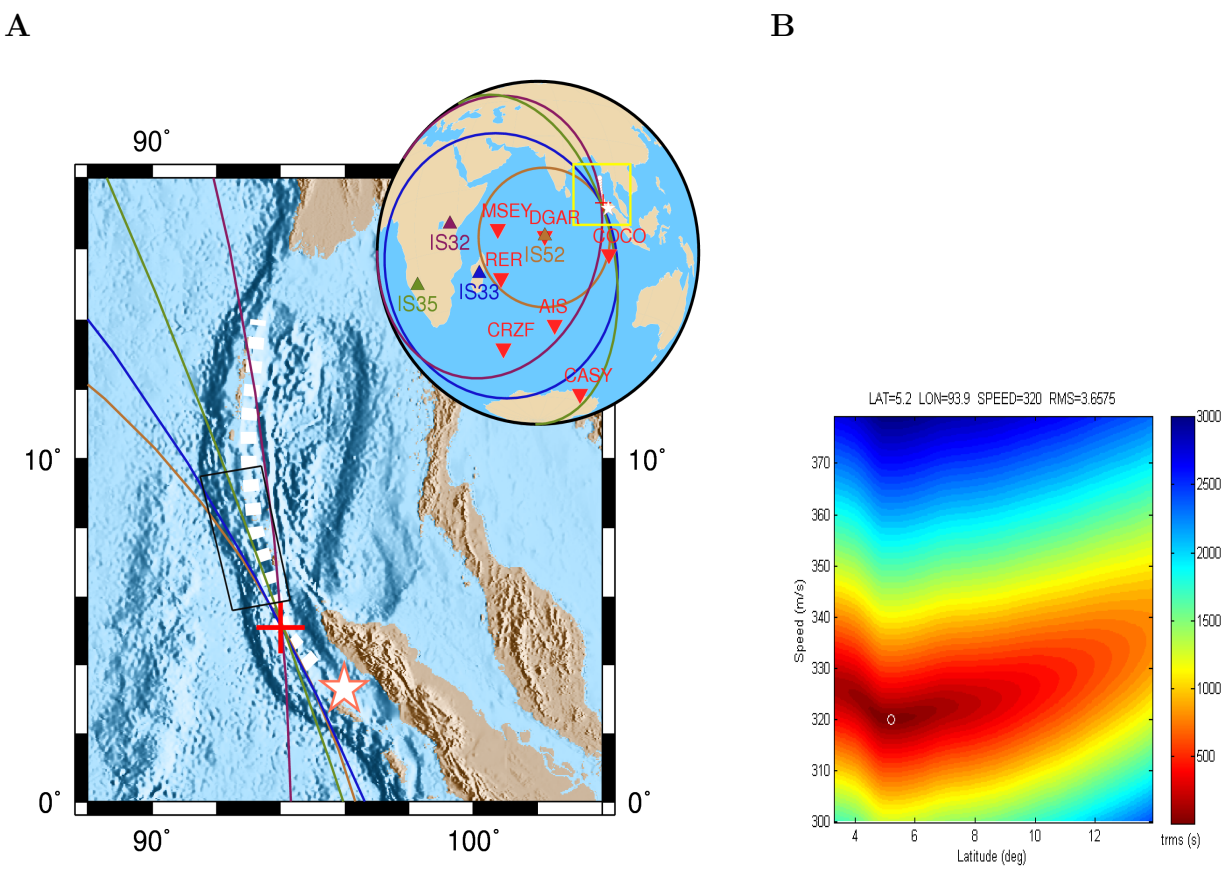


**Figure 1:** A) Seismic stations are indicated by red inverted triangles in the inset. Infrasound stations are represented by color coded triangles. The star marks the earthquake epicenter and white dashed line represents the earthquake rupture track. The red plus sign represents the location of the source of the first arriving infrasound signals at the infrasound stations. This location was determined by a grid search through the parameter space of geographical location and origin time of the tsunami and of sound velocity. The resulting best fitting parameters are: sound velocity 320 m/s, epicenter at 5°N and 94°E, origin time 01:00:37 UT. This tsunami origin time is 108 s after the earthquake origin time determined by the USGS. The earthquake rupture reached the tsunami epicenter after propagating with a rupture speed of 2.6 km/s (Lay et al. 2005) for 108 s. The circles mark the possible source location according to the infrasound travel time to each station. The infrasound epicenter is located at the intersection of all circles. The infrasound source region of Mikumo et al. (2008) is marked by the box north of our epicenter. B) Time residuals as a function of two parameters: the sound speed and the latitude along the rupture track (white dashed line). The parameter "latitude along rupture track" was chosen as an example of the space of the geographical coordinates. The actual search has been done in a much wider range of latitude and longitude. White circle describes the source location of the infrasound.

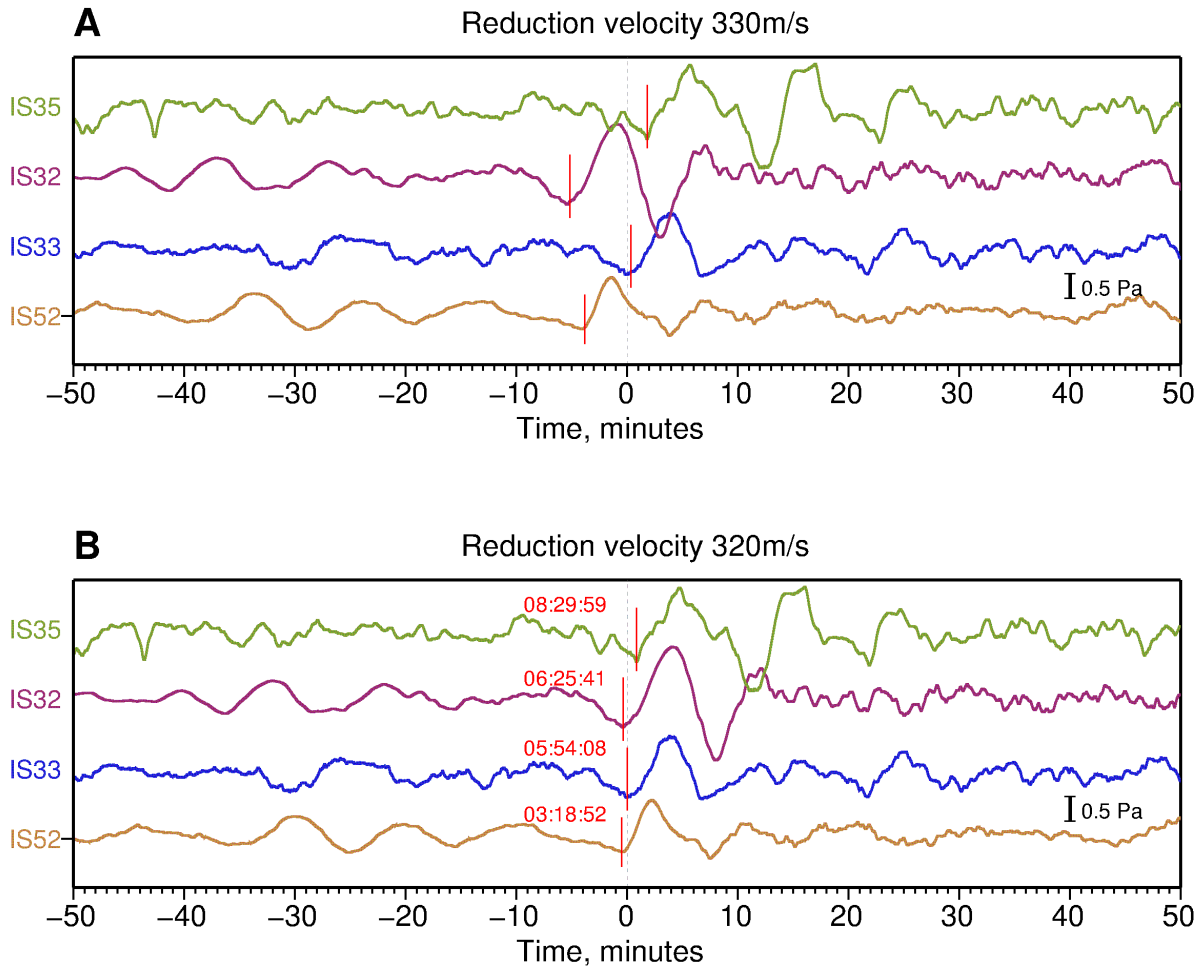


**Figure 2:** Summed infrasound records of the first arriving signal from the tsunami at each of the four infrasound arrays. The traces are filtered with an 800 s high pass filter. A) Tsunami source is assumed at earthquake epicenter and origin time. Traces are shifted according to a reduction velocity of 330 m/s (meaning a wave travelling with this velocity would arrive at zero time). The average infrasound speed to each station is close to 330 m/s, assuming the earthquake epicenter also as infrasound epicenter. B) Tsunami source parameters and infrasound velocity are taken from the caption of Fig. 1. Infrasound first arrival times are given at the traces. The scatter of the wave forms in B is clearly less than in A. That means our epicenter and origin time fit the infrasound data better than the earthquake epicenter and origin time.

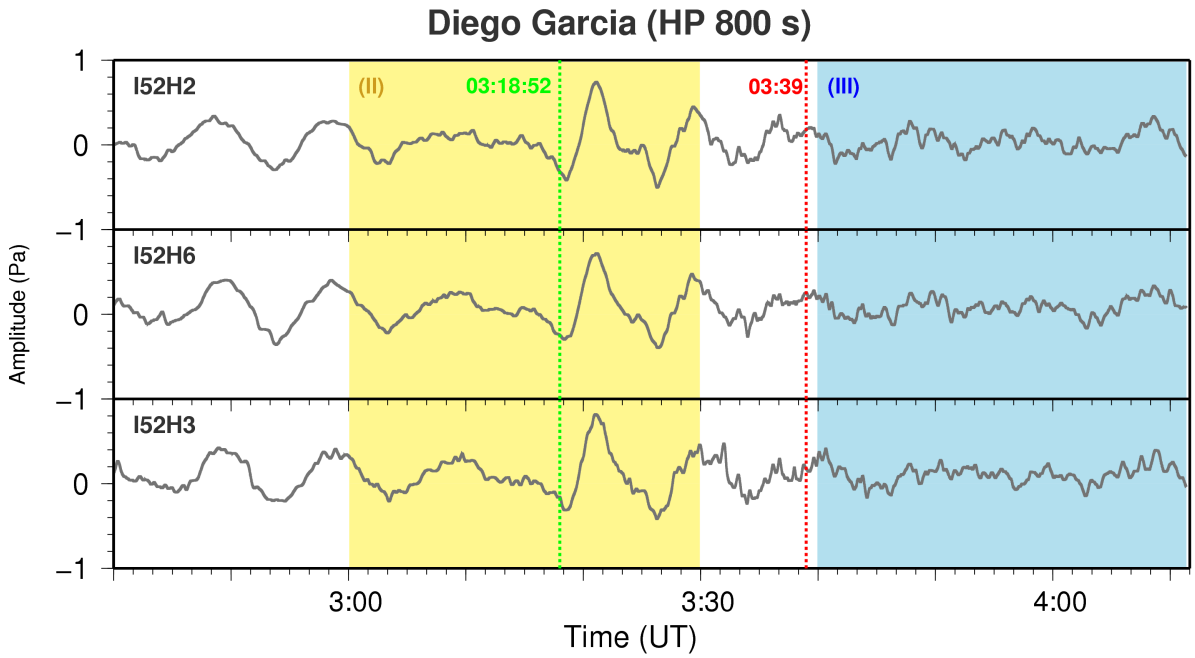


**Figure 3:** Infrasound records of the three individual components of the infrasound array at Diego Garcia filtered with an 800 s high pass filter. Le Pichon et al. (2005) located the source of the signals in group II (yellow) in the extended area of the seismic source but did not conclude that the infrasound waves have been caused by coseismic uplift and subsidence of the sea bottom and associated swelling and depression of the sea surface. They located the sources of the secondary signals in group III (blue) in the area between Sumatra and the Bay of Bengal. Mikumo et al. (2008) concluded that the first arriving signals have been caused by sea level changes in the open seas at the seismic source area. However, they gave partly questionable arrival times of the first signals. In the case of Diego Garcia their first arrival time (03:39, see vertical red line) is about 20 minutes later than ours (03:18:52, see vertical green line). We compared the infrasound time scale with the seismic time scale at Diego Garcia and found no error in our time determination (see Fig. 4 A).

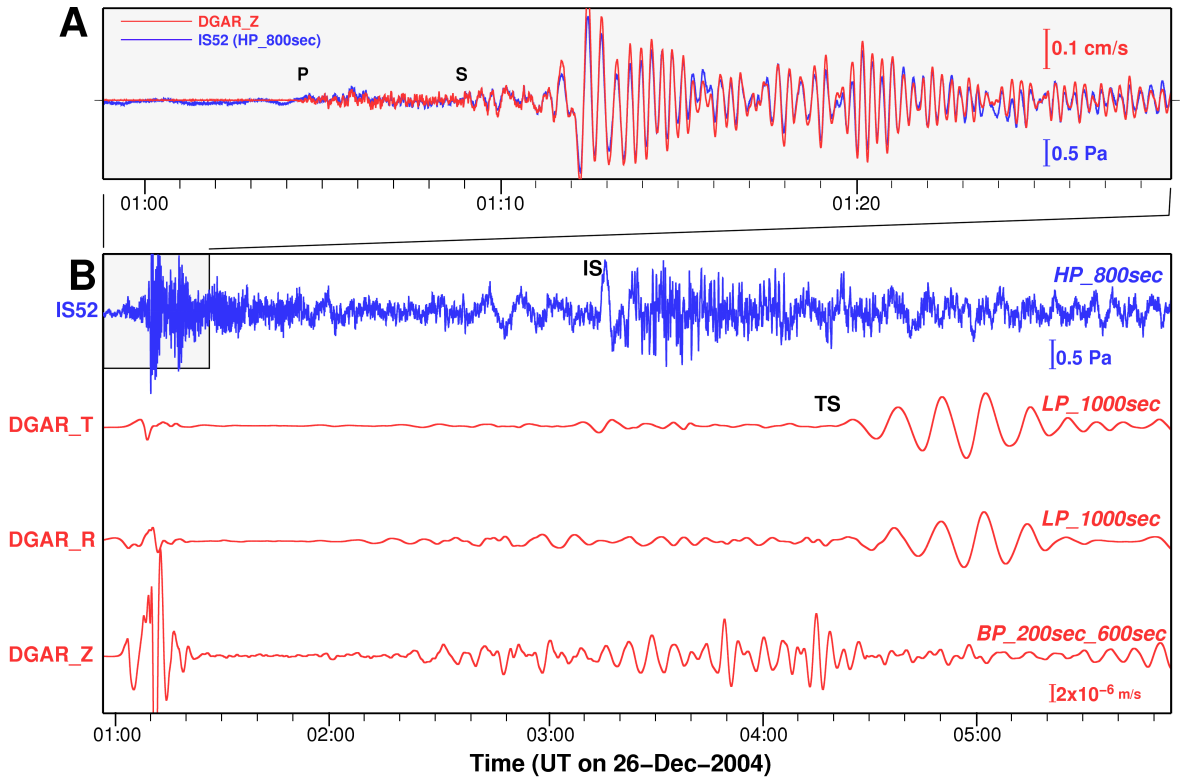


**Figure 4:** Comparison of seismic and infrasound records at Diego Garcia. A: High resolution comparison of seismic (red) and infrasound (blue) records at Diego Garcia. P and S are seismic body waves. There is a nearly perfect agreement of seismic and infrasound records. The ratio of the two traces is about 5 Pa/ (cm/s). B red: Longperiod filtered three-component seismic records of the Andaman earthquake recorded at the station on the island of Diego Garcia (DGAR) in the Indian Ocean. The vertical component shows practically only surface waves circling around the Earth. Different filters are indicated; LP = low pass, BP = band pass. The TS signals on the horizontal components are caused by tilting of the sea bottom together with the entire island by the tsunami (Yuan et al. 2005, Okal 2007). B blue: Filtered infrasound record of the earthquake also on Diego Garcia (IS52). IS marks the infrasound signal.

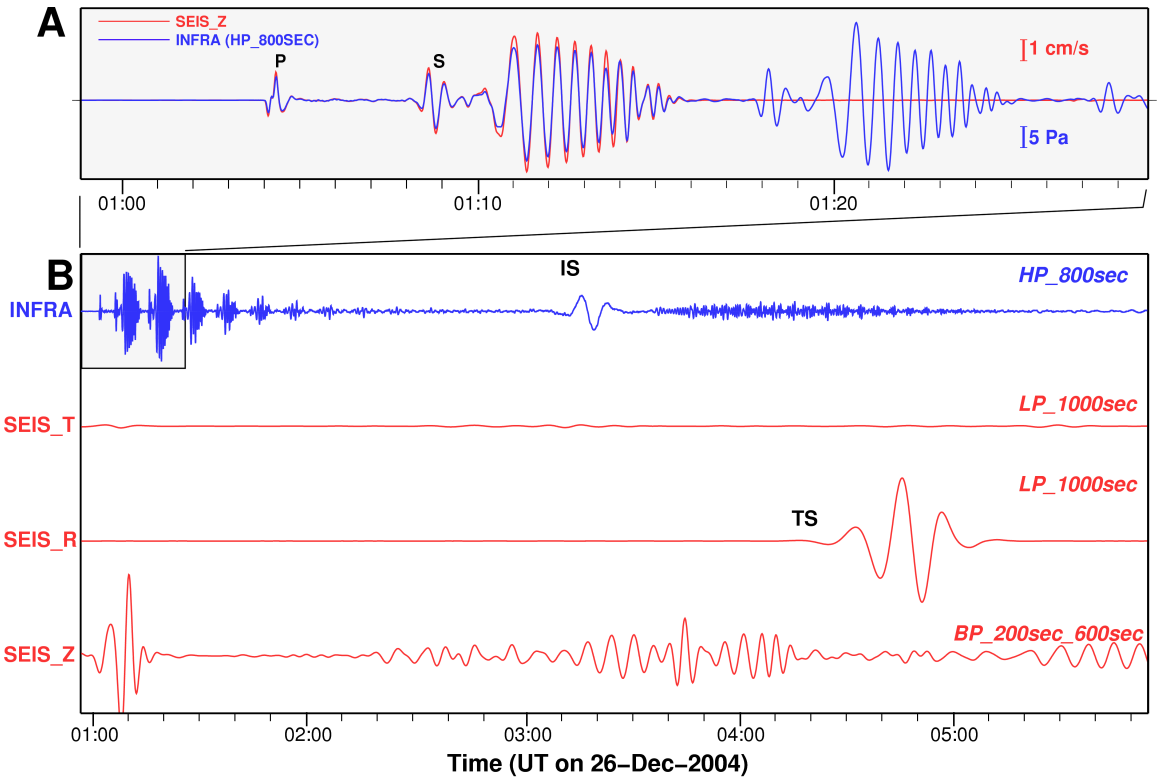


**Figure 5:** Theoretical infrasound and seismic traces for the stations at Diego Garcia. A: There is nearly perfect agreement of both types of data up to about 01:17 UT. The ratio of the two traces is, exactly like in the observed data in Fig. 4A, 5 Pa/ (cm). This indicated that the entire infrasound signal in Fig. 4A is indeed caused by leaking of seismic energy into pressure changes in the atmosphere. Shaking of the microbarograph does not contribute much to the infrasound record. There is another strong infrasound signal around 01:20 predicted by the model, which is not observed. Several more signals of similar type are following (blue trace in B). These signals are probably vertical reflections in the atmosphere which are not propagating horizontally. They may be caused by insufficient attenuation in atmosphere of our model. The red traces in B are theoretical three component (vertical, radial and transverse) seismic signals at the ocean bottom for a point source. The tsunami signal is clearly obtained on the radial component. The transverse component has no tsunami signal because of the point source.

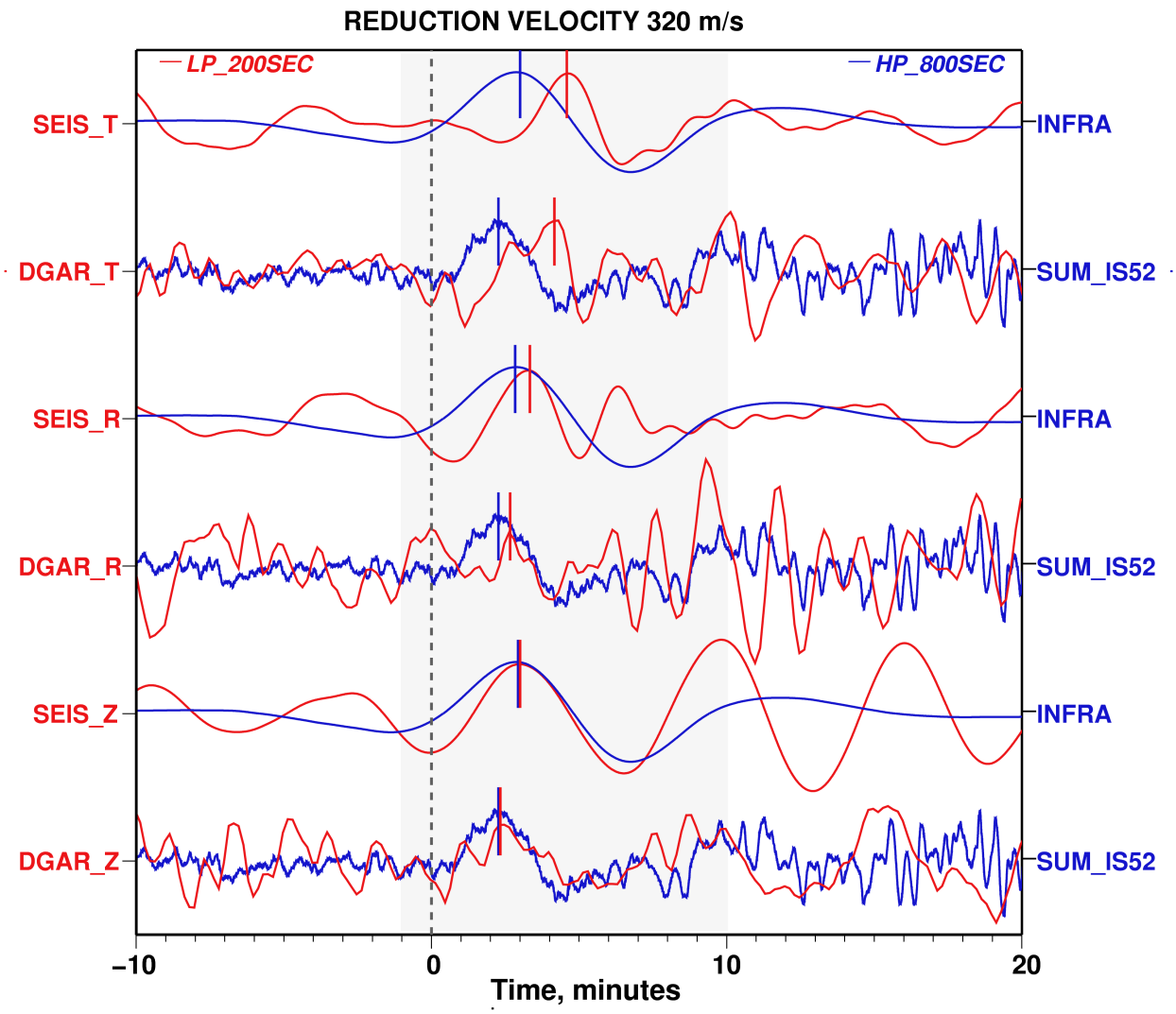


**Figure 6:** Comparison of theoretical and observed infrasound and seismic signals at the arrival time of the infrasound signal at Diego Garcia. The infrasound signals are blue (SUM_IS52 is observed and INFRA is computed). The seismic signals are red; DGAR_Z, DGAR_R and DGAR_T are the observed vertical, radial and transverse components. SEIS_Z, SEIS_R and SEIS_T are the according computed seismic signals. There are also indications of a very similar signal in the seismic traces. The vertical seismic signal and the infrasound signal are completely in phase, in the observed traces and in the theoretical traces. On the radial and transverse observed traces are the infrasound signals also visible, but out of phase. The theoretical traces behave exactly in the same way. Therefore we conclude that these observations are good evidence for infrasound signals producing seismic signals when passing a seismic station.

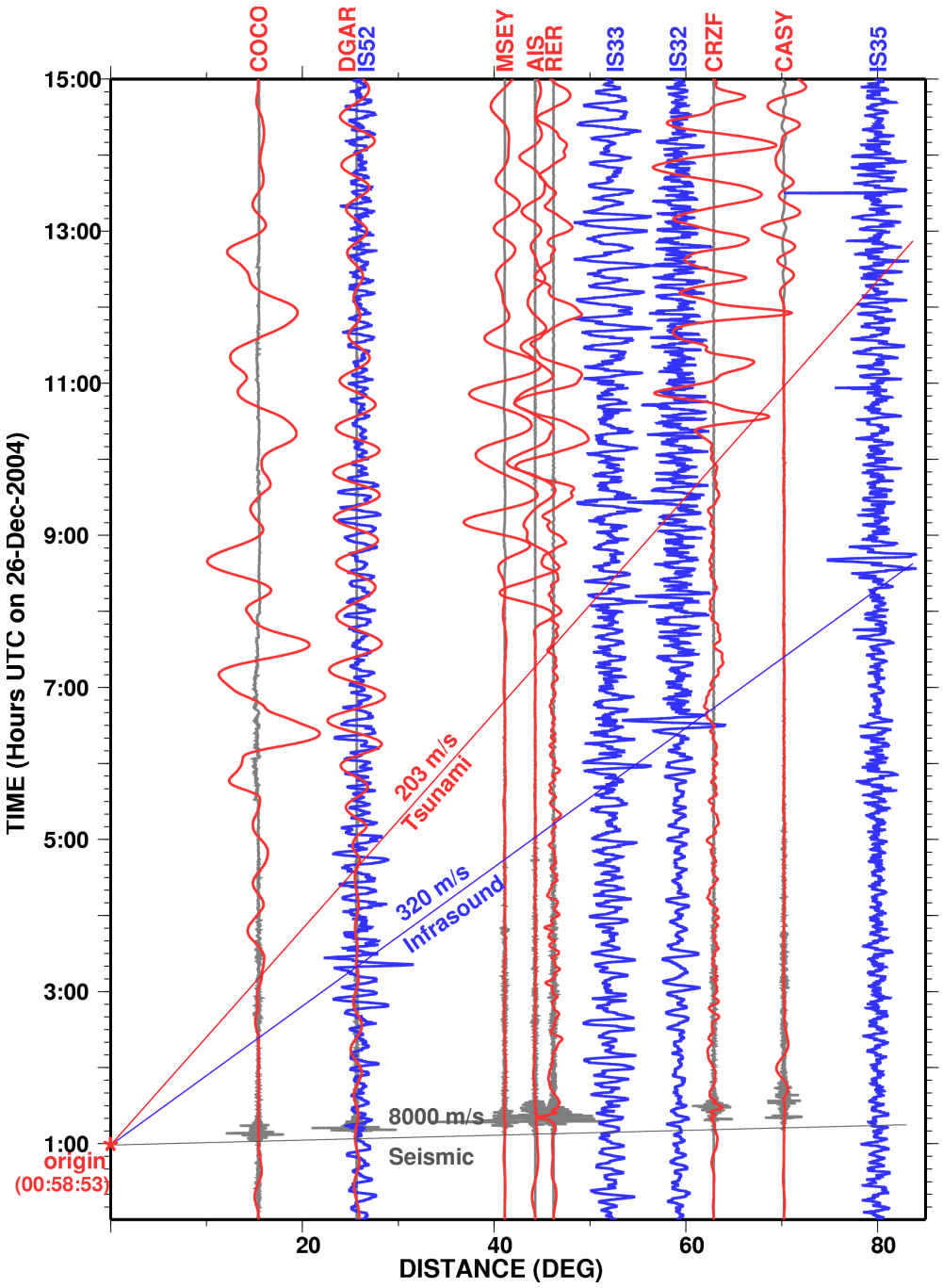


**Figure 7:** Seismic and infrasound records of the Sumatra-Andaman earthquake of 26 December 2004 sorted by epicentral distance of the stations. Original unfiltered seismic broadband records are black; long period filtered (E-W component, 1500 s low pass) seismic records are red; long period filtered (500 s lowpass) infrasound data are blue. Straight lines with velocity indications for the different wave types are also given.

**A2) Manuscript submitted to Journal of Seismology**

**Locating the Tohoku-Oki 2011 Tsunami Source using Acoustic-Gravity Waves**

A. Raveloson [1], R. Kind [1,2,*], X. Yuan[1], L. Ceranna[3]

[1] GFZ Deutsches GeoForschungsZentrum, 14473 Potsdam, Germany

[2] also at Freie Universität, Institut für Geologische Wissenschaften, 12249 Berlin, Germany

[3] Bundesanstalt für Geowissenschaften & Rohstoffe, 30655 Hannover, Germany

*Corresponding Author, email: *kind@gfz-potsdam.de*

## Abstract

The giant Tohoku-Oki earthquake of 11 March 2011 offshore Japan did not only generate tsunami waves in the ocean but also infrasound (or acoustic-gravity) waves in the atmosphere. We identified ultra longperiod signals in the recordings of infrasound stations in north-east Asia, the north-west Pacific and Alaska. Their source was found to be close to the earthquake epicenter. Therefore, we conclude that in general infrasound observations after a large offshore earthquake are evidence, that the surface and the floor of the sea have been significantly displaced by the earthquake and that a tsunami must be expected. Since infrasound is travelling faster than the tsunami, this information may be used for tsunami early warnings.

## Introduction

The magnitude 9.0 Tohoku-Oki earthquake on 11 March 2011 in Japan [e.g. *Simons et al.* 2011] caused one of the largest and most devastating tsunamis ever observed on Earth. The tsunami early warning system of the Japan Meteorological Agency saved many lives by issuing a timely warning. However, the tsunami still caused thousands of casualties because its size was not properly predicted. The first step in a tsunami warning system is the fast determination of the location and size of the offshore earthquake, which is used to

model the possible tsunami at the shorelines. However, at this point it is not even certain if a tsunami has been generated at all. The first direct observation of the tsunami may be obtained from ocean bottom pressure gauges in the vicinity of the source, if they are available. The next direct tsunami observations usually come from tide gauge stations at the shorelines. However, at this point the tsunami has already reached the shores and the warning time tends to zero.

Already *Bolt* (1964) observed acoustic-gravity waves from the great 1964 Alaska earthquake and he suggested using them for tsunami warnings. Atmospheric pressure waves travel with a speed of about 300m/sec whereas tsunami waves travel with 200m/sec in the deep sea and much slower in shallower coastal regions. This difference may result in a very useful tsunami warning time. *Mikumo et al.* (2008) identified acoustic-gravity waves with periods of about 500sec caused by the great 2004 Sumatra-Andaman earthquake and used them to estimate the dislocation of the sea level in the source region. *Raveloson et al.* (2011) also used long period acoustic-gravity waves of the same event to improve the location of the tsunami source.

## Data and Method

We searched through the data of the infrasound arrays of the International Monitoring System in Vienna (IMS, *http://www.ctbto.org/*) for signals of the Tohoku-Oki tsunami. The locations of the infrasound arrays used in our study are shown in Fig.1. Each of these arrays consists of 4-8 microbarographs located within several kilometers. Because of the small aperture of the arrays and our interest in the longest periods ( 500sec), we summed all the individual components of each array into one summation trace without applying any time shifts. That means we did not used typical array properties (like measurements of slowness and backazimuth of an incoming sound wave), but treated each array as single

station and used the individual array stations only to improve the signal-to-noise ratio. Clear signals were found thousands of kilometers away from the source in continental Asia and Alaska. These signals are displayed in Fig.2a. Picked arrival times of the infrasound signals are marked in Fig.2a at the individual traces. We located the tsunami source by a simple grid search method over the coordinates of the infrasound source location and the sound speed. The origin time of the earthquake was used as the origin time of the infrasound wave. The resulting source location is displayed in Fig.2b and the infrasound speed, which leads to the closest location of the circle intersections, is 290m/sec, using only the stations in Asia. Delays of the infrasound origin time relative to the earthquake origin time by up to 100s changed the location of the infrasound source by less than 50km.

The station in Alaska (IS53, see Fig.1) is the station with the largest outlier of its intersection points and was ignored in the source location. The best sound speed would be 356m/sec for this station. The velocities of infrasound are generally near 300m/sec with variations of ś50m/sec due to wind speed (*Arrowsmith et al.* 2010). Our observed sound speeds of 290 and 356m/sec are within this window. The wind in Japan was blowing from the west at the time of the earthquake and its speed on the ground was near 30km/h (ref). The wind speed in larger altitudes is not known to us, but could be higher than on the ground. A strong wind component (about 100km/h) blowing in the opposite direction for the Asian (backazimuth north-west) and Alaskan (backazimuth north-east) stations could be responsible for the different travel times in the different directions. Fig.3 shows the infrasound records of the stations IS39 and IS44 (stations in black in Fig.1) in comparison with the station IS53 in Alaska. A very weak signal may be detected at station IS44, which has a similar backazimuth like the Alaskan station. No signal is detectable above the noise level at station IS39 in the western Pacific, which has a backazimuth nearly opposite to the Alaskan station. This might be an effect of source directivity.

## Results and Conclusions

Fig.2b shows the locations of the earthquake epicenter according to the USGS, our location of the infrasound source and the distribution of vertical displacements of the sea bottom measured at ocean bottom GPS stations. The largest GPS displacement of the sea bottom and the two epicenters are located within about 100km of each other. It should be kept in mind that all infrasound stations (except one) used for the source location are thousands of kilometers away from the source. Data from a larger number of better distributed and closer infrasound stations would certainly increase the accuracy of the location of the infrasound source. Our most important result is therefore, that the Tohoku-Oki earthquake has generated dislocations of the sea surface in the epicentral region of the earthquake, which acted as source of ultra longperiod infrasound signals. From this we conclude that the infrasound source region is also the source region of the tsunami and the region with largest vertical displacements of the sea bottom. Modeling of the observed infrasound signals may contribute additional parameters to the earthquake source characteristics (*Mikumo et al.* 2008).

A second important aspect of our study is that real-time processing of infrasound observations may improve tsunami modeling for early warning purposes. Assuming an average water depth of 1000m, the speed of the tsunami is about three times less than the speed of infrasound. This means a tsunami needs about 15 minutes to reach a coast 100km away from the epicenter. The infrasound signal of the tsunami already indicates 5 minutes after the origin time that a tsunami is definitely coming. From the size and the regional distribution of the infrasound signals a better modeling of the tsunami arriving at the shores may be obtained.

## Acknowledgement

We wish to thank James Mechie for reading the manuscript.

## References

Arrowsmith, S.J., Johnson, J.B. and Drop, D.P., 2010, The Seismoacoustic Wavefield: A new Paradigm in Studying Geophysical Phenomena, *Review of Geophysics*, **48**, RG4003, DOI: 10.1029/2010RG000335.

Bolt, B.A., 1964, Seismic air waves from the great 1964 Alaskan earthquake, *Nature*, **202**, 1095- 1096, doi:10.1038/2021095a0.

Mikumo, T., Shibutani, T., Le Pichon, A., Garces, M., Fee, D., Tsuyuki, T., Watada, S. and Morii, W., 2008, Low-frequency acoustic-gravity waves from coseismic vertical deformation associated with the 2004 Sumatra-Andaman earthquake ($M_w = 9.2$), *J. Geophys. Res.*, **113**.

Raveloson, A., Wang, R., Kind, R., Ceranna, L. and Yuan, X., 2011, Seismic and Infrasound Signals from the 2004 Indian Ocean Tsunami, *Geophys. J. Int.*, **submitted**.

Sato, M., Ishikawa, T., Ujihara, N. et al., 2011, Displacement above the Hypocenter of the 2011 Tohoku-Oki Earthquake, *Science*, **332**, 1395-1395, DOI:10.1126/science.120740.

Simons, M., Minson, S.E., Sladen, A. et al., 2011, The 2011 Magnitude 9.0 Tohoku-Oki Earthquake: Mosaicking the Megathrust from Seconds to Centuries, *Science*, **332**, 1421-1425.

## Figures

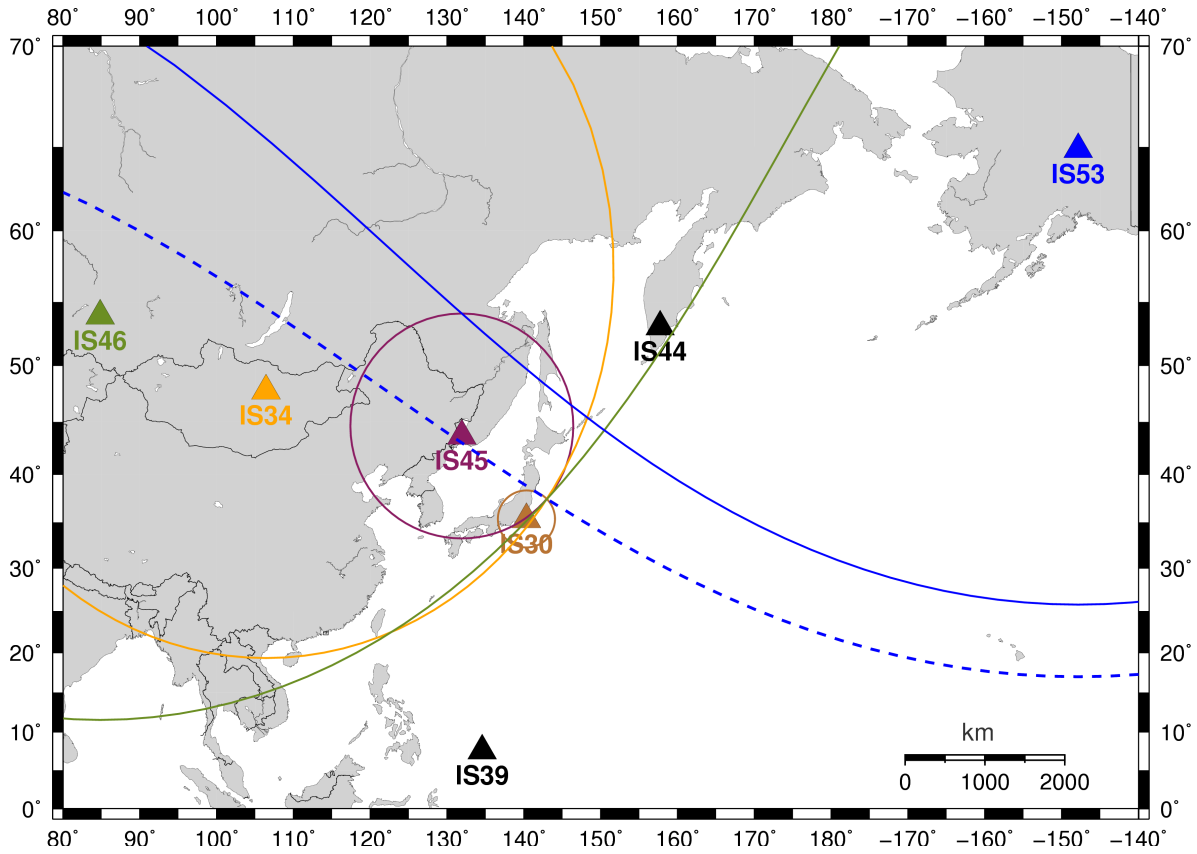


**Figure 1:** Location map of infrasound stations. Longperiod infrasound signals have been observed at the stations **IS30, IS45, IS34, IS46** and **IS53** (see Fig.2a for signal forms and arrival times). No according signals have been found at the stations **IS39** and **IS44**. Circles indicate the possible source of the infrasound for each station assuming a speed of 290m/s for the infrasound signals. The dashed circle around station IS53 is for a sound speed of 356m/s. The origin time of the earthquake was also used as infrasound origin time. Ideally the intersection of all circles would be the location of the infrasound source. A sound speed of 290m/s was found to result in the closest location of all intersection points, excluding the Alaskan station **IS53**, which has a very different backazimuth. An enlarged map of the source region is shown in Fig.2b.

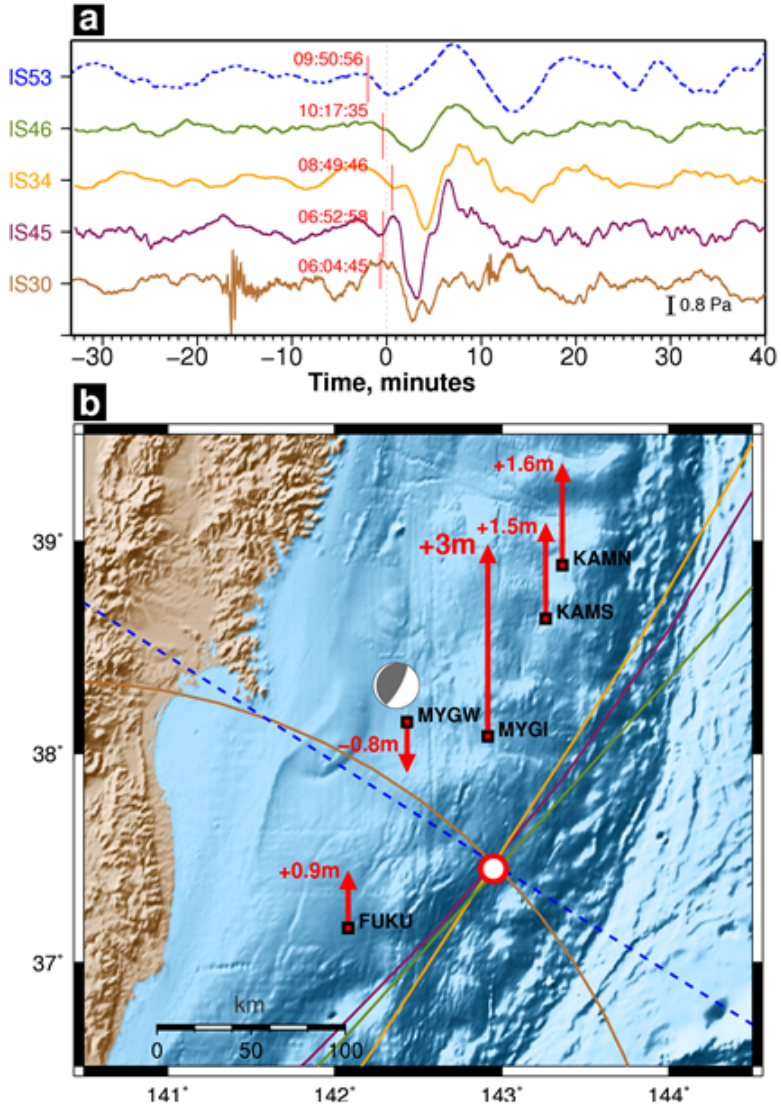


**Figure 2:** Infrasound records and source location of the Tohoku-Oki tsunami. a) Infrasound traces filtered with an 800s high pass filter. The observed periods of the signals vary between 500 and 850s. Infrasound arrival times at the station are given at each trace. The earthquake origin time is 05:46:24.12 (USGS). The seismic signal is visible about 18 minutes in front of the infrasound signal at the station **IS30** in Japan. Zero time mark indicates for Asian stations $290 m/s$ infrasound speed and for the Alaskan station (dashed lines in Fig.2a and 2b) $356 m/s$ speed. b) Location of infrasound source (red-white sphere). Only the stations **IS46, IS34, IS45** and **IS30** are used for source location. The anomalous travel times to the Alaskan station are assumed to be caused by wind direction and speed (see text). Location error is estimated not more than a few tens of kilometers. The seismic epicenter according to the US Geological Survey is shown as a grey-white beach ball marking the fault orientation. Arrows mark the vertical sea floor displacement observed with GPS [*Sato et al.* 2011]. The seismic epicenter, the largest observed GPS ground displacement and the infrasound (or tsunami) source are all located within about $100 km$.

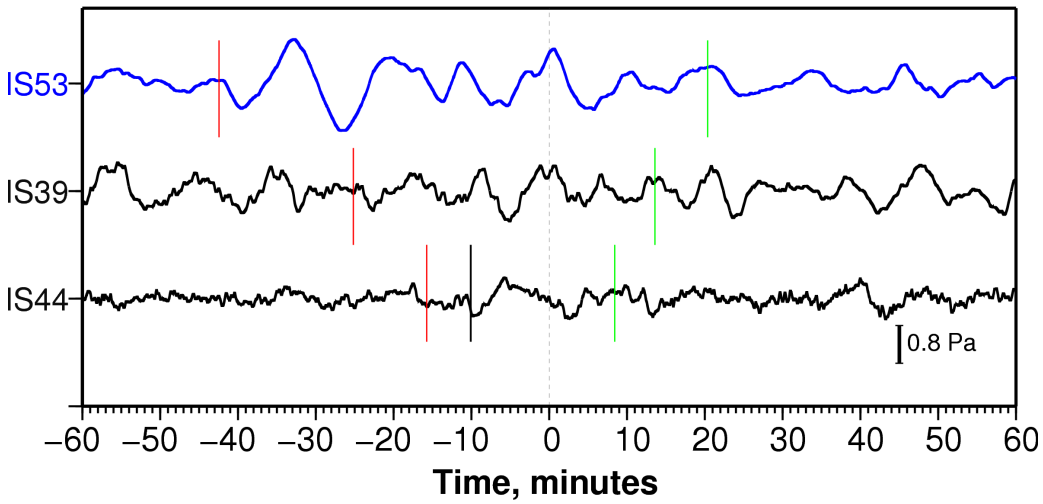


**Figure 3:** Infrasound records of the stations **IS53, IS39** and **IS44**. Zero time is the arrival time of a possible signal traveling with a speed of 310m/s. The red and green marks indicate speeds of 356 and 290m/s, respectively. At station IS53 a signal traveling with 356m/s is visible. At station IS39 no signal was detected above noise level. A weak indication for a signal traveling with a speed of 330m/s is marked in black at station IS44.